Sizing, Dynamic Modeling and Simulation of a Solar-Wind-Hydrogen Power System of the MUN Explorer Autonomous Underwater Vehicle

By

Mohamed Musbah Albarghot

A thesis submitted to the School of Graduate Studies

in partial fulfillment of the requirements for the degree of

Doctor of Philosophy

Faculty of Engineering and Applied Science

Memorial University of Newfoundland

May - 2020

St. John's, Newfoundland and Labrador

Canada

Abstract

In this doctoral research dissertation, sizing, dynamic modeling, and simulation of a solar, wind and hydrogen power system of the MUN Explorer Autonomous Underwater Vehicle (AUV) have been explored, integrating a Polymer Electrolyte Membrane (PEM) fuel cell into an existing power system which uses a lithium ion battery as the main source of its energy. Along with the batteries the integrated fuel cell was designed to power the MUN Explorer AUV to increase its hours of operation and reduce the number of batteries. The installation of hydrogen and oxygen gas tanks next to the batteries augmented the buoyancy force underwater. An electrolyzer powered by solar and wind energy, was used to produce hydrogen. The produced hydrogen was then stored in gas cylinders. A PEM fuel cell was used to consume the hydrogen gas inside the MUN Explorer AUV. The fuel cell was connected to a DC / DC Boost Converter to increase the output voltage from 24 to 48 V, as required by the battery and DC motor. It was proposed that the renewable excess energy be stored and used for recharging a battery. The system design is based on MUN Explorer data sheets and system dynamic simulation results. The system sizing was performed using Hybrid Optimization Model for Electrical Renewable (HOMER) software. The dynamic model was then built in MATLAB / Simulink environment to give a better understanding of the system's behaviour. A PI controller was applied in the dynamic model to maintain the operating conditions such as motor speed, DC bus voltage and the load torque. The simulation of dynamic models and experiment results in hydrogen production and consumption were compared and found to have an acceptable error. The

results from hydrogen production systems (solar and wind) were measured to be 7.0 ml/min. The PI controller provided satisfactory results in terms of maintaining the same operating conditions of the MUN Explorer AUV with a fuel cell.

Acknowledgments

All praises are due to almighty Allah who has given me the opportunity and patience to complete this thesis. It is my honur to acknowledge several institutions and individuals for their contribution, guidance, and support throughout my Ph.D. journey.

First, I would like to offer my sincere thanks to my Libyan government for their financial support by offering me a scholarship to complete my Ph.D. program.

I would like to thank my supervisory committee, for all their support, guidance, and encouragement throughout my program.

I would like to extend my thanks to the department of graduate studies at Memorial University for providing me with such a great opportunity to complete this work.

Lastly, I would like to thank my parents, brothers and sisters for their prayers, support, and encouragement in helping me to grow and learn in a safe environment. Many thanks to my wife whose efforts enabled me to make this journey. I also would like to thank my beloved children for their patience and understanding.

Table of Contents

List of Figures

List of Tables

List of Symbols & Abbreviations

Symbol / Abbreviation	Description
MUN	Memorial University of Newfoundland
AUV	Autonomous Underwater Vehicle
DC	Direct current
PEM	Polymer Electrolyte Membrane
Li-ion	Lithium- ion Battery
HOMER	Hybrid Optimization Model for Electrical Renewable
PV	Photovoltaic
PID	Proportional, Integral, Derivative
SPURV	Self Propelled Underwater Research Vehicles
OTEC	Ocean Thermal Energy Conversion
GC	Gas Chromatography
MPP	Maximum Power Point
MEP	Maximum Efficiency Point
MERLIN	Marine Environmental Research Lab for Intelligent Vehicles

P_b	Pressure of the tank (Pa)
F	Faraday constant
I	Current
P_{bi}	Initial pressure of the tank (Pa)
T_b	Operating temperature (K)
N_{H2}	Normal hydrogen flow rate (Liter/min)
V_b	Volume of the tank (m^3)
T	Temperature (K)
CF	Compressibility factor
V_m	Molar volume (m^3)
P	Pressure (pa)
H_2O	Water
H_2	Hydrogen gas
O_2	Oxygen gas
P_{H2}	Hydrogen pressure Anode side (Pa)
R	Universal gas constant (J/ (mol.K)
V_a	Anode's volume (m3)
H_{2in}	Hydrogen input flow rate (kg/ sec)
H_{2out}	Hydrogen output flow rate (kg/ sec)
P_{o2}	Oxygen pressure cathode side (Pa)
V_c	Cathode's volume (m^3)
O_{2in}	Oxygen input flow rate (kg/ sec)
O_{2out}	Oxygen output flow rate (kg/ sec)

E	Controlled voltage source (V)
E_{OC}	Open circuit voltage (V)
N	Number of cells
A	Tafel slope (V)
i_0	Exchange current (A)
T_d	Response time (sec)
R_{ohm}	Internal resistance (ohm)
i_{FC}	Fuel cell current (A)
V_{FC}	Fuel cell voltage (V)
τ	Constant time (Sec)
V_{Batt}	Nonlinear voltage (V)
E_0	Constant voltage(V)
Exp(s)	Exponential zone dynamics (V)
K	Polarization constant (Ah^{-1})
i*	Low frequency current dynamics(A)
i	Current(A)
it	Extracted capacity (Ah)
Q	Maximum battery capacity (Ah)
A	Exponential voltage(V) for eq. (2.14)
B	Exponential capacity (Ah^{-1})
Ah	Ampere hour
R_b	Internal Resistance of the Battery
K_m	Torque constant (V·s/rad)

e_a , e_b , e_c	Back–EMF waveforms of the phases (V)
i_a , i_b , i_c	Currents of each phases (A)
ω_r	Motor speed (rad/s)
T_e	Electromagnetic torque (N.m)
B	Damping coefficient [N.m/(rad/sec)]
J	Motor shaft (kg*m^2)
T_L	Mechanical torque (N.m)
ED	Energy density (kWh/L)
SE	Specific energy (kWh/kg)
SS	Storage system
E	Controlled voltage source (V)
EOC	Open circuit voltage (V)
COE	Levelized cost of energy ($/kWh)
NPC	Total net present cost of a system
D	Duty cycle
Vin_min	Minimum input voltage(V)
n	Efficiency (eq. 4.14)
Fs	Switching frequency(V)
Vout	Output voltage(V)
Iin	Input current(A)
dv	Output voltage ripple(V)
L	Inductance (H)

C	Capacitance (F)
Vt	DC source voltage (V)
Ia	Armature current (A)
Ra	Armature resistance (Ω)
Laa	Armature inductance (H)
J	Inertia constant (kg*m2)
B_{m}	Constant (N ∗m∗s)
Km	Torque constant (V·s/rad)
$\boldsymbol{\omega}$m	Motor speed (rpm)
D	Density (kg/L)
V	Volume (m3)
M	Mass (kg)
M_{H_2O}	Molecular weight of water
A	Area of the cell
n_d	The electro- osmotic drag coefficient
ne	Number of the Electrolyzer cells
$F_{H_2O_{eod}}$	Electro- Osmotic drag
$F_{H_2O_d}$	Water diffusion of the membrane
D_w	Water diffusion coefficient
$\boldsymbol{t_m}$	Thickness of the membrane
$\boldsymbol{C_{wa}}$	Water concentration of the Anode
$\boldsymbol{C_{wc}}$	Water concentration of the Cathode

V_{ohm}	Ohmic polarization
V_{act}	Activation polarization
α	Charge transfer coefficient
Vel	Operating Voltage of Electrolyzer

Chapter 1

Introduction and Overview

1.1. Introduction and motivation

In the 1950s, the foundation of AUV technology was built and included several unmanned, unchained submersibles' improvements that were remotely controlled. The applied physics laboratory, University of Washington, in the 1960s, developed Self Propelled Underwater Research Vehicles (SPURVs). An AUV can be defined as a self-powered vehicle with Lithium-ion (Li-ion) batteries and a self-controlled machine capable of underwater data collection and autonomous navigation. AUVs' usage can be categorized as research, and includes industrial and military applications, due to its advantages of collecting richer data sets, compared to traditional point sampling methods, which drop cameras and sensor casts from surface ships [1].

The purpose of the MUN Explorer AUV is to do underwater surveillance around the Newfoundland coast and surrounding areas. However, some problems of operating the existing power system of the MUN Explorer, which was done by the researcher at the Holyrood management facility, include mobilization costs, logistics and transport, and facility access, all of which must be considered. Furthermore, recharging the batteries for at least 8 hours is also very challenging and time consuming. There is also a risk of loss when the MUN Explorer is working in extreme environmental conditions. The short life

of the batteries can lead to the loss of the vehicle. This loss can be costly because this vehicle is expensive.

In [1], work investigated how to locate a missing AUV during a particular mission. To bring the MUN Explorer back required more power than it had. In this research, a PEM fuel cell was sized (in HOMER), integrated and simulated (in MATLAB / Simulink) into the existing power system of the MUN Explorer to increase its power capacity and to run for a long period of time. The integrated system also maintained the same operating conditions in terms of motor speed, DC bus voltage and the load torque as the old energy system. Hydrogen and oxygen gases were generated by solar and wind energy to be used by the MUN Explorer for its operations.

Renewable energy is considered as alternative energy sources as awareness of global warming increases and the fossil fuel starts to drain. Many researches and investments focus on renewable energy to eliminate the political issues related to the desirability of nuclear power. Many natural resources such as solar, wind, hydro, geothermal energies are named as renewable energy resources which have no major waste products and the resources are naturally reloaded. The advantages of these resources are environmentally friendly, low cost, low energy conversion efficiencies and alternating nature of energy sources reduces economic sustainability of the renewable energy against the fossil fuels. The support of renewables energy has involved by many governments in the last ten years. For example, the global electricity production is provided 15% of from large hydropower plants and 3.4% from new renewables (solar, wind, geothermal, biofuels, tidal) in 2006 according to the Renewable Energy Policy Network. The capital investment on new

renewable energies,2008, has been expanded with respect to the year 2006 and the total energy generated capacity has been increased by 40% [2].

PEM electrolyzers have several improvements compared to alkaline ones. There is one advantages to be considered for PEM electrolyzer is that it can operate at high pressures up to 200 bar. This high pressure eliminates the compression stage of hydrogen storge when stored to the tanks. Furthermore, the process is an isothermal one and most efficient mothed of compressing hydrogen inside the electrolyzer. Alkaline electyrolyzers have higher parasitic losses and lower efficiency than PEM electrolyzers which lower the cost of hydrogen production. Because of the simple and compact design, the PEM electrolyzers are known as smaller sizes and mass. Yet, high initial cost of equipment such as the membrane cost and special alloys for the casings, supplied pure water to the electrolyzer, and low efficiency at high pressures due to the hydrogen diffusion are considered as drawback pints for operating PEM electrolyzer. Finally, safety concerns at low loads in case of hydrogen mixing with oxygen can be disadvantages as well. While PEM Electrolyzers and fuel cells have similar material construction and design, the improving technology made parallel to the electrolyzers [2]. Figure 1.1 illustrates the main components of the PEM electrolyzer.

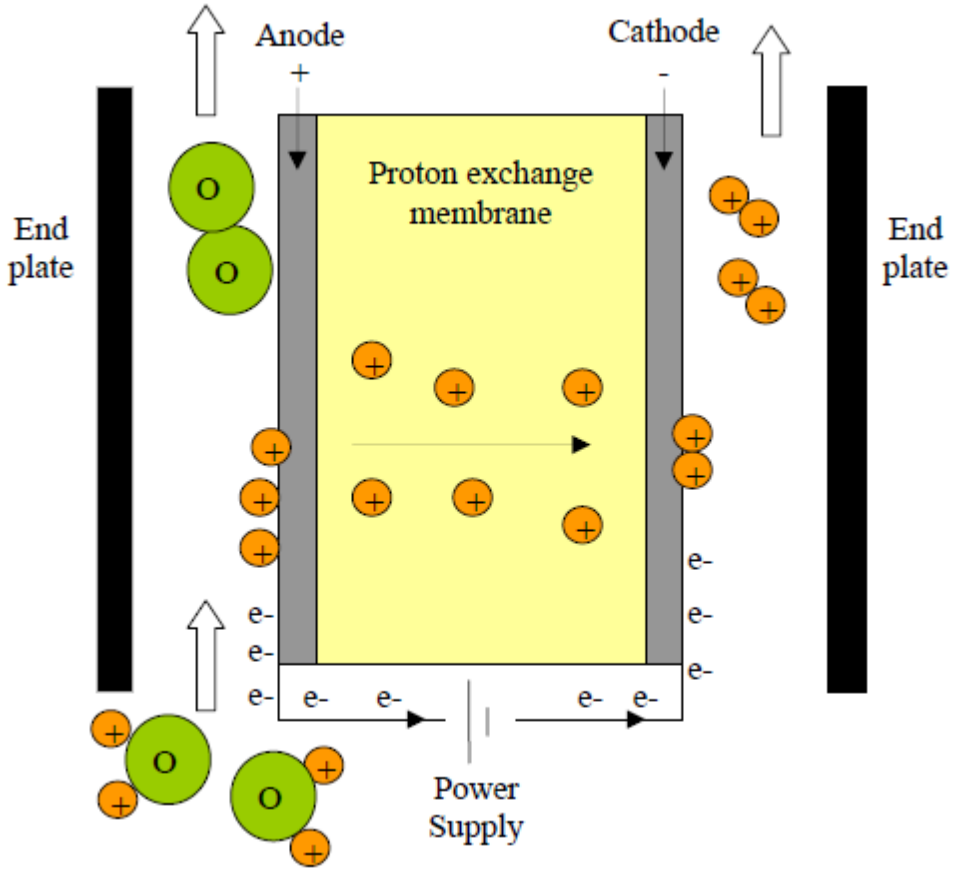

Figure 1. 1: the schematics of PEM electrolysis [2]

There are many types of fuel cells which are categorized corresponding to the electrolyte utilized. Proton exchange membrane fuel cells are known as polymer electrolyte membrane (PEM) fuel cells (PEMFC), also named the most popular type of fuel cells. A solid polymer is used in PEMFC as an electrolyte and porous carbon electrodes which included a platinum or platinum alloy catalyst and they operated with pure hydrogen form the storge systems. At the anode side in which electrons are split from protons on the surface of a platinum-based catalyst, hydrogen gas is generated. Whereas, on the cathode side of the cell the protons pass through the membrane allowing the electrons pass through

in an external circuit, generating the electrical output of the cell. The protons and electrons with oxygen mixes together by metal electrode to produce water, which is only the waste from the fuel cells. Two ways for providing an oxygen gas are in a distilled form or obtained at the electrode directly from the air [3].

One of the most applications of the fuel cells are transportation and stationary applications. For example, fuel cells which used in passenger vehicles such as cars and buses, have fast start up time and promising power-to-weight ratio. One quarter of the world total energy is consumed by transportation sector where a large part of the fuel energy is dissipated as heat in internal combustion engines due to friction loss and exhaust gas. The production of fuel cell units has increased significantly in 2012 to reach a total of 45,700 units, which have achieved substantial progress in the transport market. A massive progress was made in the transportation industry as additional fuel cell electric vehicles (FCEV) were built. For example, Hyundai established the I X 35 FCEV, while Toyota during that period also produced the Mirai 2015 [3]. Figure 1.2 shows the main components of the PEM Fuel Cell.

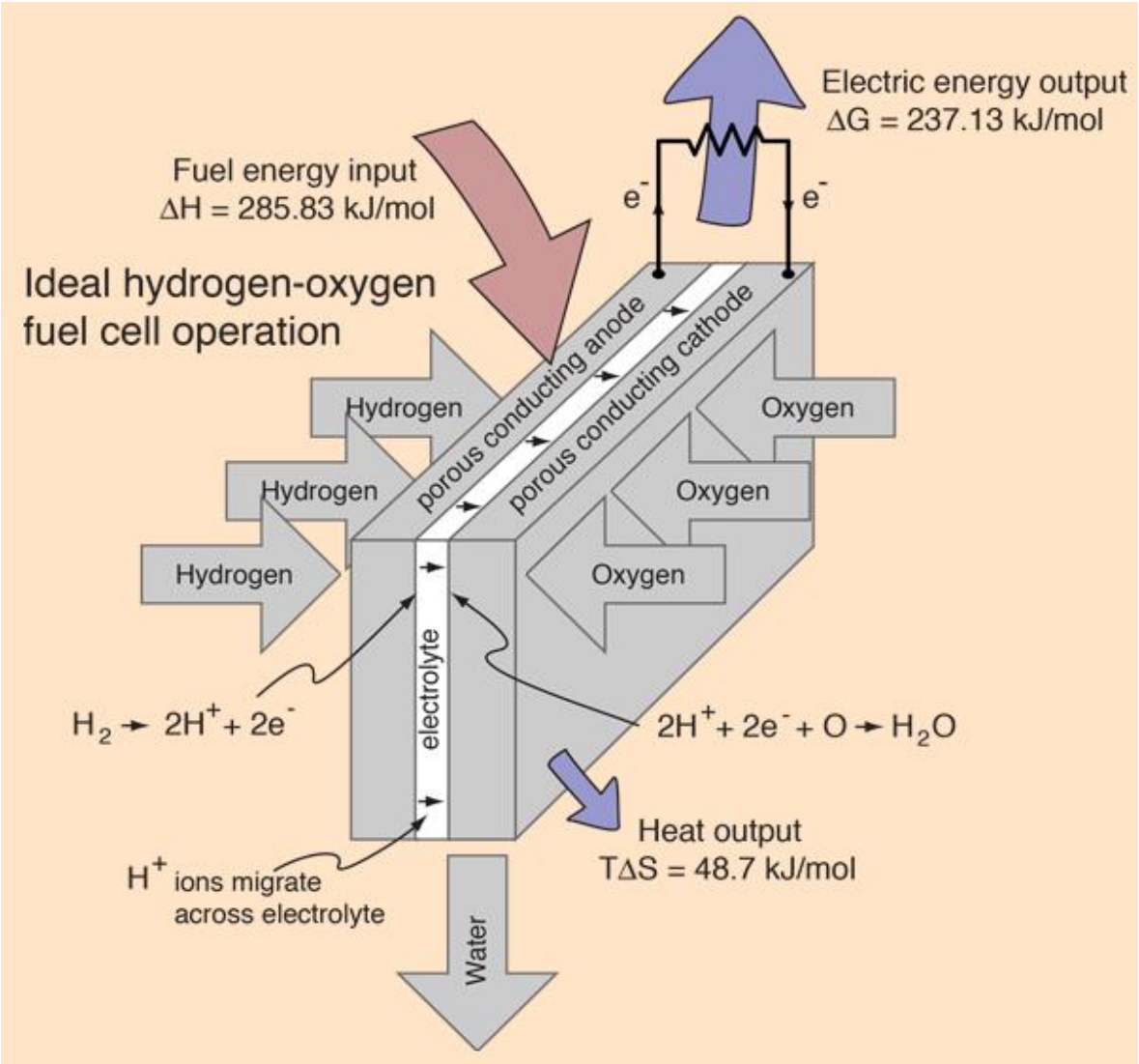

Figure 1. 2: The main components of the PEM Fuel Cell [http://hyperphysics.phy-astr.gsu.edu/hbase/thermo/electrol.html]

1.2. Research Objective and Contributions

As stated above, there are some operational problems related to the existing power system of the MUN Explorer AUV, such as mobilization costs, logistics and transport, recharging the batteries for at least 8 hours, and facility access, which have been addressed in this thesis. To eliminate these challenges and reduce the risk of loss a PEM Fuel Cell

(PEMFC) is studied and integrated into the existing power system of the AUV. The PEMFC requires hydrogen and oxygen gas in order to generate the power. Therefore, the hydrogen production is intended to be generated from renewable solar and wind energy sources, designed to be placed on shore along with PEM Electrolyzer and the hydrogen and oxygen tanks to facilitate the process of refueling.

The objectives of this research are to integrate a PEM Fuel Cell into an existing system to:

- Increase the energy capacity
- Reduce the number of batteries
- Help the buoyancy force in underwater depths.

The overall system components and research approach are shown in Figure 1.3. The research contributions are accomplished focusing on flowing: solar energy hydrogen production is investigated experimentally and from simulation, wind energy hydrogen production is investigated experimentally and from simulation, a PEM Fuel Cell is integrated into an AUV existing power system, a new AUV power system is sized and created using HOMER and MTLAB / Simulink, and a PI controller is applied to maintain the MUN Explorer operating conditions for the MUN Explorer.

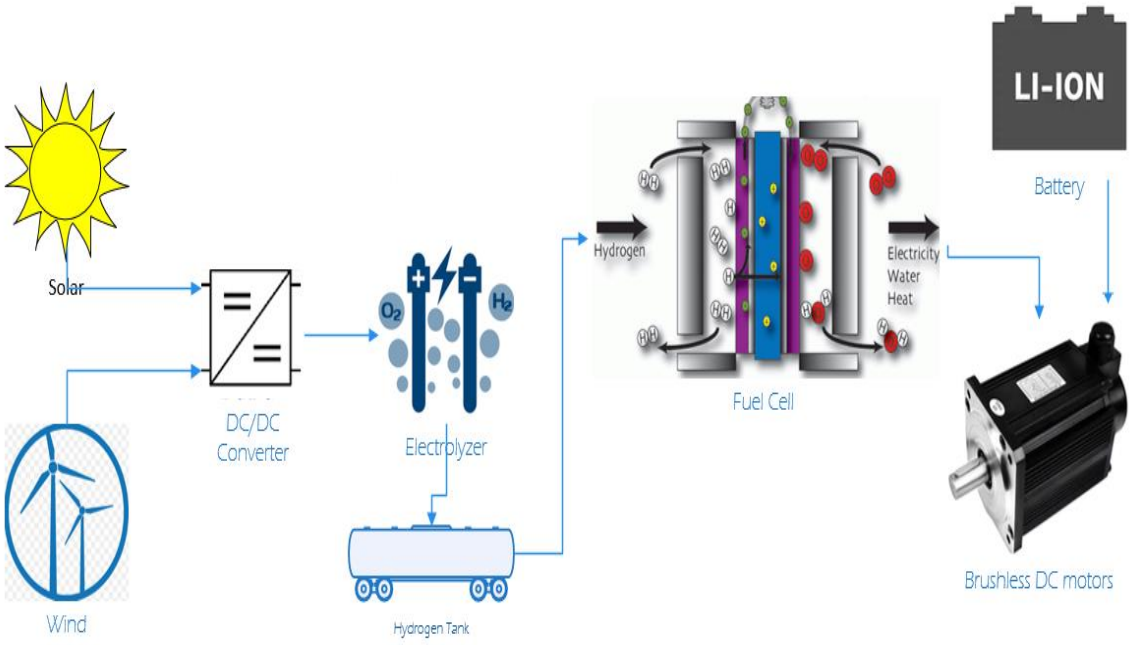

Figure 1. 3: Overall research approach components [Appendix No. 1]

1.3. Thesis Structure

This thesis is organized based on these areas. Chapter 1 is an introduction and overview of the AUV's history and foundation. The MUN Explorer AUV challenges and improvements have also been discussed. Chapter 2 depicts the required hydrogen and oxygen production from a renewable energy source (solar energy) using a PEM Electrolyzer. The generated gases are also stored in the tanks. An experimental setup and MATLAB/ Simulink modeling are also developed and simulated to be compared and discussed. In chapter 3, a renewable energy source (wind energy) is used to power a PEM Electrolyzer to generate hydrogen and oxygen gases, which are stored in tanks. An

experimental setup and MATLAB/ Simulink model are also built and simulated to be compared and considered.

Chapter 4 demonstrated the sizing technique of the power system of the MUN Explorer AUV using HOMER software. then the dynamic model of the system was built in MATLAB / Simulink to match the sizing results with the dynamic model. The proposed sizing was able to increase the power capacity of the system as well as eliminate some of the batteries. This chapter was also able to show the benefits of integrating the PEM fuel cell into the system by improving the underwater buoyancy force. Chapter 5 presented the dynamic model of the MUN Explorer AUV, including a fuel cell system to run under the same operating conditions as suggested by its manual. A PI controller was then applied to the dynamic model to maintain the operating conditions, such as motor speed, DC bus voltage and the load torque. Chapter 6 concluded the research with the key findings and contributions and suggested possible expansion ideas for this work.

This thesis follows the objective classification as defined earlier. The chapters' structure is discussed as below:

- Chapter 1includes a brief introduction and overview of this thesis. The research objective and scope, along with the limitations, are also introduced. A literature survey is included, and the dissertation's structure is outlined.
- Chapter 2 discusses the hydrogen production from solar renewable energy by powering a PEM Electrolayzer experimentally and by simulation. The DC /DC converter is used to regulate the voltage and current. All the simulation is done in MATLAB / Simulink.

- Chapter 3 demonstrates the hydrogen production from wind renewable energy by powering a PEM Electrolayzer experimentally and by simulation. The hydrogen amount is calculated to be 7.345 ml/min for the model and for the experimental set up. The DC /DC converter is used to regulate the voltage and current.
- Chapter 4 studies the sizing technique using HOMER Software as well as the new dynamic model with a PEM fuel cell to study and check the system's behaviour. The model is created in MATLAB / Simulink.
- Chapter 5 presents the dynamic model of the MUN Explorer AUV, including a fuel cell system as well as a PI controller, to maintain the operating conditions such as motor speed, DC bus voltage and the load torque.
- Finally, Chapter 6 concludes the research with the findings results and contributions and suggests possible expansion ideas for this work. This Chapter also discusses the learnings from this research work and its contribution toward the improvement of the design.

1.4. Literature Review

Shapiro et al. (2005) studied a solar electric power system which powered an electrolyzer to store energy in the form of hydrogen gas. This methodology used batteries as an alternative way for storing energy. Their system components included a PEM electrolyzer, high-pressure hydrogen and oxygen storage, and a PEM fuel cell, which was built as a prototype and tested experimentally. The goal of such a system was a proof- of-concept for general system feasibility, and electrolyzer performance characterization, with the current density of 1.0 A/cm2 at 2.0 V per cell. The power integration with a PV system was expected to be a reliable environmentally remote installation. However, the system provided high-quality power backup for critical systems, such as telecommunications and medical facilities, without PV [4].

Beainy et al. (2014) developed an electrical equivalent circuit for a PEM electrolyzer using a MATLAB / Simulink block diagram. The examination of I -V characteristic for a single PEM electrolyzer cell was shown under a steady state condition. Hydrogen production behaviour was studied based on power and current. The electrolytic hydrogen production rose with the input current in a linear manner; however, the variation of the input power was nonlinear. Some parameters such as temperature and pressure were considered for developing the model [5].

Lee et al. (2013) analytically and experimentally investigated temperature and flow rate's effects on a PEM electrolyzer to develop their model. Five ancillaries, including an anode, cathode, membrane, voltage, and storage, were simulated by MATLAB/ Simulink to build the dynamic model for an electrolyzer. Some parameters such as power, flow rate,

and temperature controllers showed the PEM electrolyzer performance, to validate the analytical polarization curve. The evaluation of four circulating water flow fields took place experimentally, using the 25 cm^2 active area of a small cell. The optimum temperature and flow rate for the electrolyzer were compared at different temperature regimes by analytical and experimental polarization curves. The hydrogen generation was also illustrated for different water flow rates[6].

Speranza et al. (2015) proposed hydrogen as a carrier gas to switch nitrogen and helium in Gas Chromatography (GC) applications and found many advantages, such as faster analysis, lower cost, and on-site generated hydrogen reliability. The carrier gas purity was critical for higher performance and lower maintenance. A proper evaluation of different hydrogen sources was produced for critical requirements of carrier gas applications [7].

Joneidi et al. (2013) simulated a small PV- fuel cell -based hybrid energy system in MATLAB / Simulink, which was constructed using mathematical and electrical models. The system components included a PV, a PEM fuel cell, hydrogen storage tanks, and a power converter. The load demand was connected from the PV when there was enough sunlight. However, when there was insufficient sunlight, the fuel cell operated to meet the needed load. The PV was also used to convert the electrical energy into hydrogen using an electrolyzer and stored in the hydrogen tank for later use in fuel cells. To control the fuel cell model, a PID controller was applied [8].

Al-Refai (2014) studied the energy storage system to improve the usage of renewable energy. An electrolyzer was used to produce the hydrogen gas from PV solar energy. The system components were demonstrated in MATLAB / Simulink environment.

The operations of photovoltaic array and electrolyzer were tested at different insulation levels. The results from both the PV and electrolyzer were determined, especially when the solar energy inputs varied continuously [9].

Sopian et al. (2009) integrated a PV - wind - hydrogen energy production / storage system. The components of the system were a photovoltaic array, wind turbine, PEM electrolyzer, battery bank, and hydrogen tank. The system also had an automatic control system for battery charging and discharging. A hydrogen quantity of 130 ml/min to 140 ml/min was generated for an average global solar radiation, between 200 W/m^2 and 800 W/m^2, and wind velocities ranging from 2.0 m/s and 5.0 m/s. For each system component, a mathematical model was built and compared to the experimental results [10].

Uluoglu (2010) built a solar hydrogen Stand-Alone Power System (SAPS) for an emergency room of a hospital. The system also operated without any external power supply and provides off-grid continuous electricity throughout the year. Some components of the system were integrated and simulated in TRNSYS commercial software, including photovoltaic panels, PEM electrolyzer, PEM fuel cells, hydrogen tanks, batteries, and a control mechanism. Auxiliary equipment such as DC/AC converters, water pump, pipes, and hydrogen dryers were also integrated into the system. An investigation of the optimal system structure and sizing component with a good performance and a low cost for different users, and control strategies were tested [11].

Kim and Peng (2007) investigated a power management strategy of a fuel cell hybrid vehicle (FCHV) for achieving optimal fuel economy. For the performance optimization of FCHVs, they designed a combined power management and design optimization problem for model subsystem scaling in order to forecast the features of

system components. The controller was applied as a design variable in the system's optimization problems, which was inspired by their Stochastic Dynamic Programming. The simulation results with an optimization approach delivered excellent fuel economy [12].

Ahmadi et al. (2013) generated hydrogen using an ocean thermal energy conversion (OTEC) system which was combined with a solar-enhanced PEM electrolyzer. Some system components, such as turbine, evaporator, condenser, pump, solar collector, and PEM electrolyzer, were integrated. The electricity from the turbine was used to power the PEM electrolyzer to produce hydrogen gas. The models of the OTEC system and PEM electrolyzer were developed and simulated using MATLAB/ Simulink. The experimental data from the literature were used to validate the simulation model for the PEM electrolyzer. The exergy efficiency of the system performed as well as the exergy destruction of each component. The energy efficiency of the simulated OTEC system was 3.6% and the exergy efficiency was 22.7%. The PEM electrolyzer exergy efficiency was calculated to be 56.5% and hydrogen production was 1.2 kg/h [13].

Kumaraswamy and Quaicoe (2016) illustrated the nonlinear output characteristics of PEM fuel cells. These characteristics may cause low efficiency and low operation power. Some tracking techniques were used to track the maximum power point (MPP) which extracts maximum power and the maximum efficiency point (MEP). For portable applications, the output power and efficiency of the PEMFC were recommended to be high but were low at the maximum power point and maximum efficiency point. This work focused on an alternative tracking technique called midpoint tracking technique (MDT), to eliminate the MEP and MPP tracking techniques. The simulation results and the analysis of the tracking techniques model were studied and illustrated. The proposed MDT

technique was found to be an effective technique with high output power and high efficiency when compared to the MEP and MPP [14].

Rigatos and Siano. (2016) demonstrated a nonlinear fuel cell control approach, utilizing differential flatness theory and a Kalman filter. The fuel cell dynamic model verified their differential flatness theory. The state variables of the system and control inputs were expressed as differential functions of specific state variables called flat outputs. The design of a state-feedback controller of the dynamic system was successfully accomplished for uncertainties and external perturbations of the model. The extension of the PEM fuel cells state-space variables were measured as extra state variables to the derivatives of the total disturbance inputs. The linearization of extended fuel cell models was implemented by using a Kalman filter-based disturbance observer, to eliminate the disturbance effect and uncertainty of the system. A complementary control element that compensates for the perturbations' effects was illustrated. Simulations and experiments were used to measure the control scheme efficiency [15].

Raugel et al. (2010) developed an adapted fuel cell system for an AUV. It was difficult to fully optimize the integration because the fuel cell was in a separate vessel. The hybridization with Lithium-ion batteries was examined by performing another experiment using the fuel cell system. The fuel cell provided the necessary electrical energy on board and stored it in the batteries to meet the peak power supply. These fuel cells were classified as innovative power sources for underwater vehicles such as AUVs and submarines [16].

Lewis et al. (2016) researched the potential of an AUV for operations in harsh naval environments. In 2005, Memorial University of Newfoundland authorized the construction of an International Submarine Engineering Explorer AUV, the management and operation

of which was led by the Marine Environmental Research Lab for Intelligent Vehicles (MERLIN). To ensure that a full service AUV research team can contend with harsh maritime and polar experiences, MERLIN's programs have developed over the past decade. AUV research has progressed from dynamic vehicle trainings with basic sensor technology to develop advanced autonomous navigation [17].

Lewis R. (2015) showed that with any operation of AUV technology, there is an actual risk of underwater loss. This risk is associated with the harsh environmental conditions under the ice, such as extreme cold and compromised visibility. The development of risk-based methodologies was to overcome the risk of loss for specific AUV stages prior to utilizations. This was a basic goal, to be aware of the overall risk of a specific task. There were successful AUV missions reported in previous studies with very little AUV loss [1].

Mebarki et al (2016) studied the ability of a hybrid power system of an electric vehicle to generate the needed energy. The system was constructed with a PEM fuel cell and a battery bank. A DC/DC converter connected to the PEMFC to adjust the voltage, and the excess energy was stored in the battery bank. The mathematical model of the system, along with the control supervision, were well studied to address each subsystem. Experimental and simulation results were collected and illustrated, and MATLAB / Simulink was used to run the simulation [18].

Motapon et al (2014) evaluated the fuel cell hybrid emergency power system of an electric aircraft that included new real-time hydrogen consumption and a minimizing energy management strategy. He compared two strategies (hydrogen consumption minimization strategy and less hydrogen consumption) based on equivalent fuel

consumption through simulations and experiments. The first was called a hydrogen consumption minimization strategy, which is well known as an equivalent consumption minimization strategy (ECMS). The sensitivity of the second strategy that he suggested was less hydrogen consumption compared to the load profile. The examination of equivalent fuel consumption has not considered the financial cost of improvement, which depended on the complete mission profile. This strategy was minimizing the hydrogen consumption for the load profile variations [19].

Five different energy management schemes (the state machine control strategy, rule-based fuzzy logic strategy, classical proportional–integral control strategy, frequency decoupling/fuzzy logic control strategy, and the equivalent consumption minimization strategy) for a fuel cell-based emergency power system of an electric aircraft were compared and analyzed by Motapon et al (2014). Their system had fuel cells, Li-ion batteries, and supercapacitors, as well as DC/DC and DC/AC converters. These energy management schemes were commonly used in fuel-cell vehicle applications. Hydrogen consumption, the state of charges of the batteries/ supercapacitors, and the overall system efficiency were compared as the main criteria of the system. All analyses and performances were validated and calculated using simulation models and an experimental bench test [20].

From the above literature, there was not enough information for sizing and storage systems for the AUV and other applications. This thesis will be focusing and exploring what is missing from the literature. Hydrogen and oxygen storge system is studied and showed to increase the power capacity during the MUN Explorer AUV's missions.

1.5. Constraints and Limitations

There has been considerable work done by researchers in the area of using fuel cells with batteries to estimate and achieve a desired power for many different applications, yet the literature on the fuel cell integration of the existing power system for the MUN Explorer Autonomous Underwater Vehicle has not been investigated by any researcher so far. A few researchers have also done experimental work on fuel cell integration into AUVs, but there has been a lack of information about the dynamic models and control approaches. Some components were also missing from the literature, such as DC motor specification, batteries, and gas tanks. For this reason, this thesis investigated and studied the sizing and the proposed dynamic model of the MUN Explorer AUV by applying a PI controller to maintain the same operating conditions, such as motor speed, DC bus voltage and the load torque, and to overcome some problems mentioned above.

There was also a limitation regarding the integration of the MUN Explorer AUV proposed dynamic model into the actual one, because the vehicle is owned by another department and the access to it is limited. Therefore, the experiment cannot be done using the MUN Explorer AUV and the proposed work mainly focuses on the simulation.

Finally, the simulation results were scheduled to be validated by experimental work in order to get basic results before integration into the AUV. However, the financial limitation prevented the completion of this work.

References - Chapter 1

[1] A. Science, “THE AUTONOMOUS UNDERWATER VEHICLE EMERGENCY LOCALIZATION SYSTEM An under ice AUV tracking technology for over-the-horizon operations,” 2015.

[2] A. Uluoğlu, “Solar-Hydrogen Stand-Alone Power System Design and Simulations,” no. May, 2010.

[3] Alaswad, Abed, Ahmad Baroutaji, Hussam Achour, James Carton, Ahmed Al Makky, and Abdul-Ghani Olabi. "Developments in fuel cell technologies in the transport sector." *International Journal of Hydrogen Energy* 41, no. 37 (2016): 16499-16508.

[4] D. Shapiro, J. Duffy, M. Kimble, and M. Pien, “Solar-powered regenerative PEM electrolyzer/fuel cell system,” *Sol. Energy*, vol. 79, no. 5, pp. 544–550, 2005.

[5] A. Beainy, N. Karami, and N. Moubayed, “Simulink model for a PEM electrolyzer based on an equivalent electrical circuit,” *2014 Int. Conf. Renew. Energies Dev. Countries, REDEC 2014*, pp. 145–149, 2014.

[6] B. Lee, K. Park, and H. M. Kim, “Dynamic simulation of PEM water electrolysis and comparison with experiments,” *Int. J. Electrochem. Sci.*, vol. 8, no. 1, pp. 235–248, 2013.

[7] G. C. Conference, B. J. Speranza, and P. Onsite, “The Effects of Hydrogen Purity on GC Analysis and Column Life,” 2015.

[8] A. Joneidi, A. A. Shayegani, and H. Mohseni, “A Control Methodology of

Dynamic for Photovoltaic (PV)/Fuel Cell (FC) Hybrid Energy System for Standalone Usage," *Int. J. Comput. Electr. Eng.*, vol. 5, no. 1, pp. 128–132, 2013.

[9] M. a Al-refai, "Matlab / Simulink Simulation of Solar Energy Storage System," *Int. J. Electr. Comput. Energ. Electron. Commun. Eng.*, vol. 8, no. 2, pp. 304–309, 2014.

[10] K. Sopian, M. Z. Ibrahim, W. R. Wan Daud, M. Y. Othman, B. Yatim, and N. Amin, "Performance of a PV-wind hybrid system for hydrogen production," *Renew. Energy*, vol. 34, no. 8, pp. 1973–1978, 2009.

[11] A. Uluoğlu, "Solar-Hydrogen Stand-Alone Power System Design and Simulations," no. May, 2010.

[12] M. J. Kim and H. Peng, "Power management and design optimization of fuel cell/battery hybrid vehicles," *J. Power Sources*, vol. 165, no. 2, pp. 819–832, 2007.

[13] P. Ahmadi, I. Dincer, and M. A. Rosen, "Energy and exergy analyses of hydrogen production via solar-boosted ocean thermal energy conversion and PEM electrolysis," *Int. J. Hydrogen Energy*, vol. 38, no. 4, pp. 1795–1805, 2013.

[14] V. K. Kumaraswamy and J. E. Quaicoe, "Tracking techniques for the PEMFC in portable applications," *2016 IEEE Electr. Power Energy Conf. EPEC 2016*, 2016.

[15] G. Rigatos and P. Siano, "A PEM fuel cells control approach based on differential flatness theory," *2016 Int. Symp. Power Electron. Electr. Drives, Autom. Motion, SPEEDAM 2016*, vol. 2, no. 2, pp. 1004–1009, 2016.

[16] E. Raugel, V. Rigaud, and C. Lakeman, "Sea experiment of a survey AUV powered by a fuel cell system," *2010 IEEE/OES Auton. Underw. Veh. AUV 2010*, pp. 1–3, 2010.

[17] R. Lewis *et al.*, “MERLIN - A decade of large AUV experience at Memorial University of Newfoundland,” *Auton. Underw. Veh. 2016, AUV 2016*, pp. 222–229, 2016.

[18] N. Mebarki, T. Rekioua, Z. Mokrani, D. Rekioua, and S. Bacha, “PEM fuel cell/ battery storage system supplying electric vehicle,” *Int. J. Hydrogen Energy*, vol. 41, no. 45, pp. 20993–21005, 2016.

[19] S. N. Motapon, L. A. Dessaint, and K. Al-Haddad, “A robust H2-consumption-minimization-based energy management strategy for a fuel cell hybrid emergency power system of more electric aircraft,” *IEEE Trans. Ind. Electron.*, vol. 61, no. 11, pp. 6148–6156, 2014.

[20] S. Njoya Motapon, L. A. Dessaint, and K. Al-Haddad, “A comparative study of energy management schemes for a fuel-cell hybrid emergency power system of more-electric aircraft,” *IEEE Trans. Ind. Electron.*, vol. 61, no. 3, pp. 1320–1334, 2014.

Chapter 2

MATLAB / Simulink Modeling and Experimental Results of a PEM Electrolyzer Powered by a Solar Panel

2.1. Chapter Overview

Solar panels are used to power an electrolyzer to separate the water into hydrogen and oxygen gas. The electrical equivalent circuit for the PEM electrolyzer was developed and implemented in MATLAB / Simulink, along with the hydrogen storage tank. The voltage (2V) and current (1A) were supplied from the DC/DC buck converter to the electrolyzer to compare simulation and experimental results. The hydrogen amount is calculated to be 7.345 ml/min for the model, as well as for the experimental set up. The experimental and simulation results were matched and validated against the Simulink model. The contribution of this chapter is to show the buck converter along with storage system (hydrogen and oxygen tanks)

2.2. Introduction

World transport depends heavily on petroleum, as it supplies 95% of total energy and is responsible for almost a quarter of global energy-related emissions. Globally, marine shipping running on fossil fuels also causes many environmental issues. Over the past decade, transport emissions have increased at a faster rate than those of any other energy

sector. The transportation sector accounts for 28% of all US greenhouse gas emissions, 34% of all carbon dioxide emissions, 36-78% of the main components of urban air pollution, and 68% of all oil consumption [1] and [2]. Global transport activity will continue to increase along with economic growth. International transportation has been dominated by ocean shipping, with ships continually increasing in size and number. Fossil fuel usage also raises many important concerns and challenges, such as climate change and supply cost increases. For example, in 2002, the use of fossil fuels was responsible for 86% of the world's energy consumption. In 2003, US electrical energy demands also reached a higher value of 24% of the total demand for the planet [3]. It has become essential to seek alternative sources of renewable energy that can be easily captured by using waves, sun and wind. Statistics suggest that changing to fuel cell technology could save more than one million U.S. dollars per ship per year in fuel costs. The sun, wind and waves provide an unlimited source of renewable energy; solar energy is known as the most sustainable source of renewable energy. For example, 27.7 GW of PV (photovoltaic) systems were installed worldwide in 2011. Compared with 2010, there were also six countries where more than 1 GW of PV has been installed by 2011[4].

Batteries are not the solution for energy storage; they provide short term solutions and their waste is comprised of significant and dangerous pollutants. Hydrogen remains the only valid source for energy storage, meaning the hydrogen gas can be stored for a long period of time without self-discharging when compared to batteries. Producing hydrogen can be achieved in large quantities from water electrolysis; water is a clean resource, available in large quantities everywhere. Electrolysis will be studied to be brought aboard vehicles such as cargo ships.

This chapter's focus is to improve the results of modeling the electrolysis system and obtain experimental results. The set-up is powering the electrolyzer with a small PV solar panel that produces 2 V and 1 A. The hydrogen is produced and stocked in the tank. The mathematical and dynamic model of the electrolysis has been implemented in MATLAB/Simulink. In Section 2.3, the system's components are detailed. In Section 2.3, the simulation and experimental set-ups are described. In Section 2.4, we examine and compare the simulation and experimental results.

2.3. Solar System Components

2.3.1. Photovoltaic Solar Panel

The solar energy is transferred directly into electrical energy in the PV panel through a basic physical process. The physical behaviour of any solar cell is very similar to the classical p-n junction diode. Two diode solar cell models are shown in Figure 2.1. The relationship between Output Current (*I*) and Output Voltage (*V*) is found using the formula below [5]:

$$I=I_{ph}-I_s * \left(e^{(V+I*R_s)/(N*V_t)}-1\right)-I_{s2} * \left(e^{(V+I*R_s)/(N_2*V_t)}-1\right) - (V+I*R_s)/R_p \quad (2.1)$$

where I_{ph} is the solar induced current equal to $I_{ph0}*\left(I_r / I_{R0}\right)$, and where I_r is the irradiance (light intensity) in W/m^2 falling on the cell. I_{ph0} is the measured solar - generated current for the irradiance I_{R0}. I_s is the saturation current of the first diode, I_{s2} is the saturation current of the second diode, and V_t is thermal voltage that is equal to

KT/Q, where *K* is the Boltzmann constant. *T* is the device's simulation temperature parameter value. *Q* is the elementary charge on an electron. N and N_2 are the quality factors of the first and second diodes, respectively. *V* is the voltage across the solar cell [5]. The *I-V* and *P-V* characteristic curves of the PV module are shown under irradiance of 1000 W/m^2 at $25^{\circ}C$, as illustrated in Figure 2.2. For solar energy performance, temperature plays an important role because the four parameters (I_r, I_s, R_s, and V_t) are functions of temperature. This proves that the lower temperature is the higher power obtained from the PV, and the greater the open circuit voltage [6].

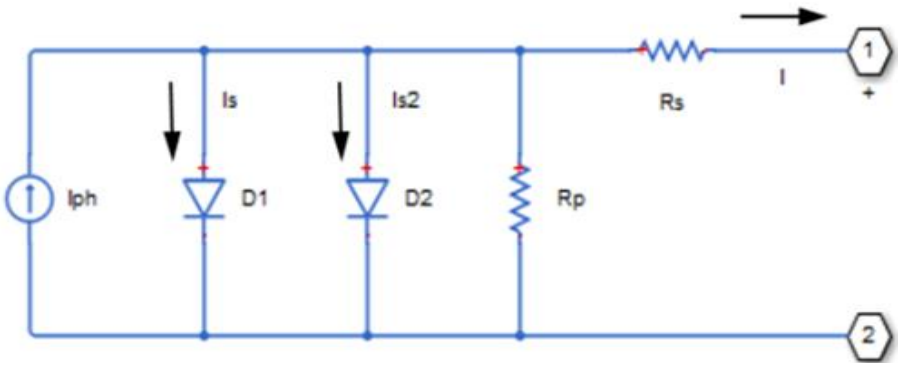

Figure 2. 1: Electrical equivalent circuit of the solar cell [28]

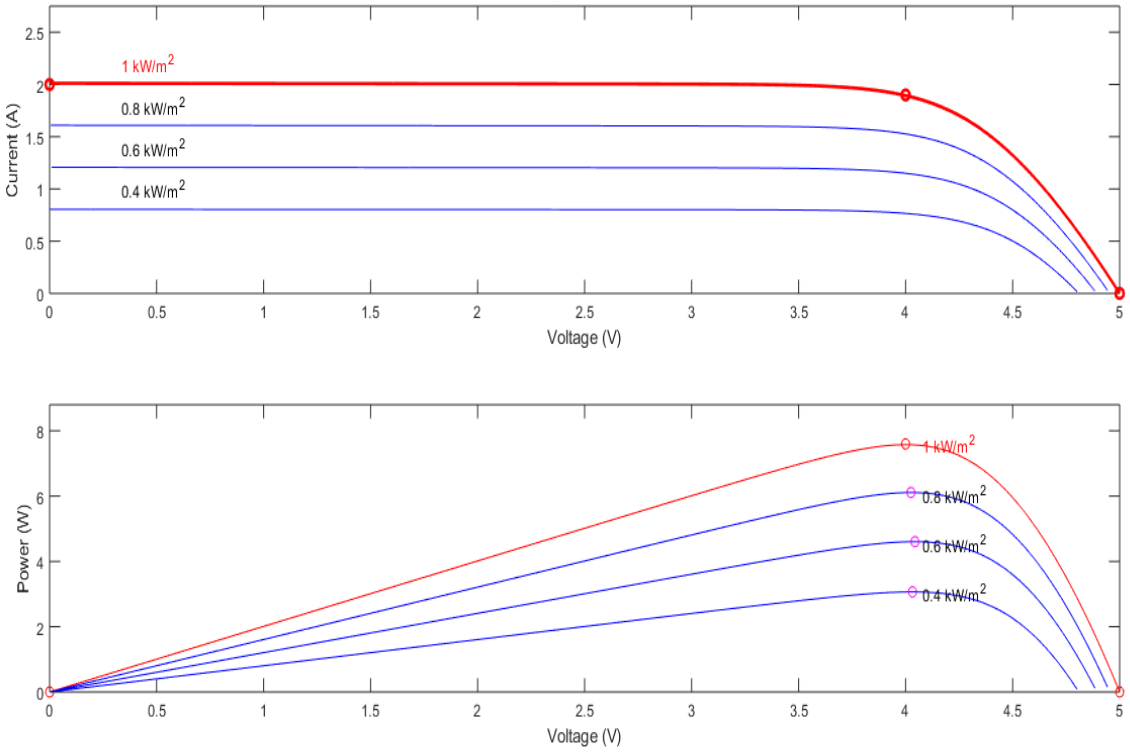

Figure 2. 2: I-V and P-V curves of the PV module

2.3.2. DC/DC Buck Converter

The buck converter is a step-down DC-DC voltage converter, where the average output voltage is always less than the input voltage. There are two operating modes for the buck converter in terms of diode circuits. In the first mode, when the switch is on, the diode becomes reverse biased, so that the supplied energy is stored in an inductor. In the second mode, the diode becomes forward biased when the switch is off, due to the load; it receives

energy from the inductor. The input stays isolated from the output [7]. The purpose of the buck converter is to regulate DC power supplies. The duty cycle (D) is the ratio of the time power is switched on to the total time, and the ratio of output voltage to the input voltage. The duty cycle is also calculated by the following equation:

$$\frac{V_o}{V_s} = D = \frac{I_s}{I_o} \tag{2.2}$$

where V_o and V_s are the output and input voltages, respectively, and I_s and I_o are input and output current, respectively [7]. The selection parameter of the buck converter is based on the voltage and current output of the PV, which is designed to be 5 V and 2 A. Since the electrolyzer load is designed for 2 V and 1 A, it becomes necessary to select a buck converter in order to regulate the voltage and current. The values of the buck converter parameters such as the inductor, capacitor, and duty cycle were obtained from the website[1] for desired input values for the electrolyzer, as shown in Table 2.1. The buck converter model is generated in MATLAB / Simulink to control the output and input between the PV and electrolyzer, as shown in Figure 2.3. The PID controller is used to check the error value as the difference between the desired set point and the measured variable voltage. The controller parameters are P = 3.04, I = 2866.4, and D = 0.000795.

[1] https://daycounter.com/Calculators/Switching-Converter-Calculator.phtml

Table 2. 1: Values of buck converter

Item	Value	Units
Volts In	5	V
Volts Out	2	V
Load Current	1	A
I_{rms}	0.99	A
Duty Cycle	36.11	%
Frequency	40	KHz
L	87e-6	H
C	29.17e-6	F

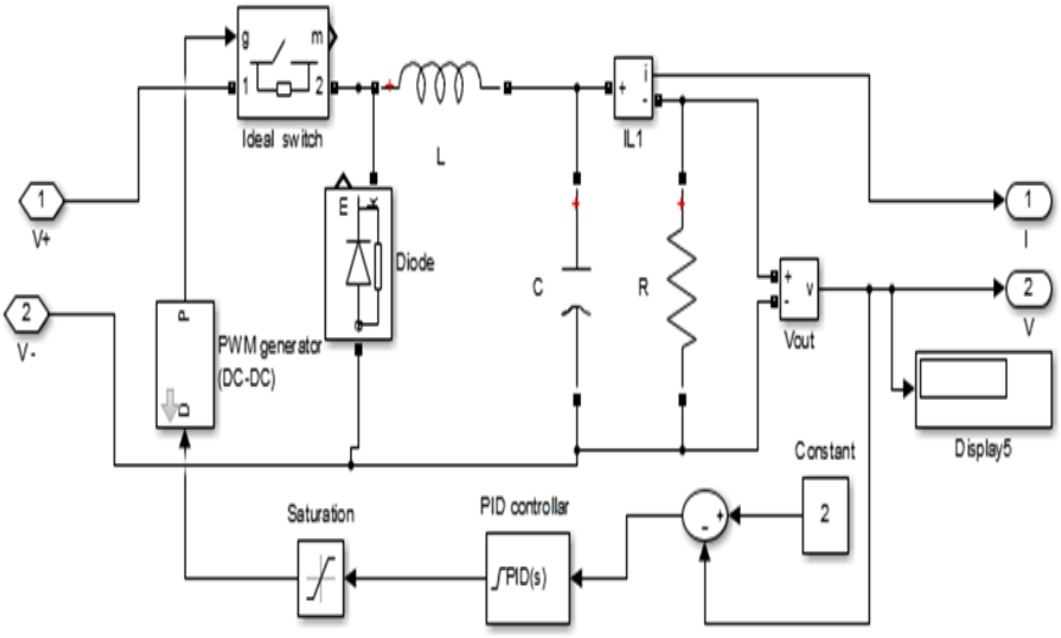

Figure 2. 3: Buck converter model in MATLAB/Simulink

2.3.3. PEM Electrolyzer Model

2.3.3.1. Mathematical model

A PEM electrolyzer is defined as a device which separates water (H_2O) into hydrogen (H_2) and oxygen (O_2). Water electrolysis may be classified as a reverse process of hydrogen that is fed into a fuel cell. An electro-chemical reaction happening in the fuel cell to generate DC electricity converts DC electrical energy into chemical energy, stored in hydrogen. An electrolyzer electrical circuit can be represented as a voltage sensitive nonlinear DC load, so that the higher voltage applied is the higher load current circulating, and more H_2 can be generated [3]. The equivalent circuit of a PEM electrolyzer is created in MATLAB / Simulink. Figure 2.4 shows the equivalent circuit of the single PEM electrolyzer [8] and [9].

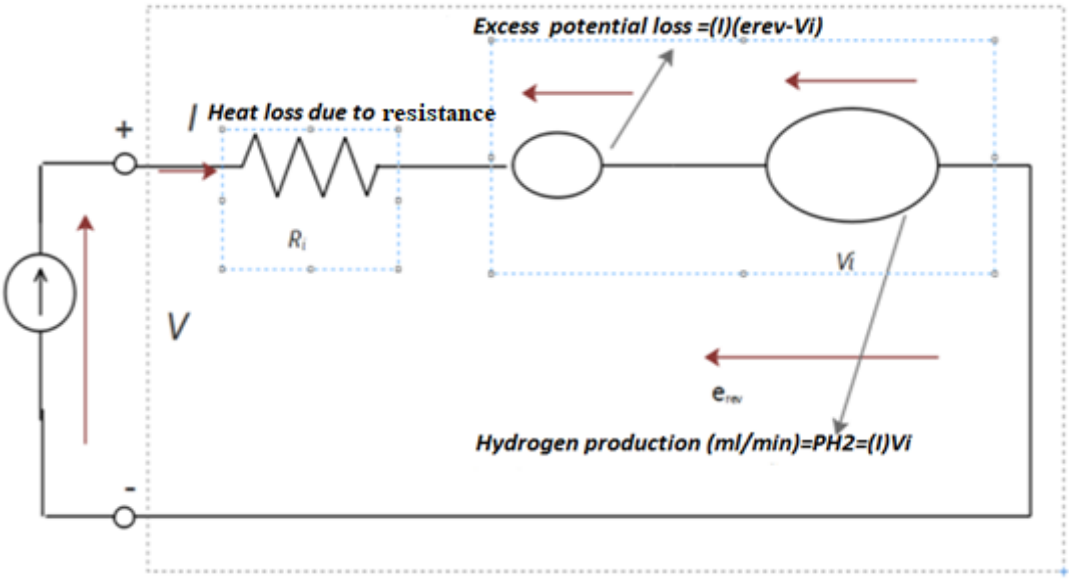

Figure 2. 4: Equivalent circuit for single PEM Electrolyzer [8]

In order to obtain the I-V and hydrogen production characteristics, some equations are developed for steady state conditions and implemented in MATLAB /Simulink. Equation 2.3 models the electrolysis process and is written as follows [8]:

$$V=\left(\frac{1}{3.064}\right)*I+1.476=0.326I+1.476 \cong IR_i+e_{rev} \quad (2.3)$$

Equation 2.3 indicates a simple equivalent circuit model for the PEM, which has an initial resistance of R_i, and reversible potential volte $e_{rev,}$ which amounts to 1.476V. The ideal potential V_i (electro chemical) is calculated by equation 2.4, [8]:

$$V_i = \frac{\Delta G}{2F} \quad (2.4)$$

where ΔG is Gibbs free energy change (J/ mol) of hydrogen gas and F is the Faraday constant (96487 C/ mol). The hydrogen production rate is V_H (ml/min) with respect to the input current I (A) and molar volume of hydrogen gas, V_m, is determined by equation 2.5. The electro chemical hydrogen energy per second P_{H2}, which is equal to the V_H, is calculated by equation 2.6 [9].

$$V_H=V_m(10^3)(60)\frac{I}{2F} \quad (2.5)$$

$$P_{H2}=V_m(10^3)(60)\frac{I}{2F}\frac{2FV_i}{V_m(10^3)(60)}=V_iI \quad (2.6)$$

From the preceding equations, the useful power which is delivered from the electrolyzer cell relies on the electrolyzer input current I and ideal voltage V_i. The input electrical power P of the PEM electrolyzer cell, which is the function of the Vh, can be determined by equation 2.7 [8]. Figure 2.5 illustrates the static model for the PEM electrolyzer.

$$P=VI=I^2R_i+Ie_{rev} \quad (2.7)$$

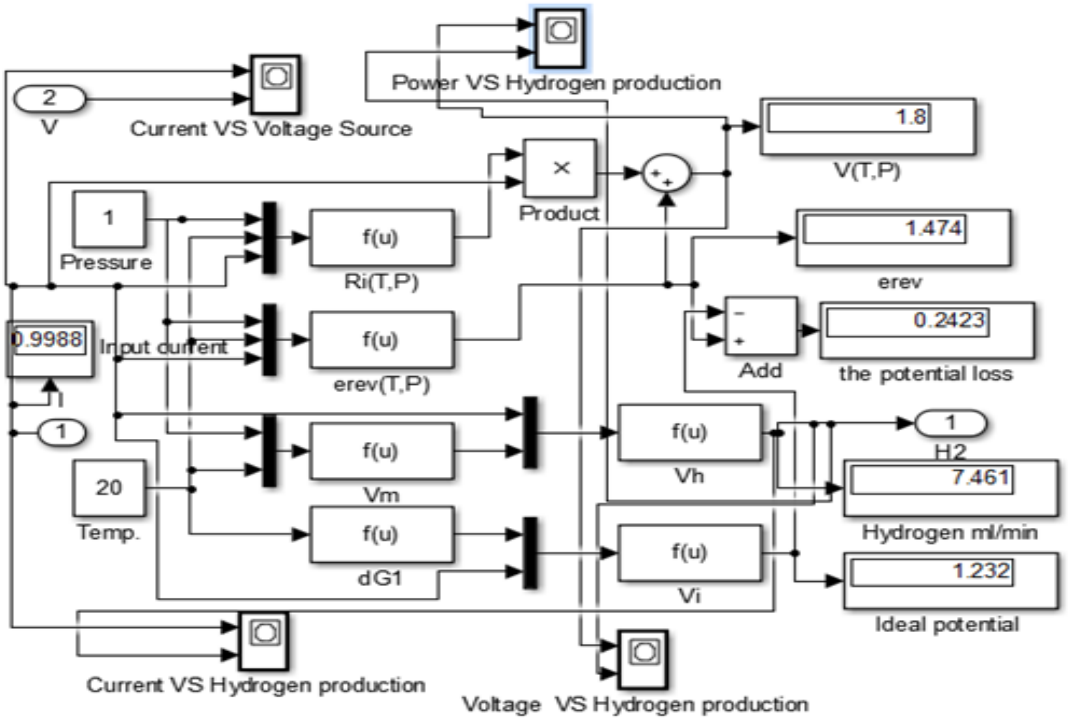

Figure 2. 5: MATLAB/Simulink Mathematical Model for PEM Electrolyzer

2.3.3.2. Dynamic model

A PEM elecrolyzer dynamic model was built in MATLAB / Simulink based on charge and mass balance and Butler-Volmer kinetics on the electrode surfaces to show the current and potential characteristics of electrolysis [10]. The hydrogen ($H_{2,g}$)and oxygen ($O_{2,g}$) reaction rates can be generated by equations 2.8 and 2.9, where the anode side of the

electrolyzer deals with oxygen production and the cathode side delivers the hydrogen gas with the water molar delayed, respectively [10].

$$H_{2,g} = \eta_F \frac{nI}{2F} \tag{2.8}$$

$$O_{2,g} = \eta_F \frac{nI}{4F} \tag{2.9}$$

The Faraday Efficiency (η_F) is defined as an internal current which allows the oxygen to move from the anode to the cathode or the hydrogen from the cathode to the anode, and it is assumed to be more than 90% [10]. Figure 2.6 shows the dynamic model for the PEM Electrolyzer in MATLAB / Simulink which consists of five main components: cathode, anode, membrane, storage, and voltage ancillary. For all these components, the mathematical details of the model are illustrated in the appendix number two (2).

For the water transport phenomena, the membrane ancillary is used in the electrolyzer. Diffusion and electro-osmotic drag are the two most important water flows taking place through the membrane, which allow the protons to move and the water molecules to accompany them. The water transportation is known as the electro-osmotic drag phenomenon and water diffusion can be found, from Fick's first law of diffusion, through the membrane, as illustrated in equations 2.10 and 2.11 [11].

$$F_{H_2O_{eod}} = n_d \frac{i}{F} M_{H_2O} Ane \tag{2.10}$$

$$F_{H_2O_d} = D_w \frac{(C_{wc} - C_{wa})}{t_m} M_{H_2O} Ane \tag{2.11}$$

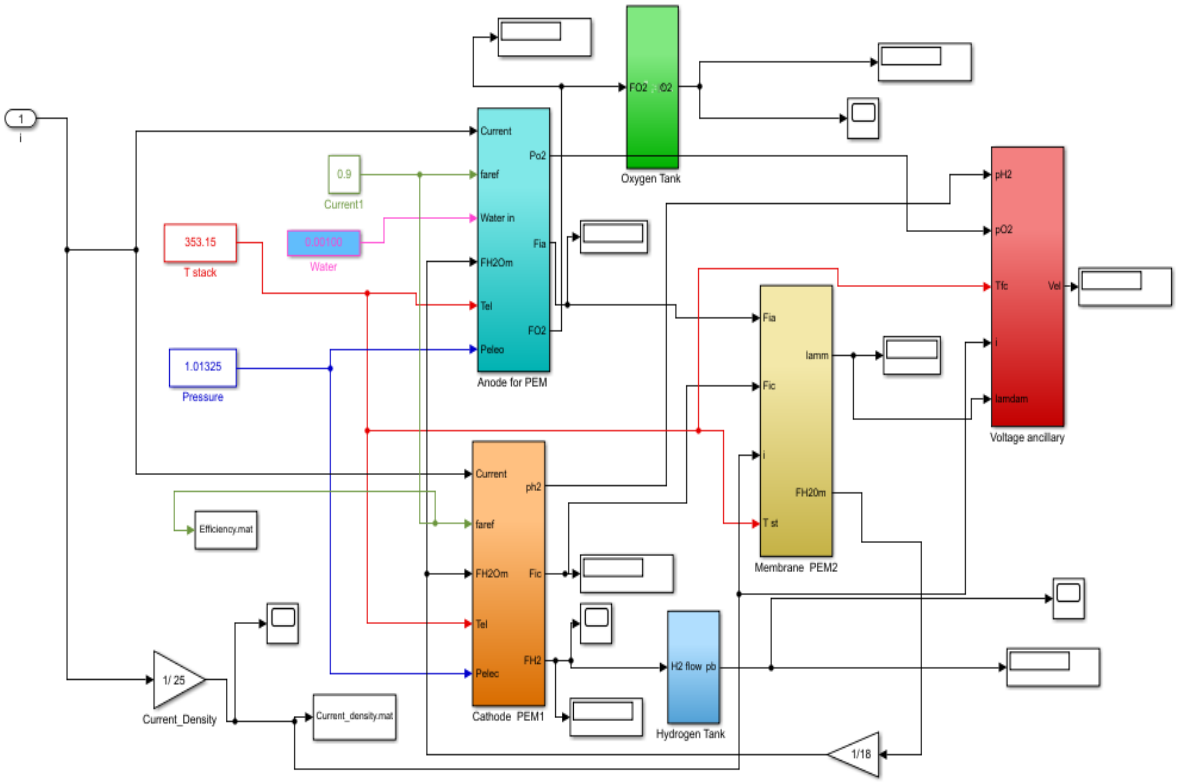

Figure 2. 6: MATLAB/Simulink Dynamic Model for PEM Electrolyzer [11]

2.3.4. Hydrogen Tank Modeling

Compressed gas or liquid hydrogen can be stored in tanks using different techniques, including physical hydrogen storage. To store hydrogen gas produced by the electrolyzer, a static model of the tank is created in MATLAB / Simulink and can be expressed by equation 2.12 [12].

$$P_b - P_{bi} = CF \times \frac{N_{H2} R T_b}{M_{H2} V_b} \tag{2.12}$$

where P_b is the pressure of the tank that is measured in Pascal, P_{bi} is the initial pressure of the storage tank in Pascal, R is the universal gas constant J/ kmol· K, T_b is the operating

temperature K, V_b is the volume of the tank m^3, T is the temperature, and CF is the compressibility factor as a function of the pressure, as shown in equation 2.13 [12].

$$CF = \frac{PV_m}{RT} \tag{2.13}$$

where P and V_m are the pressure and molar volume, respectively. This model equation determines the tank pressure using the ratio of hydrogen flow rate to the tank. Equation 2.12 is implemented in MATLAB / Simulink to store the hydrogen and deliver it to the fuel cell. Figure 2.7 shows the MATLAB / Simulink model of the hydrogen storage system.

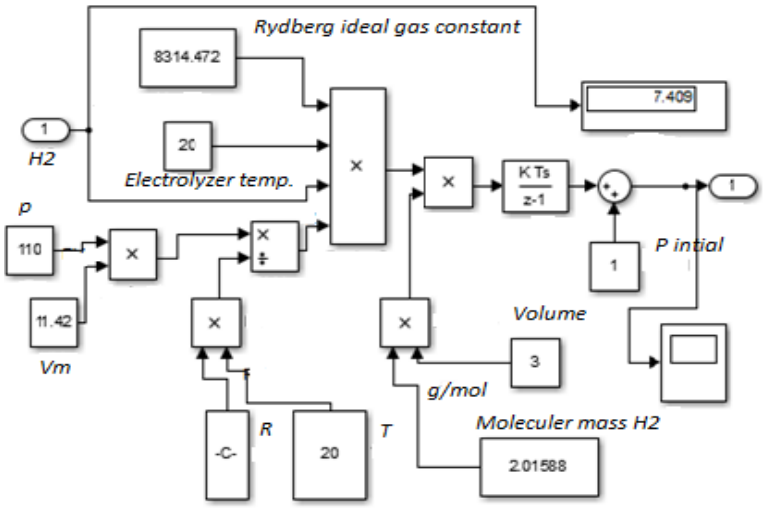

Figure 2. 7: MATLAB / Simulink model of the hydrogen storage system[12]

2.4. Simulation and Experimental Set-Up

The simulation is done in MATLAB / Simulink environment by creating each component separately, so that the error can be easily controlled, and the simulation blocks debugged. Each system block is implemented and studied to ensure that each one is sufficiently precise to run the simulation and give adequate results. The models of the PV solar, DC / DC Buck convertor, electrolyzer, and the hydrogen tank are created and well matched with each other. The simulation model is valid to simulate different cases. Figure 2.8 shows the Simulink model for the solar cells, DC / DC buck converter, electrolyzer, and hydrogen tank, and their mathematical model have shown in the previous sections. Figure 2.9 demonstrates the experimental set-up for the solar panel, DC / DC buck convertor, electrolyzer and hydrogen /oxygen tanks. The experiments are produced with a horizon kit. The reading of hydrogen production is reported in (ml/min). The PV has dimensions of 15.5 cm in length and 12.5 cm in width. Each component configuration is collected from the data sheets [2].

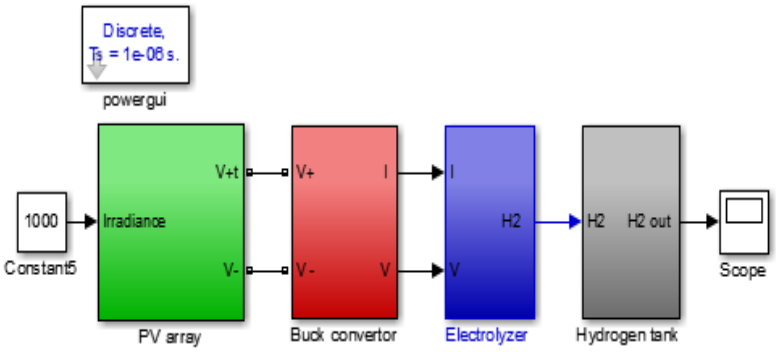

Figure 2. 8: Simulink model for the solar hydrogen production

[2]http://www.horizoneducational.com/wp

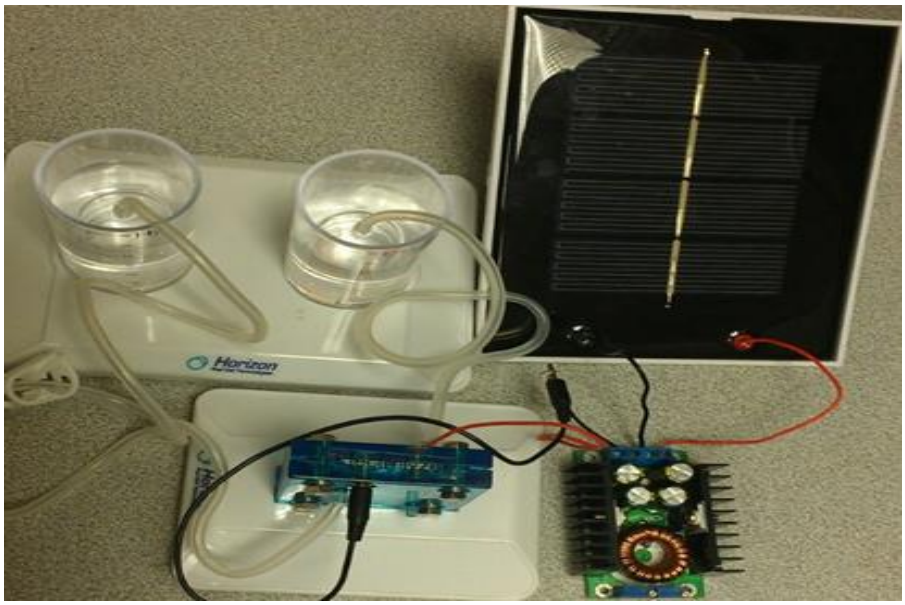

Figure 2. 9: Experimental set-up for the solar hydrogen production

2.5. Results and Discussion

The results from both simulation and experiments are now compared. The maximum voltage from the PV in the experimental set-up is designed to be 5V and the current reaches 1 A; however, the maximum power of the PV cell depends on the weather, and includes clouds and rain, which can reduce the collected energy. The maximum voltage and current from the PV panel are obtained and the electrolyzer can generate hydrogen with maximum output. Figure 2.10 shows the hydrogen production (ml/min) versus the current (A), and the simulation results are in accordance with the experimental results. Note that the characteristic response is linear [8]. The amount of hydrogen obtained from the simulation is 7.461 ml/min, and the value from the experiments amounts to 7.0 ml/min. The discrepancy is due to the solar variability. Note that the hydrogen production increases linearly with the input electrical power; as, the power increases, the hydrogen production also increases. Figure 2.11 shows the efficiency versus current density for the PEM

electrolyzer. The Faraday's efficiency decreases as the current density increases which can be defined as the relation between real hydrogen flow rate and its theoretical value.

Figure 2.12 illustrates the pressure inside the hydrogen tank model. The hydrogen quantity increases with time. The experimental storage hydrogen cylinders relate to the electrolyzer to generate the hydrogen by taking the water from the cylinders and reversing it back as hydrogen / oxygen gas. To compare the pressure from the simulation, figure 3.13 shows the hydrogen pressure tank from the experimental data as found in the literature. Table 2.2 shows the hydrogen production (ml/min) from the experiments, and the time, which was 2 min. Finally, hydrogen from the experimental results versus time is illustrated in figure 2.14; the hydrogen increases with time.

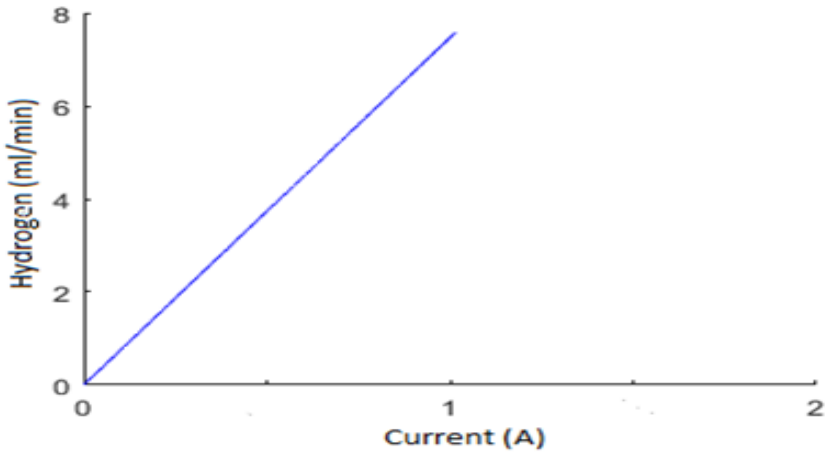

Figure 2. 10: Relationship between Current (A) verses hydrogen (ml/min) from the simulation

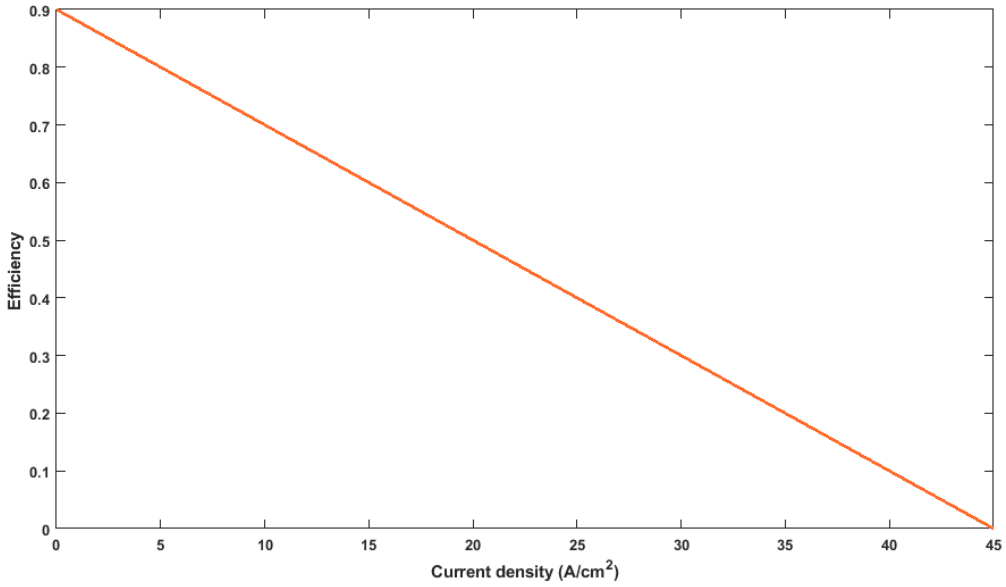

Figure 2. 11: Faraday's efficiency in % vs current density in A/cm^2 from the simulation

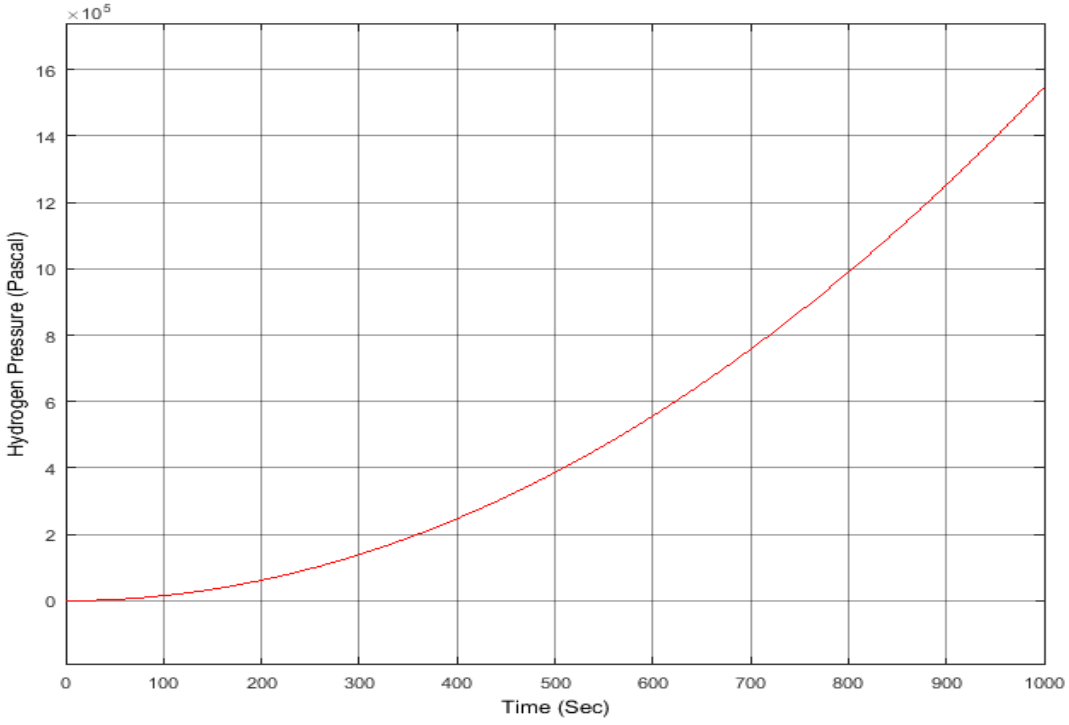

Figure 2. 12: Pressure inside the hydrogen tank for the solar system from the simulation

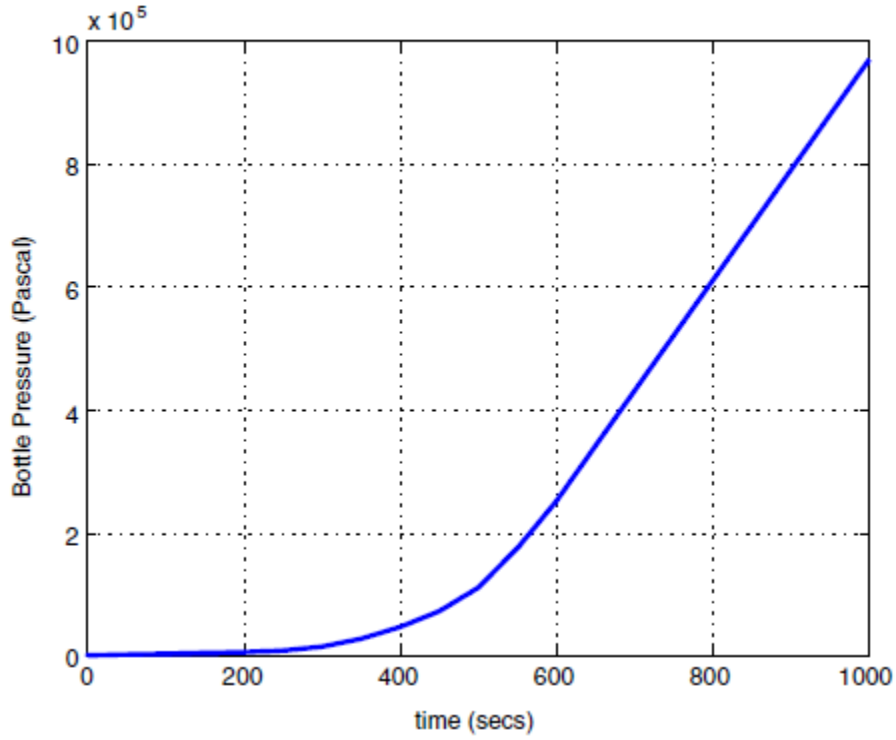

Figure 2. 13: hydrogen Pressure tank form the literature for the comparison [11]

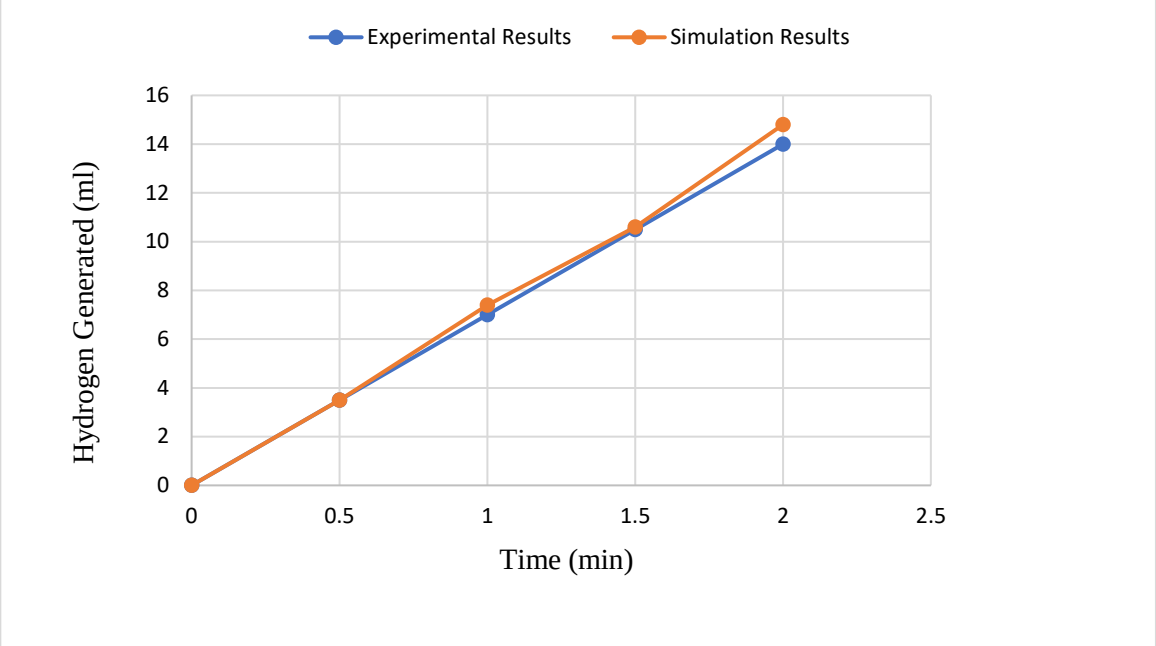

Figure 2. 14: Hydrogen production from experimental and simulation results versus time

Table 2. 2: Experimental results

Time (min)	**H2 production (ml)**
2	14
1	7
0	0

2.6. Conclusion

The solar energy hydrogen production and storage system were developed. The PV solar panels were arrayed to capture the sun as long as it was available. The electrolyzer consumed the power which generated from the PV panels. The DC/DC buck converter was used along with the system to regulate and maintain the current values, which were fed to the electrolyzer. The PID controller was used to check the error value, the difference between the desired set point and the measured variable voltage of the buck converter. It was assumed that all system components were in a steady state. The results from both the simulation and experimental trials corresponded (7.2 ml/min). MATLAB / Simulink provided the simulation environment, helping to integrate this system. The experiments confirm the results obtained from the model.

References - Chapter 2

[1] A. Kayello, P. Fazio, and J. Rao, “Ship Design Classification for Wind and Solar Energy Capture,” *Clim. Chang. Technol. Conf.*, no. 1569695823, pp. 1–12, 2013.

[2] C. E. Sandy Thomas, “Transportation options in a carbon-constrained world: Hybrids, plug-in hybrids, biofuels, fuel cell electric vehicles, and battery electric vehicles,” *Int. J. Hydrogen Energy*, vol. 34, no. 23, pp. 9279–9296, 2009.

[3] R. DUPUY, C. DUFOURMENTEL, and A. CORNET, “Sur un cas de cancer de l’estomac au début.,” 1951.

[4] T. Kerekes, E. Koutroulis, D. Séra, R. Teodorescu, and M. Katsanevakis, “An optimization method for designing large PV Plants,” *IEEE J. Photovoltaics*, vol. 3, no. 2, pp. 814–822, 2013.

[5] J. A. Gow and C. D. Manning, “Development of a photovoltaic array model for use in power-electronics simulation studies,” *IEE Proc. Electr. Power Appl.*, vol. 146, no. 2, pp. 193–200, 1999.

[6] C. Wang and M. H. Nehrir, “Power management of a stand-alone wind/photovoltaic/fuel cell energy system,” *IEEE Trans. Energy Convers.*, vol. 23, no. 3, pp. 957–967, 2008.

[7] K. F. Hussein, I. Abdel-Qader, and M. K. Hussain, “Hybrid fuzzy PID controller for buck-boost converter in solar energy-battery systems,” *IEEE Int. Conf. Electro Inf. Technol.*, vol. 2015-June, pp. 70–75, 2015.

[8] O. Atlam and M. Kolhe, “Equivalent electrical model for a proton exchange

membrane (PEM) electrolyser," *Energy Convers. Manag.*, vol. 52, no. 8–9, pp. 2952–2957, 2011.

[9] A. Beainy, N. Karami, and N. Moubayed, "Simulink model for a PEM electrolyzer based on an equivalent electrical circuit," *2014 Int. Conf. Renew. Energies Dev. Countries, REDEC 2014*, pp. 145–149, 2014.

[10] B. Lee, K. Park, and H. M. Kim, "Dynamic simulation of PEM water electrolysis and comparison with experiments," *Int. J. Electrochem. Sci.*, vol. 8, no. 1, pp. 235–248, 2013.

[11] H. Görgün, "Dynamic modelling of a proton exchange membrane (PEM) electrolyzer," *Int. J. Hydrogen Energy*, vol. 31, no. 1, pp. 29–38, 2006.

[12] M. a Al-refai, "Matlab / Simulink Simulation of Solar Energy Storage System," *Int. J. Electr. Comput. Energ. Electron. Commun. Eng.*, vol. 8, no. 2, pp. 304–309, 2014.

Chapter 3

Comparison of Experimental Results with Simulation of a PEM Electrolyzer Powered by a Horizontal Wind Turbine

3.1. Chapter Overview

One small wind turbine was used to power an electrolyzer unit to separate the water into hydrogen and oxygen gases. Two-volt voltage and 1 A current were supplied to the electrolyzer to produce hydrogen through the fuel cell unit. The electrical equivalent circuit for the proton exchange membrane electrolyzer was developed and implemented in MATLAB / Simulink along with the atmospheric hydrogen storage tank. The hydrogen production was measured during the tests and evaluated, running the simulation in order to compare the simulated and experimental results. The novel work of this chapter is to integrate the buck converter to the wind turbine system along with the storage system. The hydrogen amount was measured as 6.99 ml/min A from the experimental set-up, along with the model 7.24 ml/min A. The DC-DC buck converter was added to the Horizon kit to regulate the voltage to be 2 volts. The experimental and simulation results featured an error of 3.6 %.

3.2. Introduction

Over the past decade, transport emissions have increased at a faster rate than any other energy sector. The transportation division accounted for 34% of all carbon dioxide emissions, 28% of all US greenhouse gas emissions, 36%-78% of the main components of urban air pollution, and 68% of all oil consumption. Global transport activity will continue to increase along with economic growth [1]. Fossil fuel usage also involves many important concerns and challenges such as climate change and supply cost increases; for example, in 2002, the use of fossil fuels was responsible for 86% of the world's energy consumption [2]. It has become essential to seek alternative sources of renewable energy that can be easily captured by using wind, sun and waves. The need for renewable energy sources that will not damage the environment has increased significantly, as energy demands around the world increase. Many projections have suggested that the global energy demand will be doubled by 2050. Wind energy is a rapidly expanding field that includes many different sectors of engineering and science. The American Wind Energy Association (AWEA) showed that the installation capacity of wind expanded at an average rate of 29% per year. The worldwide installation capacity of the wind energy was approximately 159 MW at the end of 2009 [3]. The most worthen renewable generation technologies are wind and sun [4]. Statistics have suggested that changing to fuel cell technology could save more than one million U.S. dollars per ship per year in fuel costs, because wind, sun, and wave collectors provide unlimited sources of renewable energy [5].

Batteries are not the permanent solution for energy storage. They provide short term solutions, but also cause dangerous pollutants and significant waste concerns, which can

be amplified by the short life of many actual batteries' packs. Hydrogen seems to be the only valid clean source for energy storage. Hydrogen can be produced in large quantities from water electrolysis; water is a clean resource available in large quantities everywhere. Electrolysis will be studied for its suitability to be generated onshore and store it into the tanks. This section of the work proposes on potential improvements for the Ferry running between Bell Island and Portugal Cove in Newfoundland, Canada.

This chapter includes the modeling results of the electrolysis system, comparing them with experimental results. The set-up powers the electrolyzer with a small horizontal wind turbine, which is then regulated at 2 Volts and 1 Ampere. The hydrogen is produced and stocked in the tank. The mathematical model of the electrolysis has been implemented in MATLAB/Simulink. In section 3.3, the system component models are described in detail. In section 3.4, the simulation and experimental set-ups are described. In the fourth section, we examine and compare the simulation and experimental results.

3.3. Wind System Components

3.3.1. Horizontal wind turbine

The output power from the turbine can be determined by equation 3.1 [3].

$$p_m = \frac{1}{2}\rho A C_p * V_w^3 \tag{3.1}$$

where ρ is the air density, A is the swept area, V_w is the wind velocity, and

$$C_p = (0.44 - 0.0167\beta)\, sin\frac{\pi(\lambda-3)}{15-0.3\beta} - 0.00184(\lambda - 3)\beta \quad (3.2)$$

The wind turbine dynamic model is characterized by non-dimensional curves of the power coefficient (C_p) which is defined as the measure of wind turbine efficiency as, the ratio of actual electric power produced by a wind turbine, divided by the total wind power flowing into the turbine blades at a specific wind speed. It is also a function of both the tip speed ratio (λ) and the blade pitch angle (β). The value of (λ) must be kept at its optimum value in order to utilize the available wind energy. Therefore, the corresponding value of the power coefficient will become maximum too [3]. Figure 3.1 represents the mechanical power P_m as a function of the generator speed, for any different wind speeds and for the blade pitch angle of β = 0 degrees. This figure is also obtained with the specified parameters at a base wind speed = 9 m/s, maximum power at base wind speed = 0.9 pu (k_p = 0.9) and base rotational speed = 0.9 pu[3]. The wind turbine is specified in MATLAB/Simulink to generate 18W with voltage from 8-12 volts. The per-unit system (pu) is commonly used in the power system industry to show values of voltages, currents, powers, and torques of power equipment. For a given quantity like torque, the per-unit value is the value related to a base quantity [4].

[3] S. Heier, "Grid Integration of Wind Energy Conversion Systems," John Wiley & Sons Ltd, 1998, ISBN 0-471-97143-
[4] Mathworks.com, “Documentation/ per-unit-and-international-systems-of-units” 2016a.

Base value in (pu) = Quantity expressed in SI units/Base value (3.3)

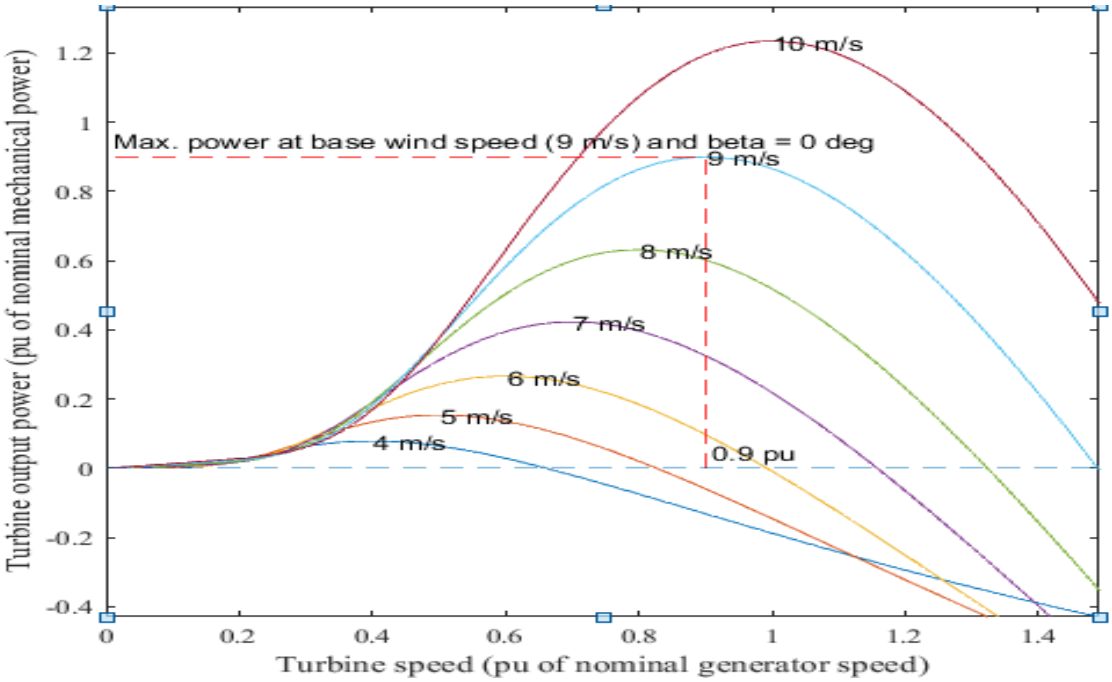

Figure 3. 1: Power wind characteristics and beta

3.3.2. DC/DC Buck Converter

The Buck Converter (BC) values for an inductor, capacitor, and duty cycle were taken from the website for desired input values for the electrolyzer. Table 3.1 shows the values of the selected buck converter which can be obtained by a special website[5]. The BC model was generated in MATLAB / Simulink to control the output and input between the wind turbine and electrolyzer, as shown in Figure 3.2. The calibration of the buck converter, which was powered by a DC power supply, was performed in the lab to ensure that the

[5] https://daycounter.com/Calculators/Switching-Converter-Calculator.phtml

output voltage and current were adjusted properly before the converter was connected to the wind turbine.

Table 3. 1: Buck converter parameters

Item	**Value**	**Unit**
Input Voltage	12	**V**
Output Voltage	2	**V**
Load Current	1	**A**
Irms	0.99	**A**
Duty Cycle	12.2	**%**
Frequency	40	**KHz**
L	2851.4e-6	**H**
C	76.65e-6	**F**

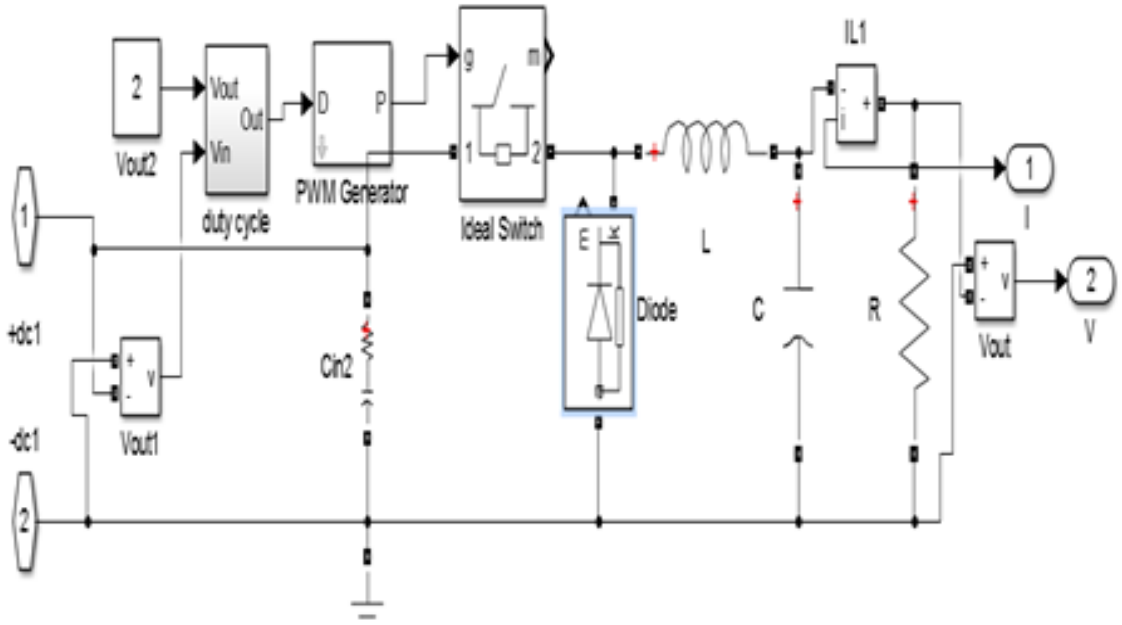

Figure 3. 2: Buck converter in MATLAB / Simulink

3.3.3. PEM Electrolyzer

3.3.3.1. Mathematical Equations and I-V curves

In order to illustrate the *I-V* curves and hydrogen production characteristics in wind hydrogen production, some equations have been developed for steady and unsteady state conditions and implemented in MATLAB/Simulink. Equations 3.4 and 3.5 represent the unsteady and steady state conditions for the electrolysis process, respectively, and they are written as follows [6]:

$$V = 1.4760 - 1.4760e^{\frac{5}{0.02}I} + 0.3264I \quad (3.4)$$

$$V(T,P) = IR_i + e_{rev}(T,P) \quad (3.5)$$

Equation 3.5 is used to simplify and determine the input of the I-V model of the PEM electrolyzer cell as a function of pressure and temperature. The two equations are implemented in MATLAB / Simulink to plot the voltage and current in linear and nonlinear behaviour. From equations 3.4 and 3.5, it can be observed that there is a threshold voltage at which the current starts to flow. The characteristic shapes are nonlinear, but the curve of the current flow can be approximated and plotted as almost linear, with an error not exceeding 5% [6]. Figures 3.3 and 3.4 are illustrated linear and non-linear *I-V* curves in MATLAB / Simulink environment, respectively.

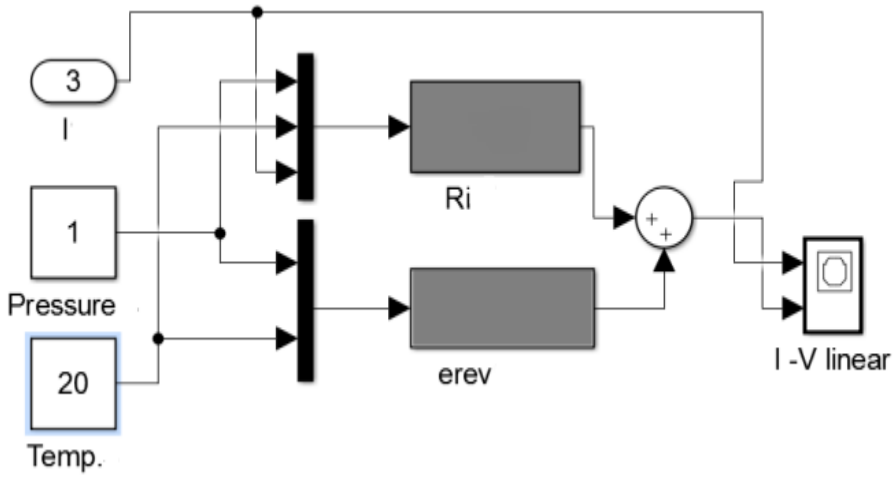

Figure 3. 3: I-V Linear mode in Simulink

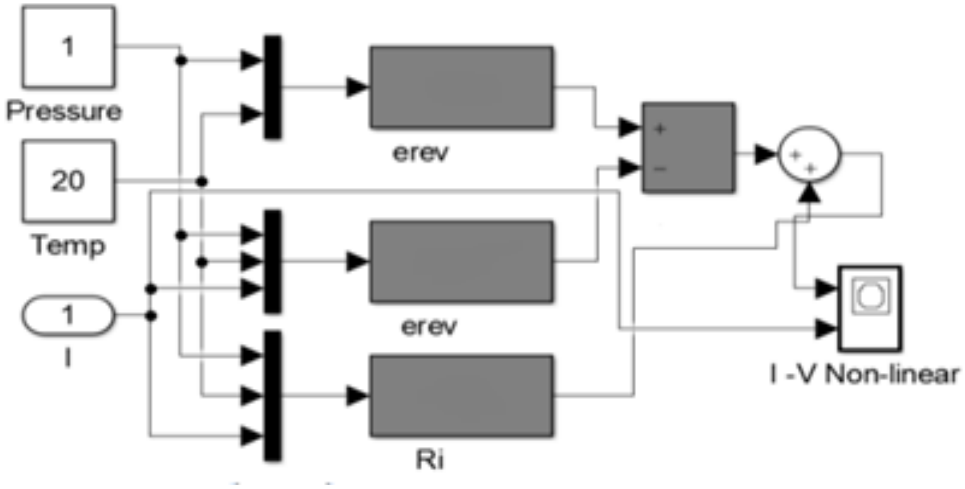

Figure 3. 4: I-V Nonlinear mode in Simulink

3.3.3.2. Hydrogen Production (Faraday Efficiency)

In an electrolyzer cell, the hydrogen production rate (ml/min) is directly proportional to the transfer rate of electrons at the electrodes according to Faraday's law, which is also equivalent to the electrical current in the circuit. Therefore, in any electrolyzer, the total hydrogen production which has many cells connected in a series can be determined, as shown in equation 3.6 [7].

$$P_{H2} = \eta_F \frac{n_c I}{2F} \tag{3.6}$$

where P_{H2} is the hydrogen production in ml/min, η_F is the Faraday's efficiency, n_c is the number of cells in series, and n is number of moles of electrons per moles of water, n=2. Faraday's efficiency is known as the ratio between the actual and theoretical maximum amount of hydrogen that is produced in the electrolyzer. Faraday's efficiency can be calculated by equation 3.7. Figure 3.5 illustrates the electrolyzer model in MATLAB / Simulink to find the hydrogen production rate. Equations 3.6 and 3.7 are illustrated in

MATLAB / Simulink as functions of current, to calculate the efficiency and then the hydrogen production [8].

$$\eta_F = 96.5\, exp(\, 0.09/i - 75.5/i^2) \tag{3.7}$$

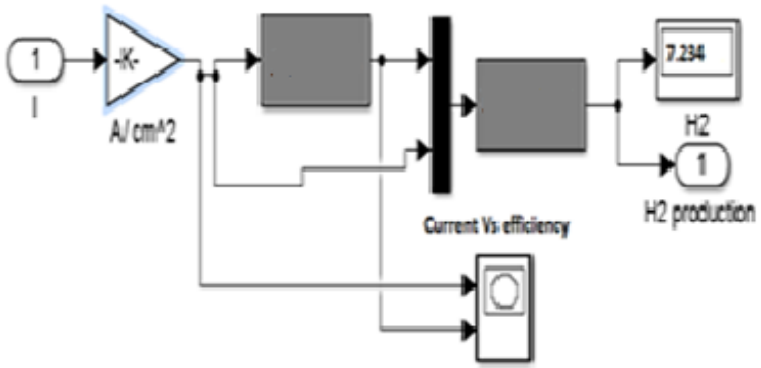

Figure 3. 5: MATLAB/Simulink module for PEM electrolyzer

3.3.3.3. Dynamic model

The dynamic model for the PEM electrolyzer is constructed in MATLAB / Simulink, as shown in Figure 3.6, and runs in two modes, current or voltage. The full mathematical model of each block is shown in the appendix number two. The voltage is supplied to the electrolyzer during the voltage mode, and it extracts the current from the source under operating conditions. A steady state value can be reached after many transient cycles. Moreover, commercial electrolyzers operate in current mode and the operating voltage electrolyzer can be calculated by equation 3.8 [9].

$$V_{el} = E + V_{act} + V_{ohm} \tag{3.8}$$

The Nernst equation is used to show an open circuit voltage for the electrolyzer, as shown in equation 3.9. The activation polarization can be found by equation 3.10 and the ohmic polarization is obtained by equation 3.11 [10].

$$E = E_0 + \frac{RT_{el}}{2F}\left[ln\left(\frac{P_{H2}P_{O2}^{1/2}}{a_{H2O}}\right)\right] \tag{3.9}$$

$$V_{act} = \frac{RT_{el}}{2\propto F} ln\left(\frac{i}{i_0}\right) \tag{3.10}$$

$$V_{ohm} = iR_{ohm} \tag{3.11}$$

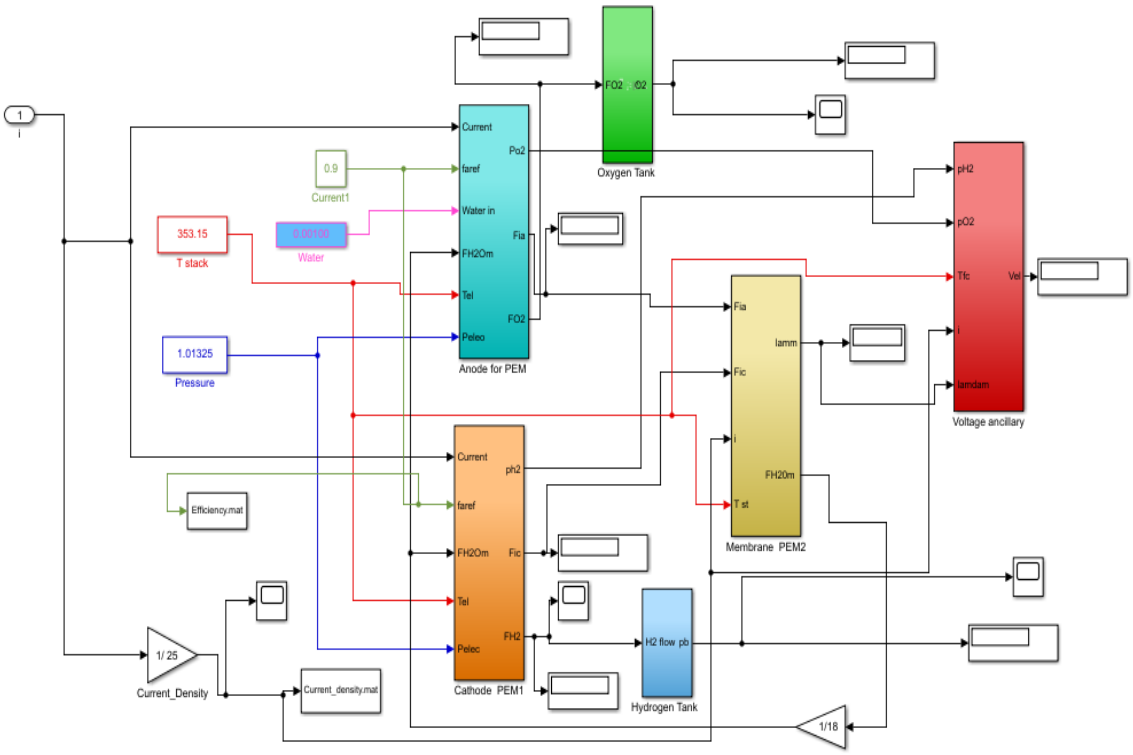

Figure 3. 6: MATLAB/Simulink dynamic Model for PEM Electrolyzer [10]

3.3.4. Hydrogen Model Tank

Liquid or compressed hydrogen can be stored in tanks using different techniques, such as the physical hydrogen storage of ideal gas [7]. To store the hydrogen gas, a dynamic model for the tank is created in MATLAB / Simulink, which is connected to the electrolyzer, as addressed by equation 3.12 [11].

$$P_b - P_{bi} = z \times \frac{N_{H2} R T_b}{M_{H2} V_b} \tag{3.12}$$

where P_b, P_{bi}, R, T_b, V_b, and T are the pressure of the tank in Pascals, the storage tank initial pressure in Pascals, the universal gas constant (J/kmol K), the operating temperature (K), the tank volume in (m^3), and the temperature (T), respectively[11].

3.4. Simulation and Experimental Set-Up

Figure 3.7 shows the experimental set-up for the horizontal wind turbine, DC/DC buck converter, electrolyzer and hydrogen / oxygen tanks. The equipment for this experiment is provided by the Horizon kit[6]. The simulation is completed in MATLAB / Simulink environment by modeling each component individually. Each system block has been applied and studied to ensure that each one is sufficiently precise to run the simulation and give adequate results. The best error is less than 5%, which can be represented in terms of calibration, and losses. The models for wind turbine, DC/DC buck converter, electrolyzer, and the hydrogen tank are created and well matched with each other to run the simulation and validate the model with different cases. Figure 3.8 illustrates the Simulink model for the whole energy system. The hydrogen production is measured and reported in (ml/min). This is achieved experimentally by generating the power from the wind turbine and feeding it to the electrolyzer; and then storeing the energy as hydrogen gas to be used whenever needed. Every component configuration is collected from the data sheets. The

[6] http://www.horizoneducational.com/wp

small wind turbine has three blades, a wind speed of around 12 (mph), output voltage of 8.5 (V), and a rotor speed of 1550 (RPM).

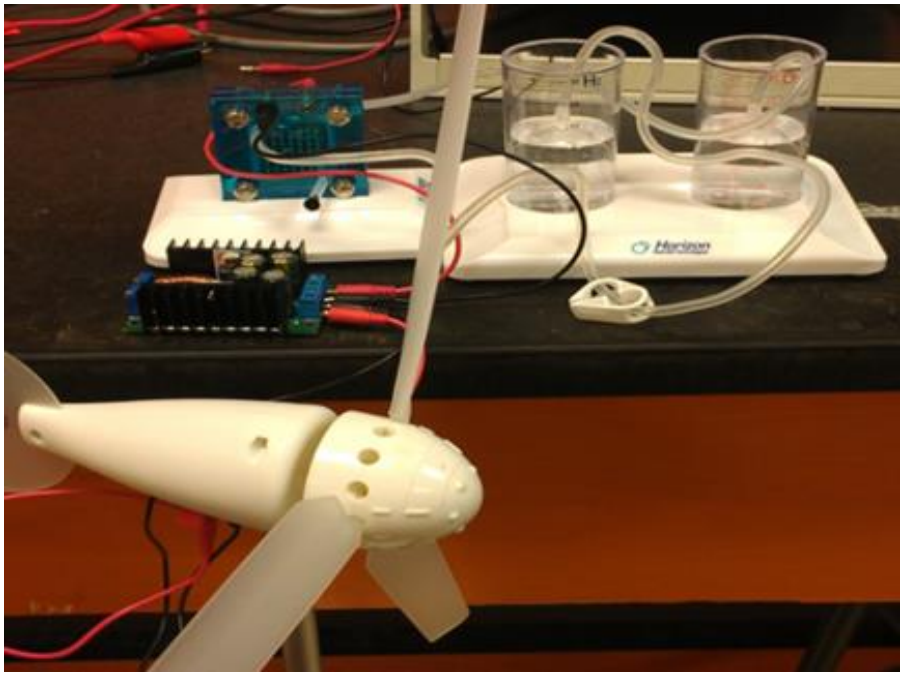

Figure 3. 7: Experimental set-up for the wind hydrogen production

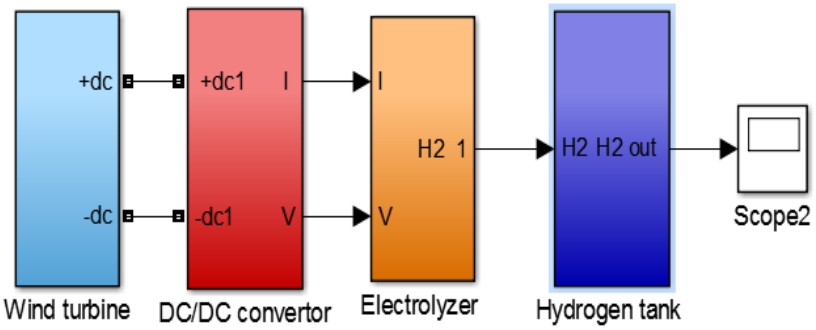

Figure 3. 8: Simulink model for the wind hydrogen production

3.5. Results and Discussion

The results from both experiments and simulation are examined and compared. The maximum voltage from the wind turbine is regulated to be 2V and the current is held at 1A in both experiments and simulation. However, the maximum power of the wind turbine is dependent on many factors such as wind speed and pitch angle. These factors can reduce the collected energy from the wind turbine if the converter is not included in the energy collection unit, but the converter ensures that no effects occur if the wind is sufficiently rapid to reach the selected thresholds. The maximum voltage and current from the wind turbine are obtained and supplied to the electrolyzer to generate hydrogen with maximum output. Figure 3.9 demonstrates the hydrogen production ml/min on the Y-axis and the current A on the X-axis, and the simulation and experimental results are in accordance with each other.

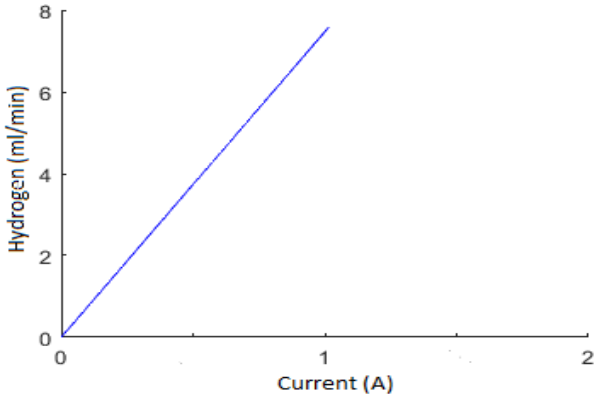

Figure 3. 9: Linear relationship between current and hydrogen production from the simulation

The results of I-V curves are represented in both linear and non-linear behaviour, and they share close results, as shown in Figures 3.10 and 3.11, respectively. The error ratio is acceptable, 3.4 % in the design application. The linear vs non-linear results are also confirmed by Atlam and Kolhe to yield an of error 2% [6]. The production of hydrogen obtained from the simulation is 7.23 ml/min, and the value from the experiments amounts to 6.99 ml/min. The discrepancy of the hydrogen production is due to the wind variability.

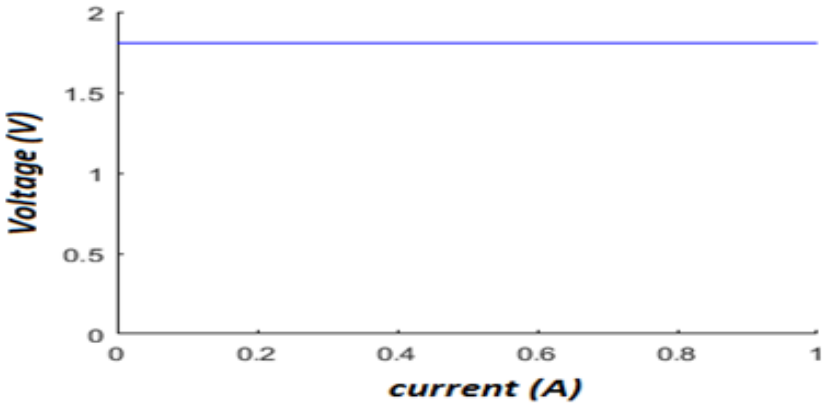

Figure 3. 10: Relationship between current vs voltage linear behaviour for the electrolyzer (simulation)

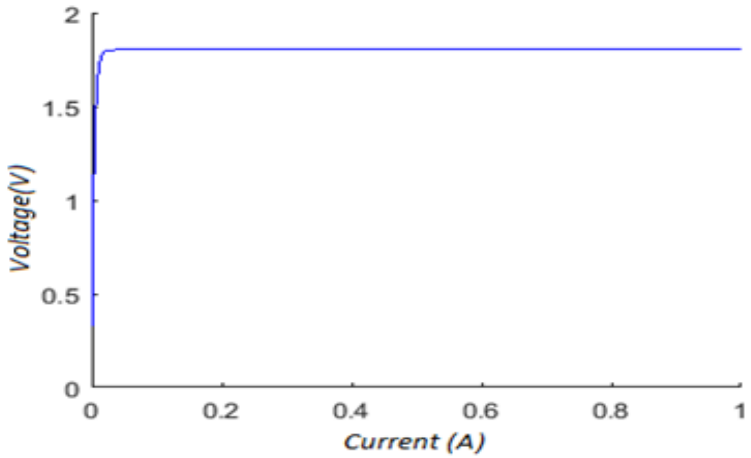

Figure 3. 11: Relationship between current vs voltage non-linear behaviour for the electrolyzer (simulation)

Figure 3.12 shows the input power w with the hydrogen production in ml /min. Note that the hydrogen production rises linearly with the input power; therefore, as the power increases, the hydrogen production will also increase. Table 3.2 illustrates the hydrogen production from the experiments. The time was 2 min. Figure 3.13 shows the current density A/cm^2 with the Faraday efficiency percent. Figure 3.14 shows the pressure inside the hydrogen tank model. The hydrogen's quantity increases with time.

Table 3. 2: Experimental results for two minutes

Time (min)	**H2 production (ml)**
2	14
1	7
0	0

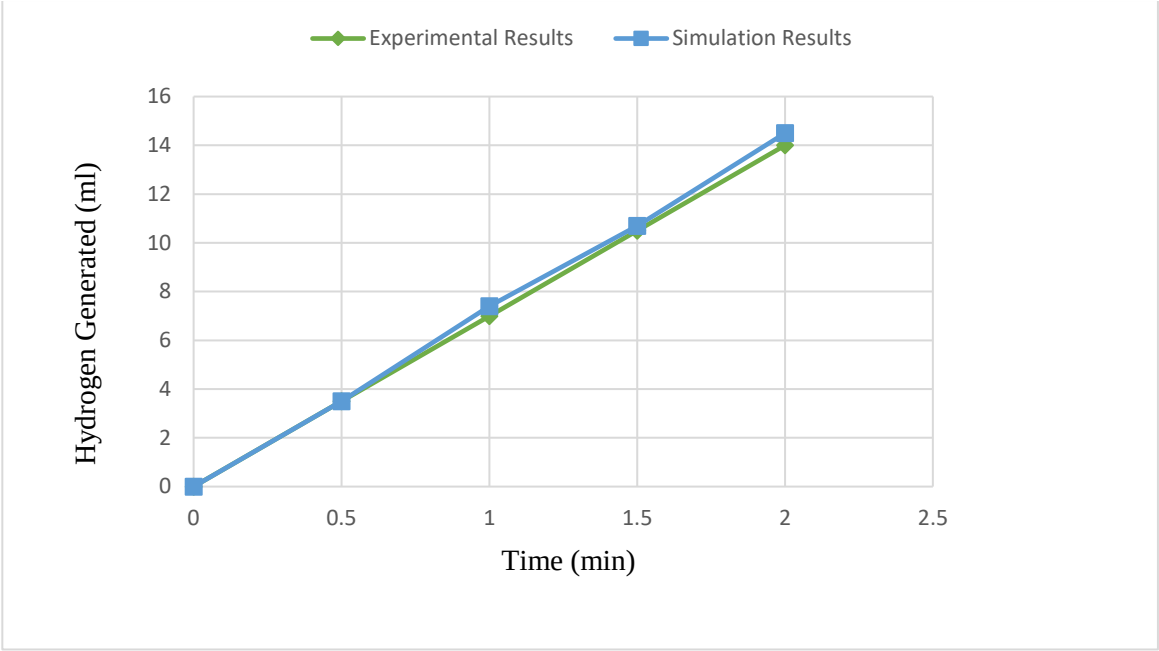

Figure 3. 12: Experimental and simulation results for the hydrogen production

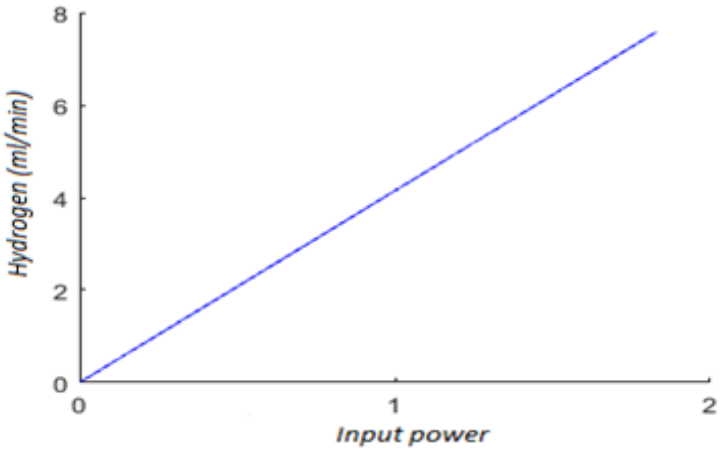

Figure 3. 13: Electrical power (w) vs Hydrogen production from the simulation

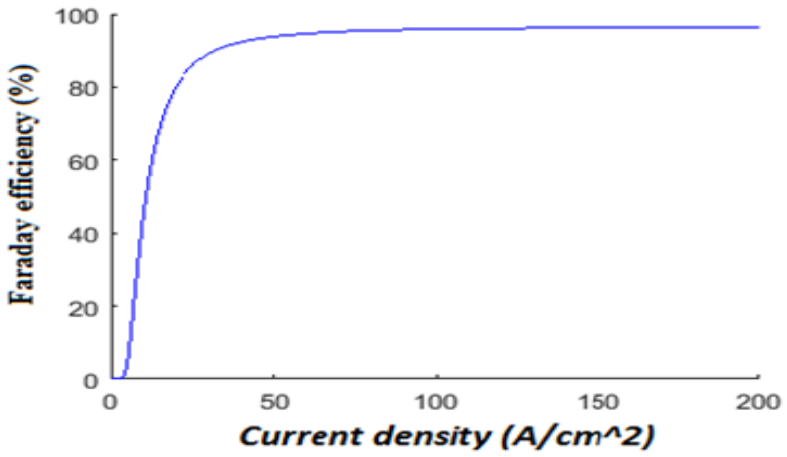

Figure 3. 14: Current density vs Faraday efficiency form the simulation results

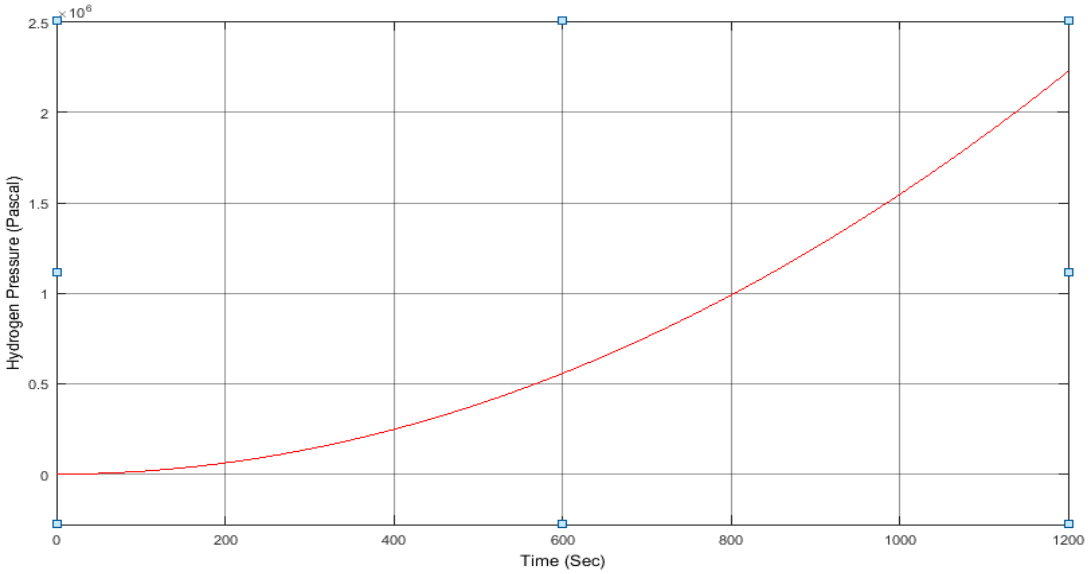

Figure 3. 15: Pressure inside the hydrogen tank for wind system from the simulation

3.6. Conclusion

The renewable energy system for hydrogen production and storage was created and simulated using MATLAB / Simulink. The horizontal wind turbine was used to generate the power from the wind as long as it was available at an acceptable wind speed. The electrolyzer consumed the electrical power, which was generated from the wind turbine. The DC / DC buck converter was also used along with the system, to maintain and regulate the voltage and current values which were fed to the electrolyzer. The *I-V* curves for linear and nonlinear behaviour were matched with an acceptable error of 3.4%. The results from both the experimental trials and simulation corresponded, 7.2 ml/min. MATLAB / Simulink provided the simulation environment, helping to integrate and implement this system. The experiments validate and confirm the results obtained from the model.

References - Chapter 3

[1] C. E. Sandy Thomas, "Transportation options in a carbon-constrained world: Hybrids, plug-in hybrids, biofuels, fuel cell electric vehicles, and battery electric vehicles," *Int. J. Hydrogen Energy*, vol. 34, no. 23, pp. 9279–9296, 2009.

[2] R. DUPUY, C. DUFOURMENTEL, and A. CORNET, "Sur un cas de cancer de l'estomac au début.," *Archives des maladies de l'appareil digestif et des maladies de la*, vol. 40, no. 11. pp. 1210–1214, 1951.

[3] F. A. R. Abbas and M. A. Abdulsada, "Simulation of Wind-Turbine Speed Control by MATLAB," *Int. J. Comput. Electr. Eng.*, vol. 2, no. 5, pp. 912–915, 2010.

[4] C. Wang and M. H. Nehrir, "Power management of a stand-alone wind/photovoltaic/fuel cell energy system," *IEEE Trans. Energy Convers.*, vol. 23, no. 3, pp. 957–967, 2008.

[5] A. Kayello, P. Fazio, and J. Rao, "Ship Design Classification for Wind and Solar Energy Capture," *Clim. Chang. Technol. Conf.*, no. 1569695823, pp. 1–12, 2013.

[6] O. Atlam and M. Kolhe, "Equivalent electrical model for a proton exchange membrane (PEM) electrolyser," *Energy Convers. Manag.*, vol. 52, no. 8–9, pp. 2952–2957, 2011.

[7] Ø. Ulleberg, "Stand-alone power systems for the future: optimal design, operation & control of solar-hydrogen energy systems," 1998.

[8] A. Beainy, N. Karami, and N. Moubayed, "Simulink model for a PEM electrolyzer based on an equivalent electrical circuit," *2014 Int. Conf. Renew. Energies Dev.*

Countries, REDEC 2014, pp. 145–149, 2014.

[9] B. Lee, K. Park, and H. M. Kim, "Dynamic simulation of PEM water electrolysis and comparison with experiments," *Int. J. Electrochem. Sci.*, vol. 8, no. 1, pp. 235–248, 2013.

[10] H. Görgün, "Dynamic modelling of a proton exchange membrane (PEM) electrolyzer," *Int. J. Hydrogen Energy*, vol. 31, no. 1, pp. 29–38, 2006.

[11] M. a Al-refai, "Matlab / Simulink Simulation of Solar Energy Storage System," *Int. J. Electr. Comput. Energ. Electron. Commun. Eng.*, vol. 8, no. 2, pp. 304–309, 2014.

Chapter 4

Sizing and Dynamic modeling of a Power System for the MUN Explorer Autonomous Underwater Vehicle using a Fuel Cell and Batteries

4.1. Chapter Overview

The combination of a fuel cell and batteries has promising potential for powering autonomous vehicles. The MUN Explorer Autonomous Underwater Vehicle (AUV) is built to do mapping- type missions for seabeds as well as survey missions. These missions require a great deal of power to reach underwater depths (i.e. 3000 meters). The MUN Explorer uses 11 rechargeable Lithium-ion (Li-ion) batteries as the main power source with a total capacity of 14.6 kWh to 17.952 kWh, and the vehicle can run for 10 hours. The drawbacks of operating the existing power system of the MUN Explorer, which was done by the researcher at the Holyrood management facility, include mobilization costs, logistics and transport, and facility access, all of which should be taken into consideration. Recharging the batteries for at least 8 hours is also very challenging and time consuming. To overcome these challenges and run the MUN Explorer for a long time, it is essential to integrate a fuel cell into an existing power system (i.e. battery bank). The integration of the fuel cell not only will increase the system's power, but will also reduce the number of

batteries needed, as suggested by HOMER software. In this chapter, an integrated fuel cell is designed to be added into the MUN Explorer AUV along with a battery bank system to increase its power system. The system sizing is performed using HOMER software. The results from HOMER software show that a 1-kW fuel cell and 8 Li-ion batteries can increase the power system capacity to 36.8 kWh. The dynamic model is then built in MATLAB / Simulink environment to provide a better understanding of the system behaviour. The 1-kW fuel cell is connected to a DC / DC Boost Converter to increase the output voltage from 24 V to 48 V, as required by the battery and DC motor. A hydrogen gas tank is also included in the model. The advantage of installing the hydrogen and oxygen tanks beside the batteries is that it helps the buoyancy force in underwater depths. The design of this system is based on MUN Explorer data sheets and system dynamic simulation results.

4.2. Introduction

The MUN Explorer AUV is an autonomous underwater vehicle used for missions such as mapping, surveillance, oceanographic data gathering, environmental monitoring, mine detecting and coastal defence [1]. One of the challenges facing the MUN Explorer is the power system's capacity to complete its missions. To improve the system's energy capacity, the MUN Explorer AUV is taken as a real example to do sizing and build a dynamic model. The MUN AUV has a length of 5.3 m, a diameter of 0.69 m and a dry weight of 820 kg. In water, the flooded front and back sections of the AUV make the mass around 1400 Kg, with an average speed of 1.5 m/s, graphing over 80 Km. Some components have also been integrated into the vehicle, such as computers and sensors.

Hydrogen production by Proton Exchange Membrane (PEM) water electrolysis is a promising method that has been successfully developed and integrated into renewable and hydrogen energy-based systems. Renewable energy sources, such as solar and wind, are desirable for hydrogen production, due to random power variations and significant current density capabilities [2]. PEM water electrolysis technology that generates hydrogen primarily emits water moisture, nitrogen and oxygen [3]. Energy storage or backup power systems are needed for photovoltaic and wind energy systems, due to their discontinuous energy production. Batteries can be a good solution for daily storage but not for seasonal storage, due to self-discharge. Storing energy in the form of hydrogen gas that is generated from renewable sources is a possible solution for both daily and seasonal storage [4]. For example, Sopian et al. (2009) integrated a Photovoltaic- wind- hydrogen energy production / storage system. The components of the system were a photovoltaic array, wind turbine, PEM electrolyzer, battery bank, and hydrogen tank. The system also had an automatic control system for battery charging and discharging. A hydrogen quantity of 130 ml/min to 140 ml/min was generated for an average global solar radiation between 200 W/m^2 and 800 W/m^2 and wind velocities ranging from 2.0 m/s to 5.0 m/s. For each system component, a mathematical model was built and compared to the experimental results [5].

Lithium–ion (Li-ion) battery technology has improved in the past decade. Li-ion batteries have higher energy and power density, higher efficiency and lower self-discharge compared to other batteries (NiCd, NiMH, and Lead Acid). To ensure the Li-ion battery is operating at a proper temperature and state of charge (SOC), a battery management supervision system (BMSS) must be applied [6]. Fuel cells' high energy density, quiet operation, and high efficiency have allowed them to be used as a portable energy source.

The capacity of fuel cells increased worldwide from 65 MW in 2009 to 181 MW in 2014 [7] and [8]. Many types of fuel cells, such as the proton exchange membrane fuel cell, alkaline fuel cell, and phosphoric acid fuel cell use hydrogen as fuel to produce electricity and water. Hydrogen-specific energy is high compared to other fuels' specific energy. Fuel cells have many applications, such as stationary, transportation, and portable applications. Proton exchange membrane fuel cells have a higher efficiency compared to phosphoric acid fuel cells and alkaline fuel cells [9].

Using compressed hydrogen in composite cylinders for fuel cells is an alternative for underwater vehicles. Composite cylinders have a low weight and can increase the total performance of a deep-diving AUV. Furthermore, hydrogen cylinders may help buoyancy compensation in underwater depths. The design for underwater depths makes the weight of the pressure hull increase, and as a result, the amount of energy carried in a vehicle with neutral buoyancy is minimized with the design's depth. Considering this, the batteries inside the vehicle should be as light as possible [10]. AUV energy supply powered by a fuel cell has been integrated on an IFREMER survey AUV called IDEFX by HELION, an AREVA Renewable subsidiary. Several experiments have demonstrated the interest in underwater power sources by installing a fuel cell along with a hydrogen gas tank. Figure 4.1 shows the pressure parameters as well as a schematic drawing of the hydrogen, oxygen gases, and produced water tank of real experimental set-up [11].

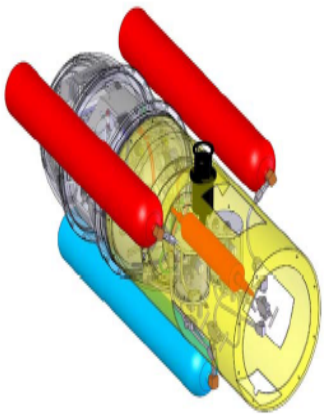

Power	0 to 2kW 1.5 kW at 48Vdc
Gas storage capacity	H2 : 100litres at 300 bars O2 : 50 litres at 250 bars
Autonomy	36 kWh
Mass	800 kg
Lenght	1.5 m
maximal depth	800m (limitation due to gas cylinders)

Figure 4. 1: Parameters of real experimental set-up using a fuel cell with storage system [11]

This chapter aims to design, size, and integrate a fuel cell into an existing power system that uses a battery bank as the main energy source to power the MUN Explorer AUV. By adding a fuel cell into the MUN Explorer, the power system capacity will be increased. The weight and the number of batteries can be reduced accordingly, and the number of hours of operation will increase. In this chapter, the focus will be on the main four components: the oxygen and hydrogen tanks, PEM fuel cell, Li-ion battery, and DC motor (load). This chapter is divided into three sections: the first section illustrates the components and system sizing using Hybrid Optimization Model for Electrical Renewable (HOMER) software; the second section demonstrates the dynamic modeling, simulation and results; and the third section is the conclusion.

4.3. Components and System Sizing

4.3.1. Hydrogen / Oxygen Tanks and PEM Fuel Cell

The MUN Explorer Autonomous Underwater Vehicle, as shown in Figure 4.2, has plenty of vacant space that could be used to install the hydrogen and oxygen tanks as well as the fuel cell.

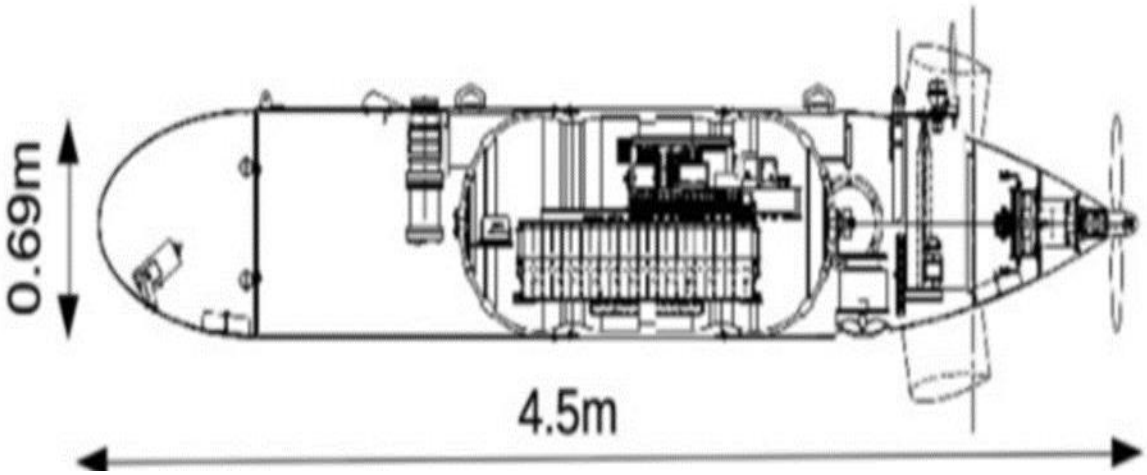

Figure 4. 2: Hull structure of the MUN Explorer AUV

The hydrogen consumed by the Proton Exchange Membrane Fuel Cell (PEMFC) can be generated directly from the electrolyzer. The hydrogen gas also depends on the relationship between the output power and the hydrogen needed for the PEMFC system. Excess hydrogen is directed to the storage tank. Due to the lack of an oxygen gas underwater surface, the fuel cell operation in underwater vehicles requires oxygen gas storage to complete the reaction between the cathode and the anode. By carrying the oxygen instead of atmospheric air into the AUV, the fuel cell performance is increased by 2 to 3 times. To remove the produced water from the fuel cell during the operation, extra oxygen

must be brought into the vehicle. This should be measured when the sizing of the oxygen storage is completed [12]. There are many ways to store hydrogen and oxygen. For example, compressed gas or liquid hydrogen and oxygen can be applied. HOMER software is designed to deal with renewable / non-renewable energy components and to integrate them. HOMER works by providing inputs (i.e. capital cost and size to consider kW) and design information about any given power system. HOMER simulation will give the system configurations and then create a list of feasible system designs and sort that list according to cost-effectiveness. The electrolyzer efficiency which converts electricity into hydrogen, is equal to the energy of the hydrogen produced that based on higher heating value divided by electricity consumed. “For Example: The higher heating value of hydrogen is 142 MJ/kg, which is equal to 39.4 kWh/kg. So, an electrolyzer that consumes 50 kWh of electricity to produce one kilogram of hydrogen has an efficiency of 39.4 kWh/kg divided by 50 kWh/kg, which is 79%” [HOMER Help Sources]. Finally, a sensitivity analysis can be performed. A real example for the calculation of the sensitivity is attached in the appendix number four. The complete HOMER block diagram is illustrated in Figure 4.3.

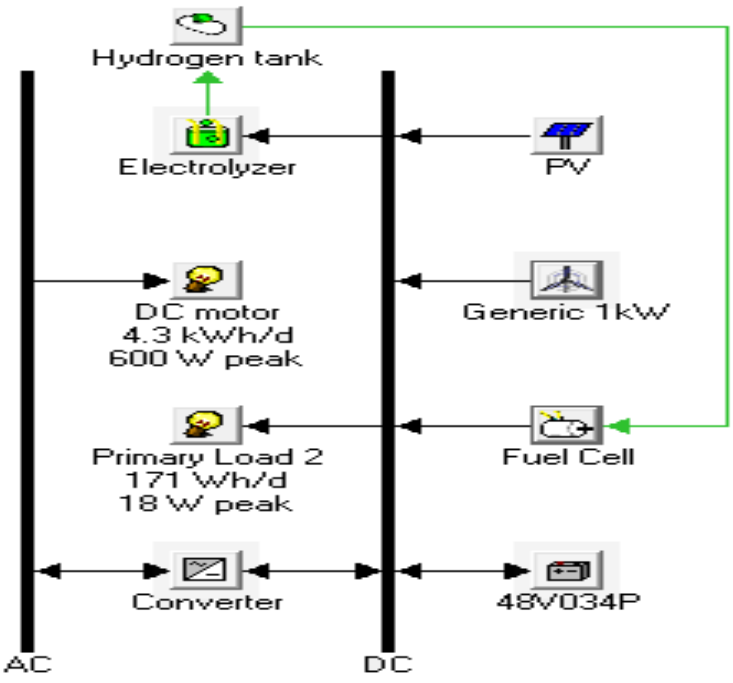

Figure 4. 3: HOMER block diagram

This diagram consists of renewable energy sources such as solar and wind to generate electricity to power the electrolyzer and then charge the battery. Subsequently, the electrolyzer will generate the hydrogen and oxygen gases. Finally, the fuel cell and the battery will power the DC motor. It is understood that the wind energy, solar energy and electrolyzer will be onshore, and hydrogen and oxygen will be transferred to the AUV when it is docked. To run the HOMER software, the capital cost (i.e. commercial prices) of three different hydrogen tanks along with the sizes to consider (kg or kW) need to be entered into the hydrogen tank inputs. However, the reason for selecting three or more different hydrogen tanks is to give HOMER software more options to choose from so it can select the most optimal results. The same procedure is done for the fuel cell inputs, electrolyzer inputs, battery inputs, convertor inputs, PV inputs, and wind turbine inputs. The data sheet of each input and its price can be found in the attached appendix four. Figure 4.4 shows the

simulation result of HOMER software in terms of the hydrogen tank storage level (in kg) and monthly statistics as well as a frequency histogram.

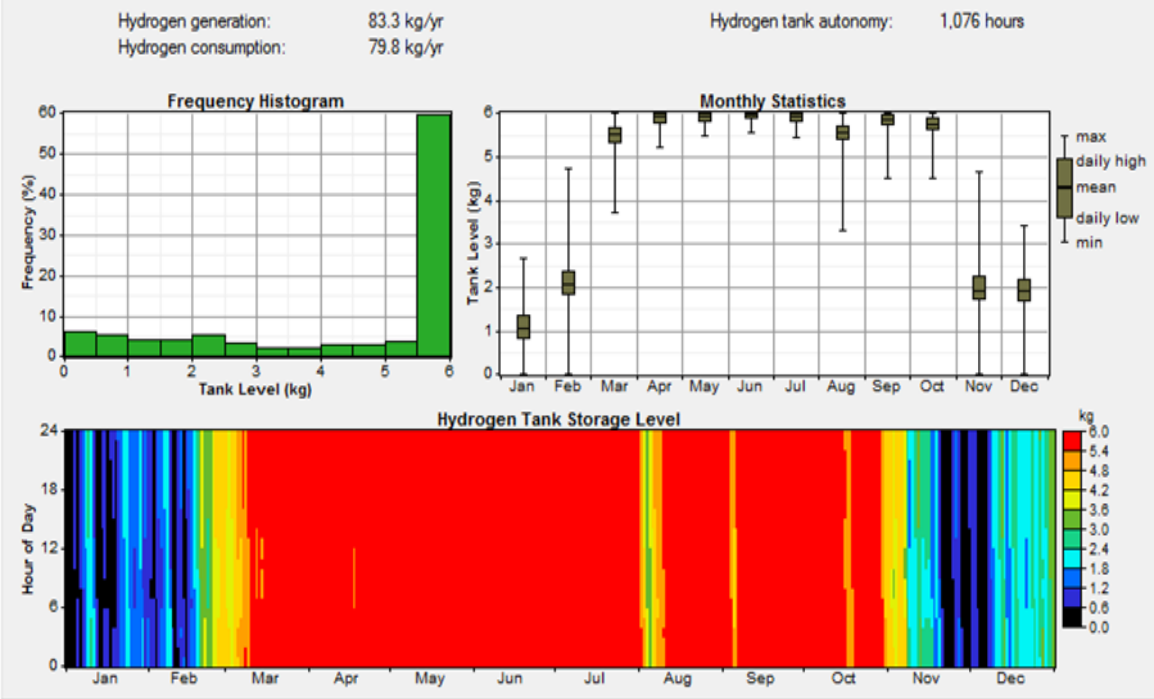

Figure 4. 4: Simulation results from HOMER software for the hydrogen tank

Since HOMER software does not have an oxygen tank input, the sizing will only be performed analytically in the next sections. After the capital cost and sizes to consider (0.2kW, 0.3kW and 0.5kW) have been set for the fuel cell inputs, the simulation runs to give the results as shown in Figure 4.5. The values in the gray line have been chosen from HOMER software. The fuel cell results are shown in Figure 4.6.

PV (kW)	G1	FC (kW)	48V034P	Conv. (kW)	Elec. (kW)	H2 Tank (kg)	Initial Capital	Operating Cost ($/yr)	Total NPC	COE ($/kWh)
7.02	1	1.0	10	2.0	2.4	6.000	$ 109,276	760	$ 118,997	5.717
5.46	1	0.5	11	1.5	1.2	7.000	$ 96,130	1,792	$ 119,036	5.721
7.02	1	0.5	11	2.5	1.2	6.000	$ 98,769	1,589	$ 119,079	5.721
6.24	1	0.5	8	2.5	2.4	6.000	$ 101,409	1,385	$ 119,113	5.726
7.80	1	0.5	9	1.5	1.2	6.000	$ 100,089	1,490	$ 119,140	5.725
7.80	1	1.0	8	2.0	2.4	6.000	$ 111,196	626	$ 119,199	5.729
5.46	1	0.5	11	1.0	2.4	6.000	$ 99,429	1,548	$ 119,217	5.728
6.24	1	0.5	9	1.5	2.4	6.000	$ 101,649	1,381	$ 119,297	5.733
7.02	1	1.0	11	1.5	2.4	6.000	$ 109,816	744	$ 119,327	5.733
7.02	1	1.0	10	2.5	2.4	6.000	$ 109,576	763	$ 119,331	5.733
5.46	1	0.5	11	2.0	1.2	7.000	$ 96,430	1,795	$ 119,370	5.737
7.02	1	0.5	11	3.0	1.2	6.000	$ 99,069	1,591	$ 119,413	5.737

Figure 4. 5: Suggested results simulation by HOMER software

Quantity	Value	Units
Hours of operation	1,226	hr/yr
Number of starts	280	starts/yr
Operational life	122	yr
Capacity factor	3.20	%
Fixed generation cost	0.0270	$/hr
Marginal generation cost	0.00	$/kWh

Quantity	Value	Units
Electrical production	280	kWh/yr
Mean electrical output	0.228	kW
Min. electrical output	0.00126	kW
Max. electrical output	0.681	kW

Quantity	Value	Units
Hydrogen consumption	79.8	kg/yr
Specific fuel consumption	0.285	kg/kWh
Fuel energy input	2,661	kWh/yr
Mean electrical efficiency	10.5	%

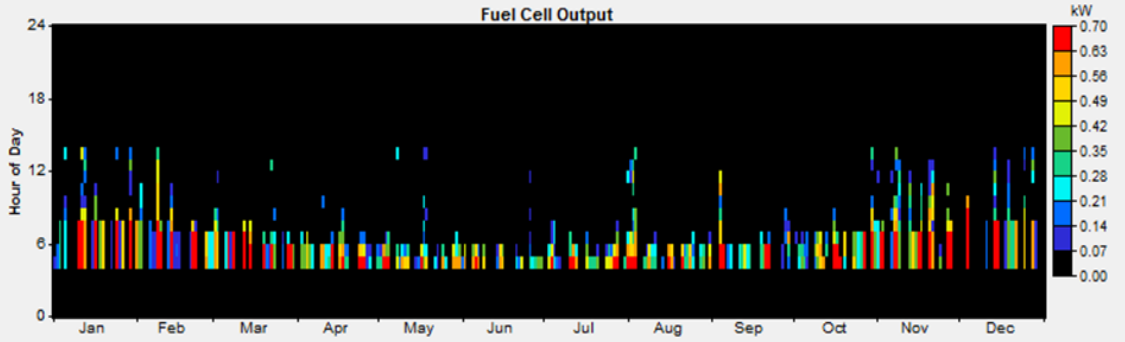

Figure 4. 6: HOMER software results for the fuel cell inputs

4.3.2. Lithium-Ion Battery and Converter

The MUN Explorer uses Li-ion batteries as its main source of energy to power loads, which include all electronics onboard and the emergency lights. This is because these batteries have high energy density and efficiency compared to other types of batteries. A Li-ion battery is more attractive in portable applications such as automotive and autonomous vehicles. The cost of the Li-ion batteries and sizes to consider (i.e. number of batteries) have been entered into HOMER software inputs. Figure 4.7 shows the battery's characteristic results. The battery has a nominal voltage of 48 V and nominal capacity of 34 Ah. The DC bus of the system is set to be 48 V, which means the battery also must be 48 V. Those characteristics were provided by the battery's data sheet as well. The DC / DC boost converter is well known as a step-up converter, which takes a lower voltage to a higher voltage. The HOMER results suggested that a 2 kW DC / DC converter should be used in the system. The efficiency of a DC / DC converter is always above 90%, and it has a lifetime of up to 15 years.

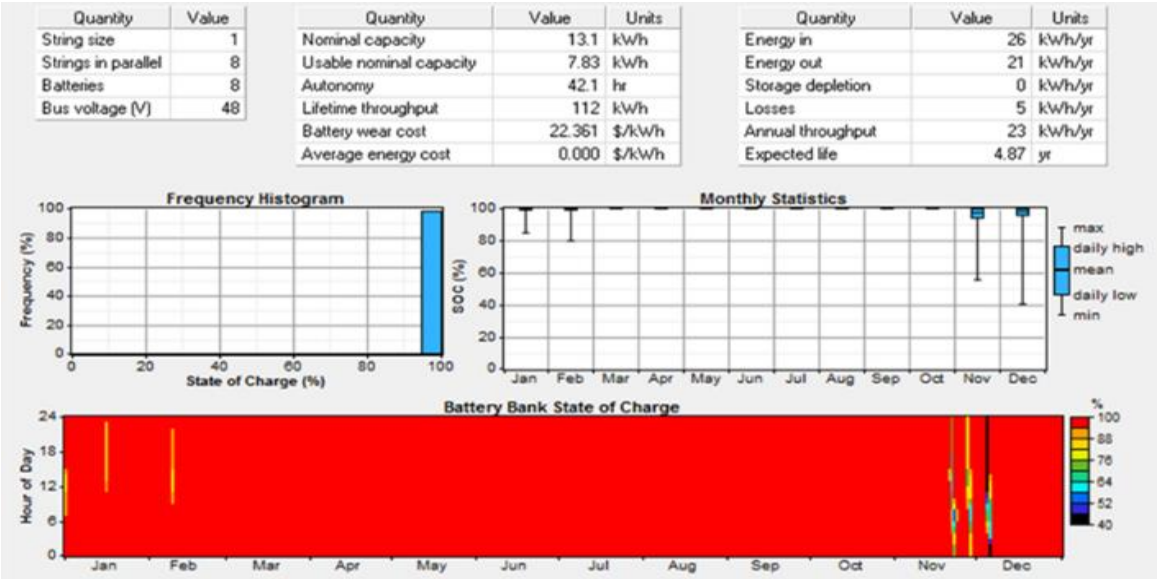

Figure 4. 7: HOMER software results for the battery

4.3.3. Permanent Magnetic DC Motor

In this case, the PMDC motor represents the load in HOMER software, and it is powered by the fuel cell and the battery. Permanent magnetic direct current (PMDC) motors are electrical machines that convert direct current electrical energy into mechanical energy. They are commonly used in many industrial, residential, and commercial applications [13]. The MUN Explorer AUV runs for ten (10) hours, so that the load has been specified based on the hours of operations (i.e. 10 hours) to be 600 W, as illustrated in Figure 4.8. The load is also divided into two sections: a DC load, which represents the electronics on-board, and the AC load, which is a variable speed motor. The MUN Explorer has only DC components, so the reason for selecting AC in HOMER is to represent the motor drive in our sizing.

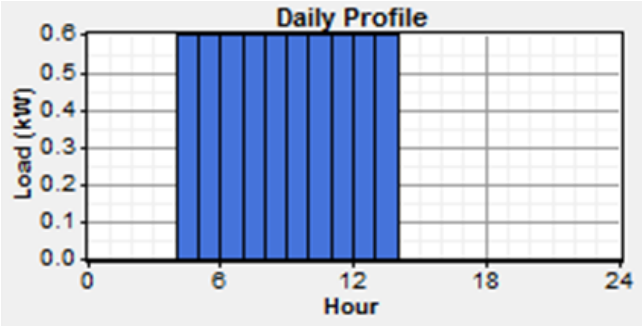

Figure 4. 8: Load for the DC motor in HOMER

4.4. System Dynamic Model

4.4.1. Hydrogen / Oxygen Tank and PEM Fuel Cell model

The storage system in the MUN Explorer could be challenging to install. As mentioned above, there are many ways to store compressed or liquid hydrogen and oxygen, especially for the MUN Explorer applications. Compressed or liquid hydrogen and oxygen storage gases can be implemented in terms of specific energies and energy densities. Effective storage systems that have higher energy density (ED) and specific energy (SE) are preferred [12].

The advantages of compressed hydrogen include that it does not need preprocessing and is the easiest and cheapest solution for dealing with fuel storage. However, to maximize hydrogen content, high pressures (up to 700 bar) can be applied, due to the low energy density of hydrogen gas. Liquid hydrogen has a higher density than gas. Liquid hydrogen also needs a temperature that is less than 20.15 K, so the stored liquid hydrogen must be in cryogenic Dewars (multi-shell flasks using an evacuated interstitial space) to eliminate heat transfer throughout the flask and prevent gas from reaching the boiling stage. Table 4.1 shows the specific energy and the energy density for compressed and liquid hydrogen storage systems, respectively [12].

Table 4. 1: Hydrogen storage system for SE and ED

Hydrogen	**Specific Energy (kWh/kg)**	**Energy Density (kW/L)**
Compressed	**1.71- 1.82**	**0.56 - 0.82**
Liquid	**2.05**	**1.86**

Lightweight tanks for transporting the compressed oxygen applications are more accessible than the hydrogen ones, because hydrogen tanks are used in automotive vehicle applications, while oxygen tanks are often used in medical applications. In short, hydrogen tanks can be modified for oxygen storage systems [14]. “Since high-pressure oxygen has a simple delivery mechanism, the desired oxygen tank wall thickness increases with pressure, which causes a reduction in the energy density advantages” [15]. Liquid oxygen storage can be a suitable solution for limited space applications. Some drawbacks of this storage system are its complexity, due to the safety concerns associated with the handling and refueling process[15]. A liquid oxygen storage system prototype has been designed by Sierra Lobo, Inc. with a diameter of 54 cm (21 inches) [14]. This prototype can store 50 kg of liquid oxygen at 452 k to run a 1-kW output PEM fuel cell. The system is 0.94-m long and 0.32 m in diameter. The weight is 13.6 kg when it is empty and 63.6 kg when it is full [16]. Table 4.2 shows the specific energy and the energy density for compressed and liquid oxygen storage systems, respectively [14].

Table 4. 2: Oxygen storage system for SE and ED

Oxygen	**Specific Energy (kWh/kg)**	**Energy Density (kW/L)**
Compressed	**0.77 - 1.68**	**0.6 - 1.09**
Liquid	**2.9 - 3.3**	**2.78 - 2.98**

In this chapter, the model for the compressed oxygen / hydrogen tank corresponds to the one used by [17] and [18]. The model of the oxygen / hydrogen tank was built based on equations 4.1 and 4.2 in the MATLAB / Simulink environment. The compressibility factor is defined as a function of temperature and pressure. Its value equals 1 when the

pressure is less than 2000 psi and is higher than 1 when the pressure is higher than 2000 psi at room temperature[18].

$$P_b - P_{bi} = CF * \frac{N_{H2} R T_b}{M_{H2} V_b} \quad (4.1)$$

$$CF = \frac{P V_m}{RT} \quad (4.2)$$

To evaluate the fuel cell in terms of specific energy and energy density, a commercial fuel cell (Horizon 1000W PEM Fuel Cell) is integrated into the storage systems. It is selected due to the effectiveness of the Horizon fuel cell and its recognised experience in AUV fuel cell applications. Table 4.3 shows the fuel cell parameters.

Table 4. 3: Fuel cell parameters

Weight (kg)	**Dimensions (cm)**	**Volume (L)**	**Specific Power (W/kg)**	**Power Density (W/L)**
4	**23.3*26.8* 12.3**	**7.68**	**250**	**130**

The calculation of the ED and SE of the complete storage system is represented as follows [12]:

$$ED_{ss} = \frac{ED_{H2} * ED_{O2}}{ED_{H2} + ED_{O2}} \quad (4.3)$$

$$SE_{ss} = \frac{SE_{H2} * SE_{O2}}{SE_{H2} + SE_{O2}} \quad (4.4)$$

These equations were applied for reactant storage combinations of liquid hydrogen / liquid oxygen and compressed hydrogen / compressed oxygen.

A polymer electrolyte membrane is an important component of a PEM fuel cell that is connected between the electrodes (anode and cathode). The cathode must be supplied by oxygen gas, whereas the anode must be supplied with hydrogen. The overall electrochemical dynamic can be represented by following equations[19]:

Cathode: $O_2 + 4H^+ + 4e^- \leftrightarrow 2H_2O$ (4.5)

Anode: $2H_2 \leftrightarrow 4H^+ + 4e^-$ (4.6)

Overall: $2H_2 + O_2 \leftrightarrow 2H_2O + electricity + heat$ (4.7)

For any fuel cell, both the anode and cathode can be represented by the mole conservation equations, as follow [19]:

$$\frac{dP_{H2}}{dt} = \frac{RT}{V_a}[H_{2in} - H_{2used} - H_{2out}] \quad (4.8)$$

$$\frac{dP_{O2}}{dt} = \frac{RT}{V_c}[O_{2in} - O_{2used} - O_{2out}] \quad (4.9)$$

The fuel cell dynamic is built in Simulink model, using a controlled voltage source in series with a constant resistance, as illustrated in Figure 4.9 [20].

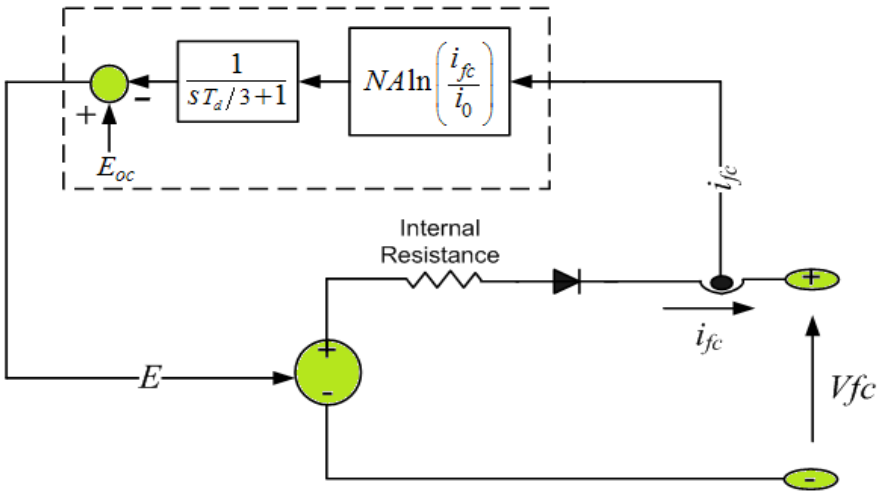

Figure 4. 9: Fuel cell stack model [19]

Equation (10) describes the controlled voltage source (E), so that

$$E = E_{oc} - NAln\left(\frac{i_{fc}}{i_0}\right) * \frac{1}{sT_d/3+1} \tag{4.10}$$

$$V_{fc} = E - R_{ohm} * i_{fc} \tag{4.11}$$

Equation 4.10 shows the fuel cell stack voltage as a function of activation losses, because of the slowness of chemical reactions at the electrode surfaces [20]. A parallel RC branch is used to model the losses electrically. Thus, for the rapid changes in the fuel cell current, the stack voltage will demonstrate a delay response that can be 3 times to the time constant $(\tau = RC)$ prior to equilibrium. Equation 4.10 also illustrates a phenomenon which delays the activation losses with a first order transfer function $\left(\frac{1}{sT_d/3+1}\right)$ where T_d is the stack settling time. Equation 4.11 represents the total fuel cell voltage by considering the losses due to electrodes and electrolyte resistances (ohmic losses). This model is a simplified model that can simulate a fuel cell stack at a nominal condition of pressure and

temperature operations. To eliminate the flow of negative current into the fuel cell, a diode is used [20]. Polarization curves (*V-I* and *P-I*) from the simulation and data sheet are presented in Figure 4.10 and Figure 4.11, respectively. The results from both MATLAB / Simulink and the manufacturer's data sheet align well. The performance characteristics data of the stack are given for baseline operating conditions and defined at sea level and room ambient temperature. More information about the fuel cell is attached in the appendix.

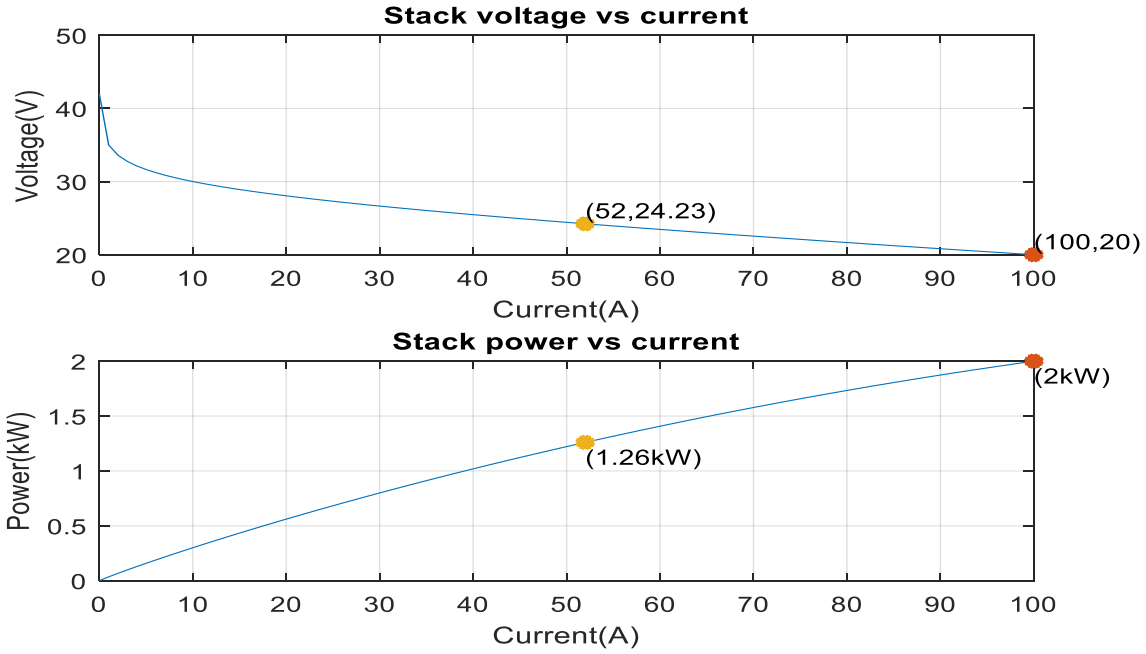

Figure 4. 10: Polarization curves, voltage vs current and power vs current from simulation results

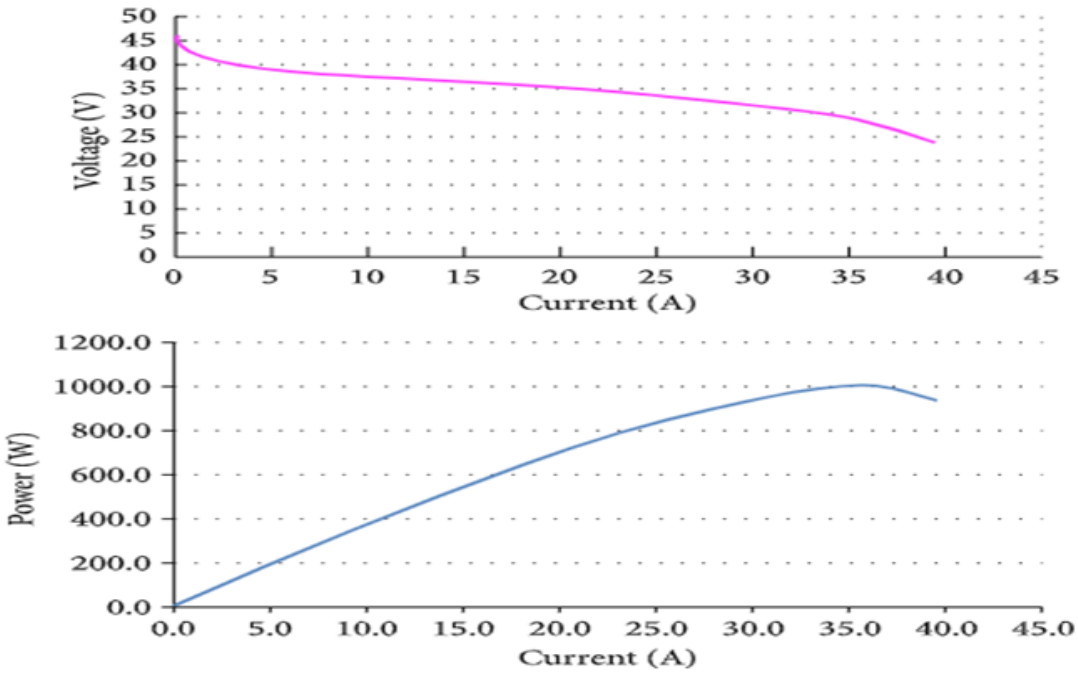

Figure 4. 11: Polarization curves, voltage vs current and power vs current from data sheet results

4.4.2. Lithium-Ion Battery and Converter model

MATLAB / Simulink already has a built-in dynamic model for a Li-ion battery that depends on a modified Shepherd curve-fitting model. The voltage polarization term was added to the battery discharge voltage expression to ensure the representation of the battery's SOC effect on the battery performance. For the simulation stability, the filtered battery current is implemented instead of the actual battery current for the polarization resistance.

The model uses equations 4.12 and 4.13 for discharging and charging as follows [21]:

Discharge Model when i^* is greater than Zero

$$V_{batt} = E_0 - K\frac{Q}{Q-it}\cdot i^* - K\cdot\frac{Q}{Q-it}\cdot it + A\cdot exp(-B\cdot it) - R_b.I \quad (4.12)$$

Charge Model when i^* is less than Zero

$$V_{batt} = E_0 - K.\frac{Q}{it+0.1Q}\cdot i^* - K\cdot\frac{Q}{Q-it}\cdot it + A\cdot exp(-B\cdot it) \quad (4.13)$$

Figure 4.12 illustrates the dynamic model for a Li-ion battery in MATLAB / Simulink. Table 4.4 also shows the battery model input parameters. The simulation discharge curves for the Li-ion battery system (i.e. 48 V and 34 Ah) are shown in Figure 4.13.

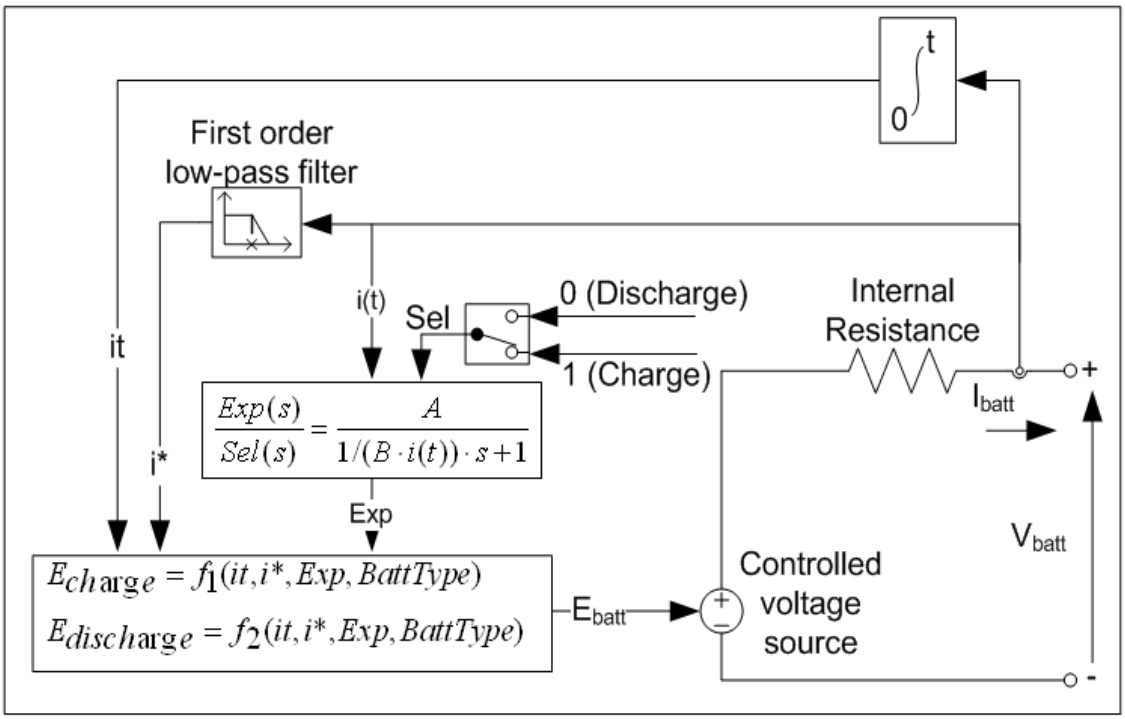

Figure 4. 12: Dynamic model for Li- ion battery [21]

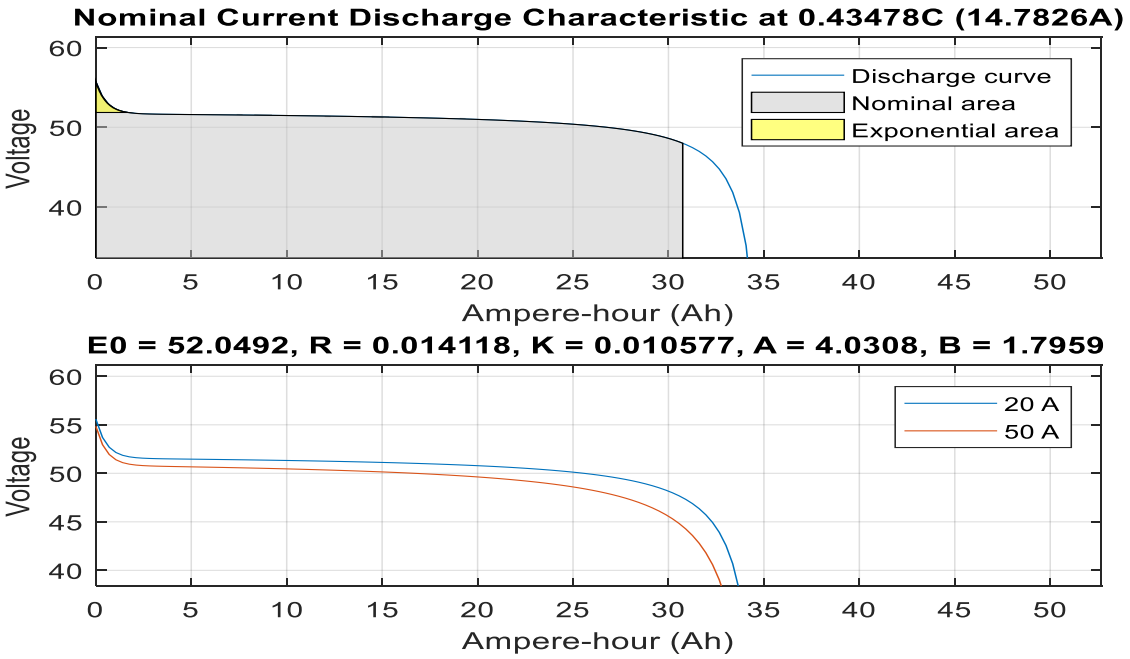

Figure 4. 13: Simulation discharge curves for the Li-ion battery

Table 4. 4: Battery model input parameters

Battery Model Input Parameters	**Value**
Nominal Voltage	48 (V)
Rated capacity	34 (Ah)
Maximum capacity	34 (Ah)
Fully charged Voltage	55.87 (V)
Nominal Discharge Current	14.78 (A)
Internal Resistance	0.014(Ohm)
Capacity at Nominal Voltage	30.74 (Ah)

The average mode boost converter is used in this simulation, and its parameters are illustrated in Table 4.5. For the DC / DC converter parameters, some equations have been implemented to calculate the values for duty cycle (D), inductance (L), and capacitance (C) [22]:

$$D = 1 - \frac{(V_{in\_min} * n)}{V_{out}} \tag{4.14}$$

$$L = \frac{(V_{in} * (V_{out} - V_{in}))}{(I_{in} * f_s * V_{out})}, and \tag{4.15}$$

$$C = \frac{I * D}{f_s * dv} \tag{4.16}$$

where D is the duty cycle, which equals the fraction of time when the switch is connected in position 1, and hence $0 \leq D \leq 1$. V_{in_min} is the minimum input voltage; n is the efficiency set to 90%. The variable F_s is the switching frequency, V_{out} is the output voltage, I_{in} is the input current and dv is the output voltage ripple[23].

Table 4. 5: Boost converter parameters

Parameters	**Value**	**Units**
Switching freq. F	20	kHz
Inductance L	500	µH
Capacitance C	7500	µF
Load Resistor R	0.2	Ω

4.4.3. Permanent Magnetic DC Motor (PMDC) model

The dynamic model for any PMDC motor can be represented by the following equations [24]:

$$\frac{dI_a}{dt} = \frac{1}{L_{aa}} * (V_t - I_a * R_a - K_m * \omega_m) \quad (4.17)$$

$$\frac{d\omega_m}{dt} = \frac{1}{J} * (T_e - T_L - B_m * \omega_m) \quad (4.18)$$

Table 4.6 shows the parameters for the DC motor implemented in MATLAB / Simulink. Most of these values were collected from the DC motor datasheet. Figure 4.14 shows the system dynamic flow rate regulators and flow rate selector. The blue and green blocks represent the hydrogen and oxygen tanks, respectively. They both enter the fuel cell stack in order to be powered. The fuel cell is connected to the boost converter to increase the voltage from 24 V to 48 V, which is required by the battery and the load (i.e. DC motor). The yellow block illustrates the MUN Explorer's motor.

Table 4. 6: PMDC motor parameters

Parameters	**Value**	**Unit**
Armature V	48	V
Armature Ra	0.3	Ohms
Armature La	0.00208	H
Torque constant	0.099	N.m/A
Total Inertia J	15e-5	Kg.m^2

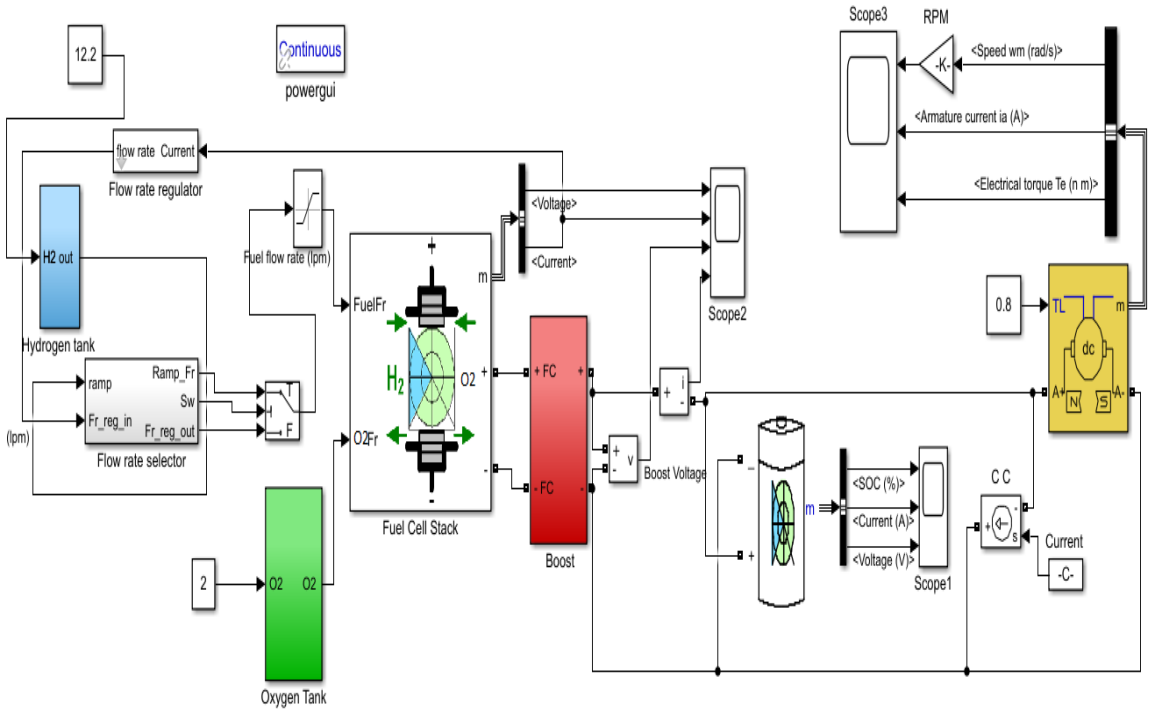

Figure 4. 14: Dynamic model in MATLAB/Simulink Software

4.5. Results and Discussion

The simulation in HOMER software was performed to obtain the sizing results for the integrated power system. The system component inputs were specified based on the cost and sizes to consider for each block. Figure 4.3 demonstrates that the components of the PV wind turbine and electrolyzer cannot be applied to the MUN Explorer, due to the lack of space available, and they will be used to generate the required oxygen and hydrogen gases to run the fuel cell. From Figure 4.5, the assumptions of the wind and PV energy are determined based on the wind speed directions and solar radiation of St. John's, Newfoundland, which is where this technology will be integrated. The oxygen / hydrogen tanks and fuel cell along with the batteries are planned to be installed in the MUN Explorer.

The gray line also shows the most optimal results. The results have shown the lowest operating cost and reduce the number of batteries from 11 to 8. The advantage of minimizing the number of batteries is that this leaves more space for installing the fuel cell and the tanks. The hydrogen stored in the cylinders can be generated from renewable energy sources as a step prior to running the MUN Explorer. Figures 4.15 and 4.16 show the pressure inside the oxygen and hydrogen tanks, respectively. They show the compressed pressure inside the cylinders which is increased exponentially. The oxygen gas is filled the tank until its pressure reaches the elecrolyzer anode pressure. Similarly, the hydrogen gas is filled the tank until its pressure reaches the electrolyzer cathode pressure [18].

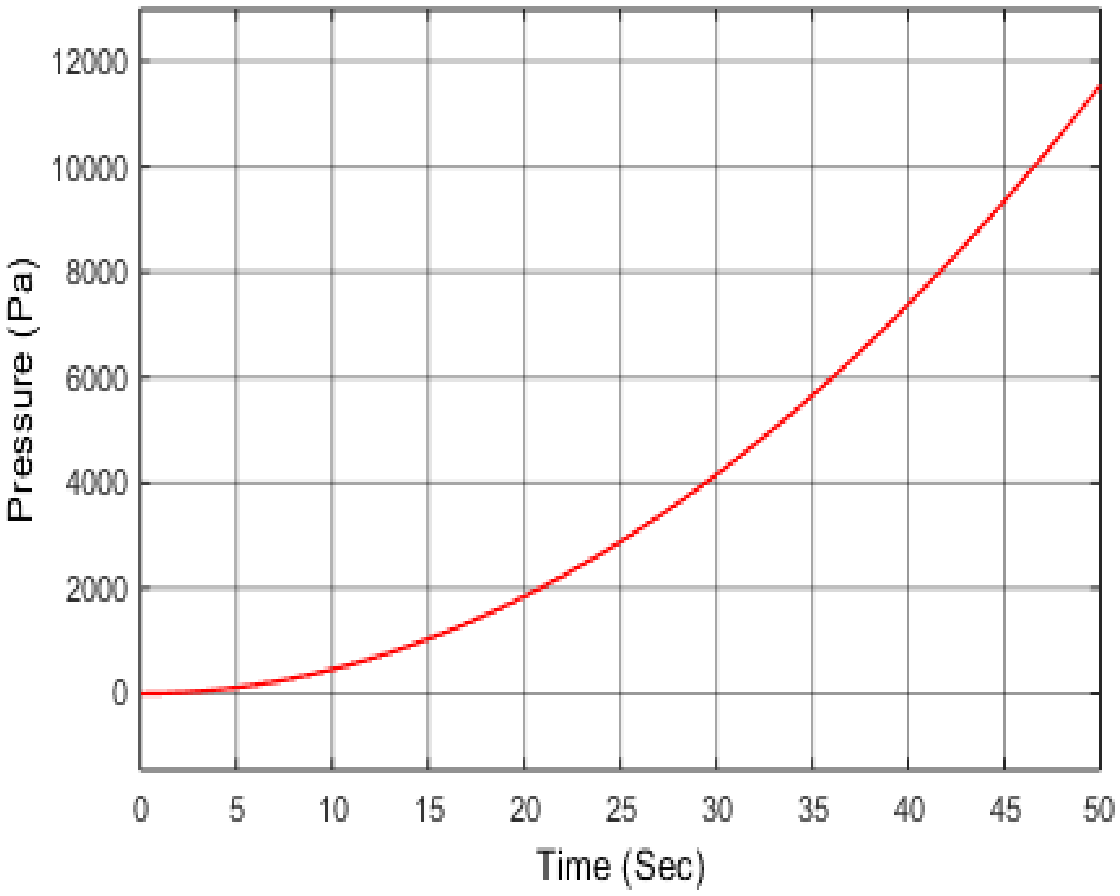

Figure 4. 15: Pressure of compressed oxygen tank

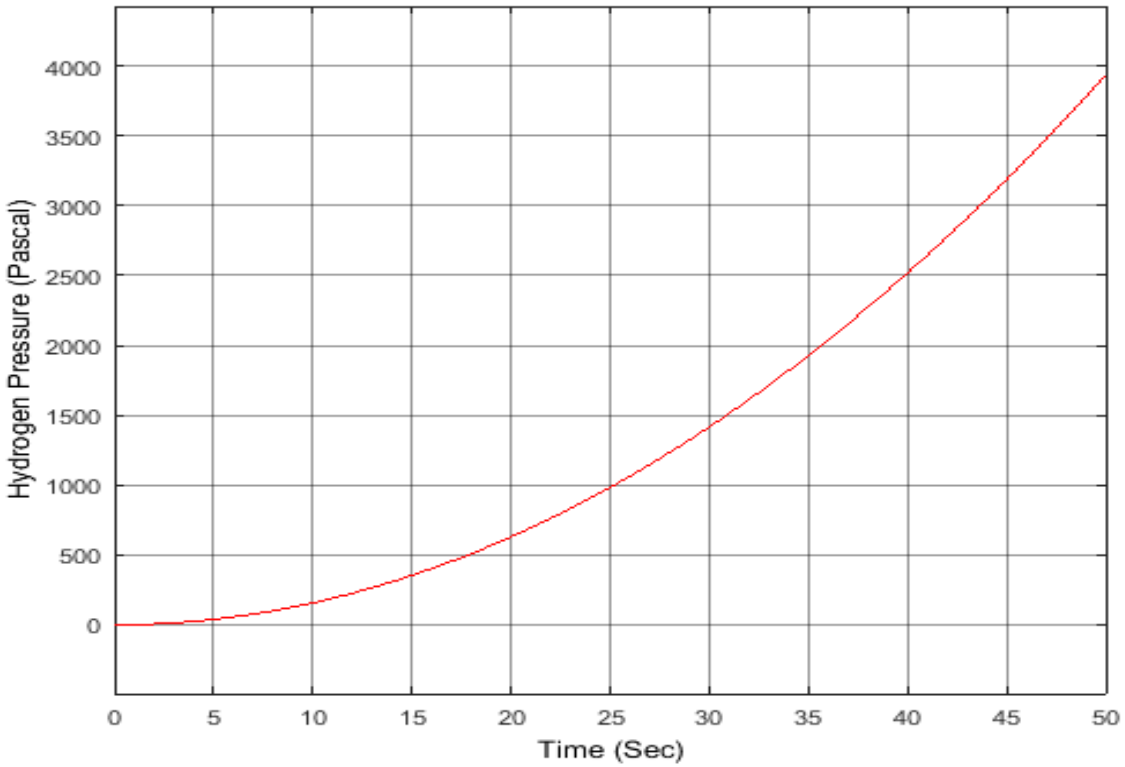

Figure 4. 16: Pressure of compressed hydrogen tank

A 6-kg hydrogen tank needs to be installed inside the Explorer to run the fuel cell. The oxygen tank can be installed according to the hydrogen tank specifications, which was suggested in the literature. The oxygen tank size is considered to be the same as the one in [16]. The fuel cell has 1 kW of power to feed the DC motor and to charge the battery once it accumulates enough power. Firstly, the fuel cell is connected to the boost converter, which takes 24 V to 48 V, which is required by the battery and DC motor, as shown in Figure 4.17. The assumptions of the fuel cell model are that all gases are ideal, pressure drops across flow channels are negligible (maximum temperature 65 ºC and the pressure form 0.45 to 0.55 bar), and cell voltage drops are due to reaction kinetics and charge transport[19]. A PI controller is used to control the output voltage from the boost converter

to maintain the 48 V for the battery and DC motor. The PI coefficients are shown in Table 4.7.

Table 4. 7: PI coefficients for boost converter

Parameter	**Value**
K_P	0.0005
K_i	0.15

From Figure 4.17, we can clearly see that after 20 seconds, the fuel cell started to run to power the DC motor. This starting time is recommended by the fuel cell manufacturer and controlled by the fuel cell regulator. The battery is set to 50% state of charge (SOC) to prevent any damage to the battery and this does not allow it to charge to 100%. The nominal discharge current is 14.78 A. Figure 4.18 shows the fuel cell power profile in HOMER through the year.

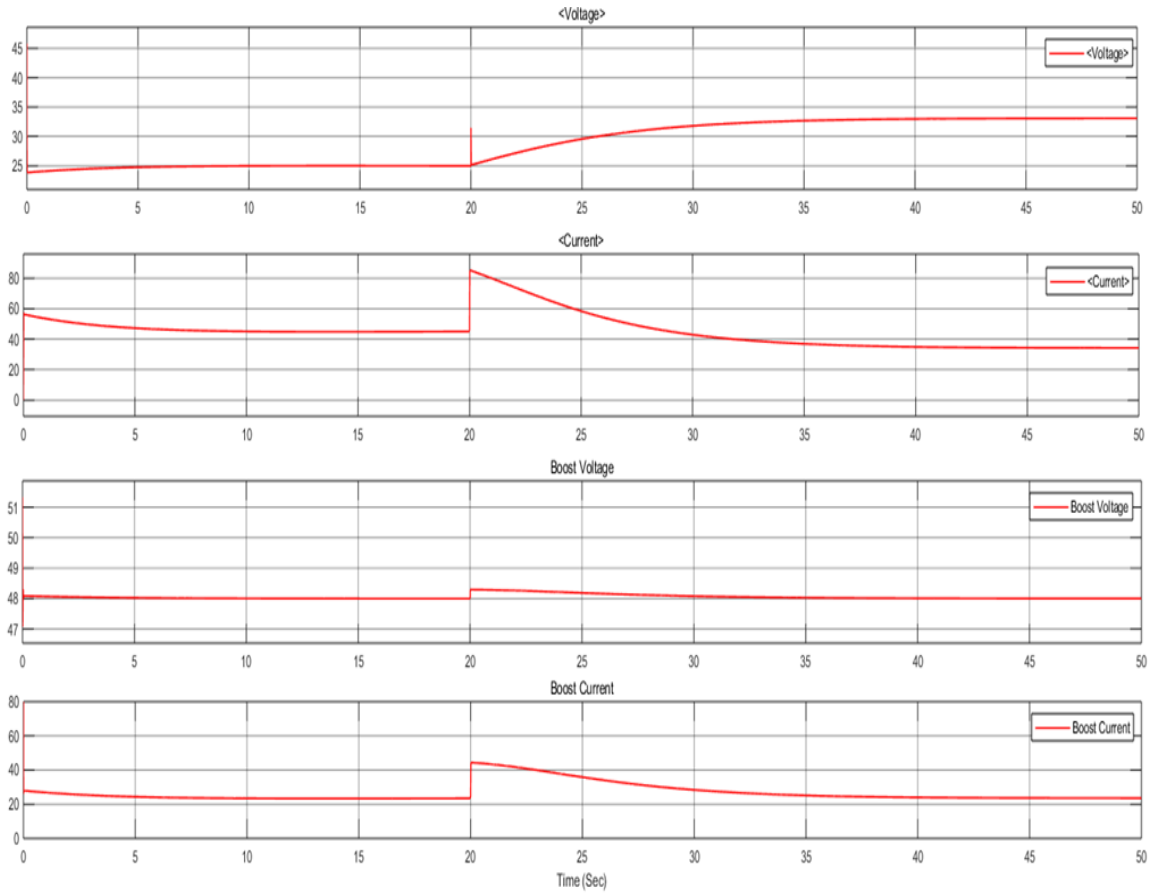

Figure 4. 17: Voltage and current of fuel cell and Boost converter

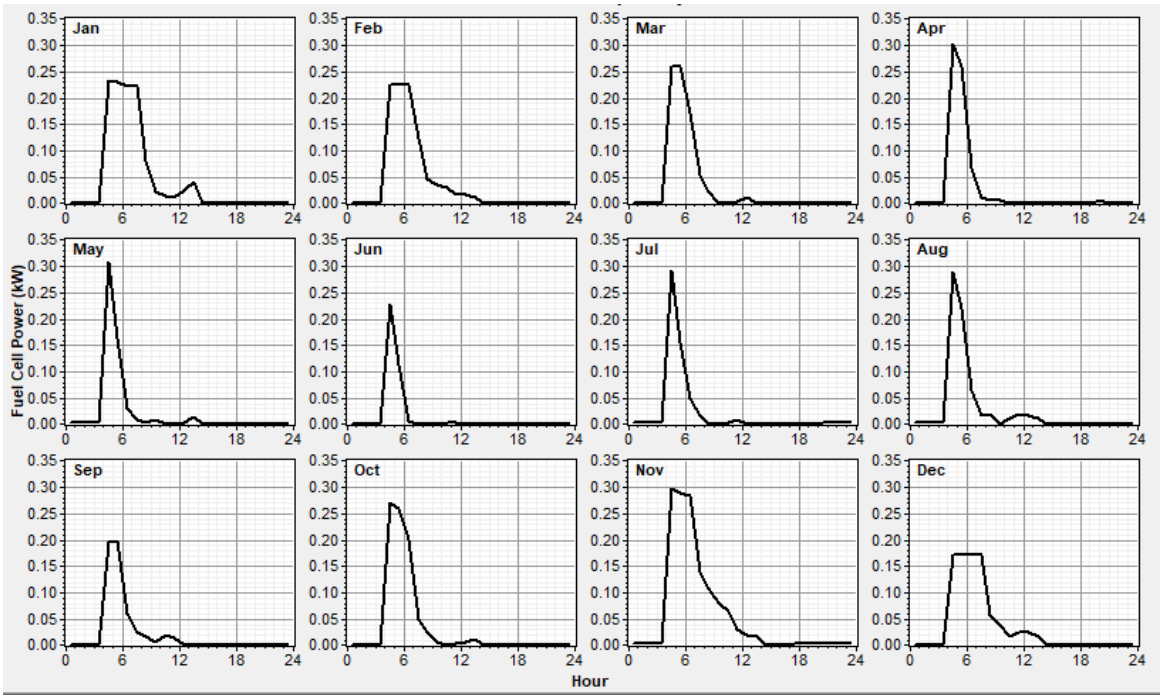

Figure 4. 18: The fuel cell power profile

There are 11 batteries connected in series inside the dry section of the MUN Explorer to power the AUV for 10 hours, as shown in the drawn Figure 4.19. The total weight of 11 batteries is 137.5 Kg (12.5*11). Figure 4.20 illustrates the battery behaviour in terms of SOC, current and voltage from the Simulink model, and Figure 4.21 shows the state of charge profile from HOMER sizing during a year. Figure 4.22 illustrates the PMDC motor, which runs at a constant speed. This constant speed is maintained by the AUV's boost converter. Then the DC motor runs at its highest efficiency. The armature current is 16, which is very close to the manufacturer's data sheet value. Figure 4.23 demonstrates the DC motor's power profile during the year in HOMER software. The energy consumption by the DC motor in kW is shown for each month.

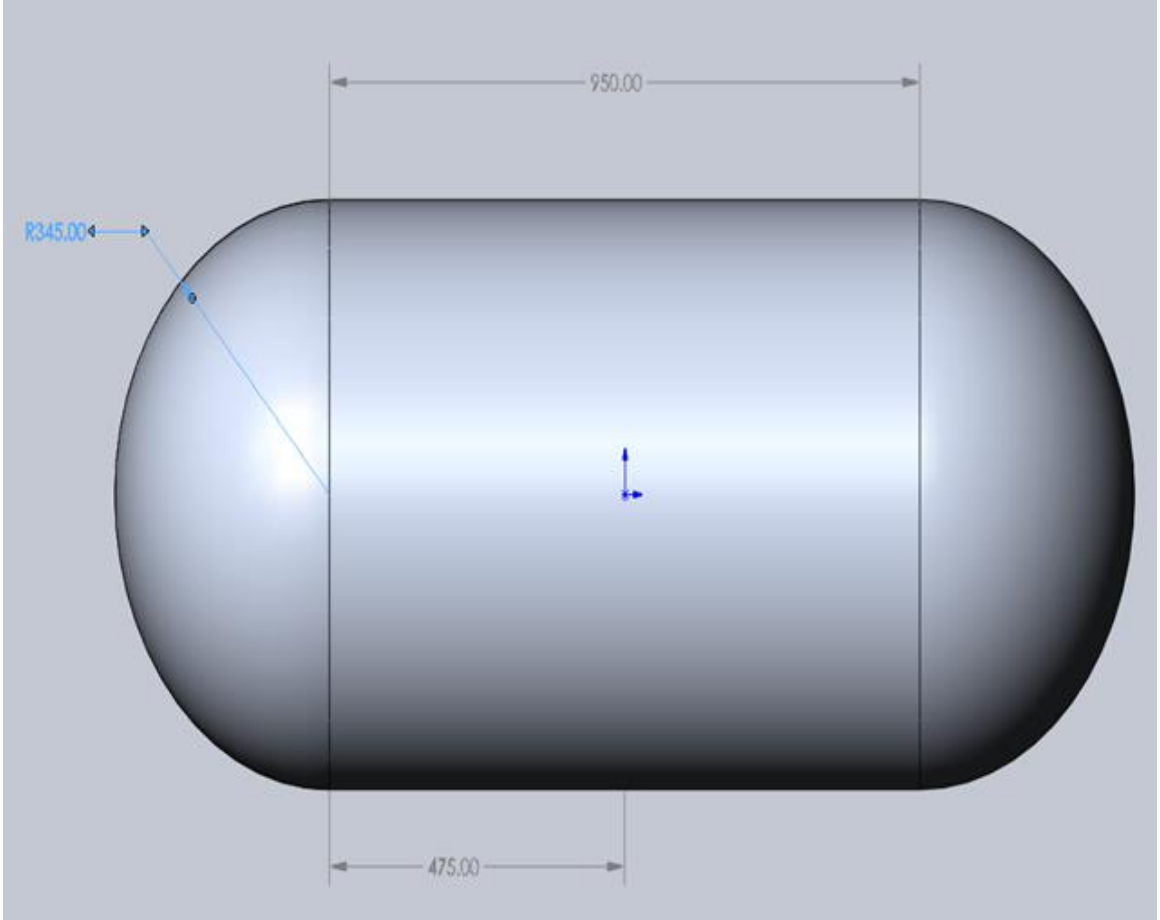

Figure 4. 19: The dry section inside the MUN Explorer (dimensions in mm)

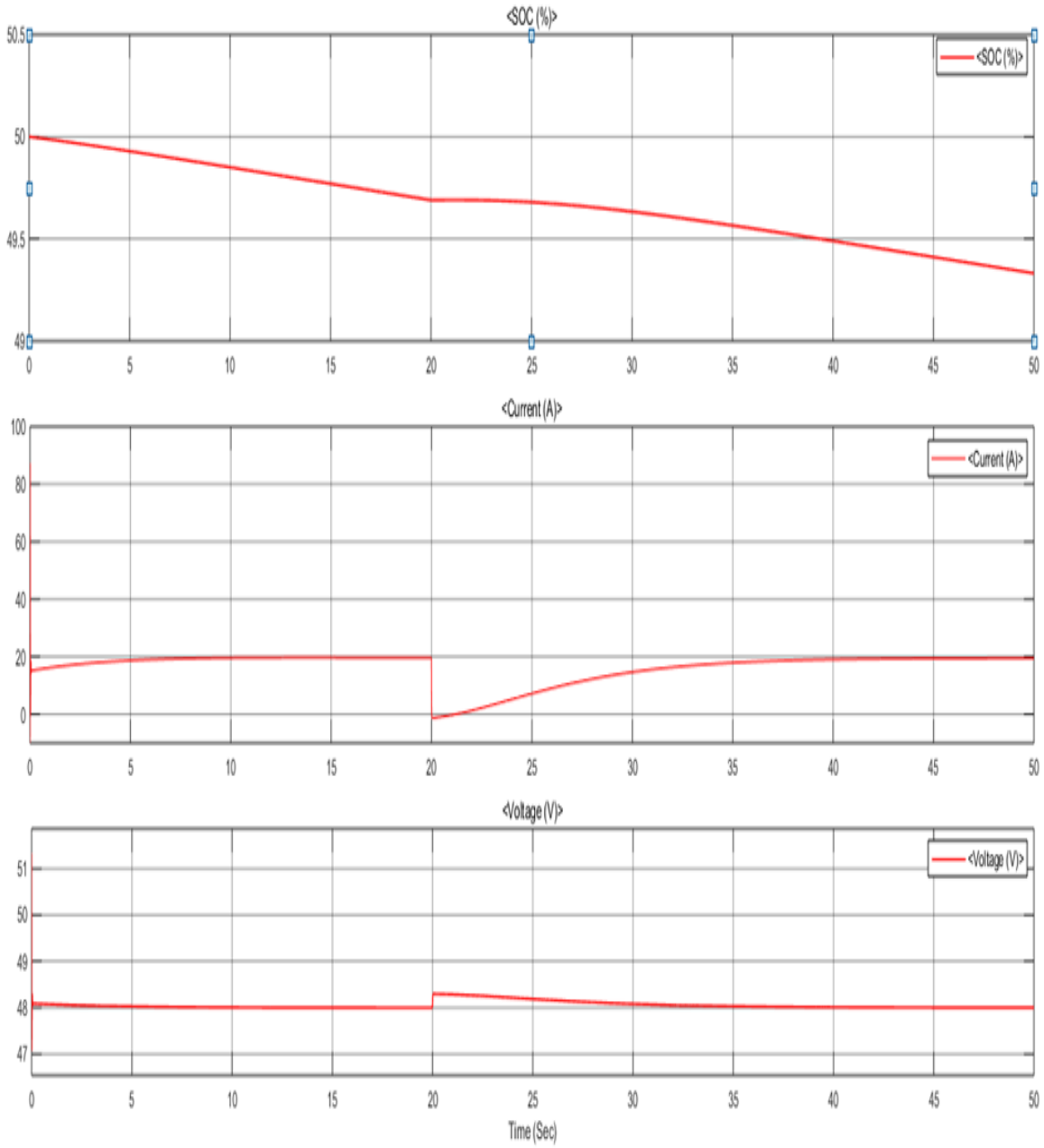

Figure 4. 20: Battery characteristic SOC, current and voltage

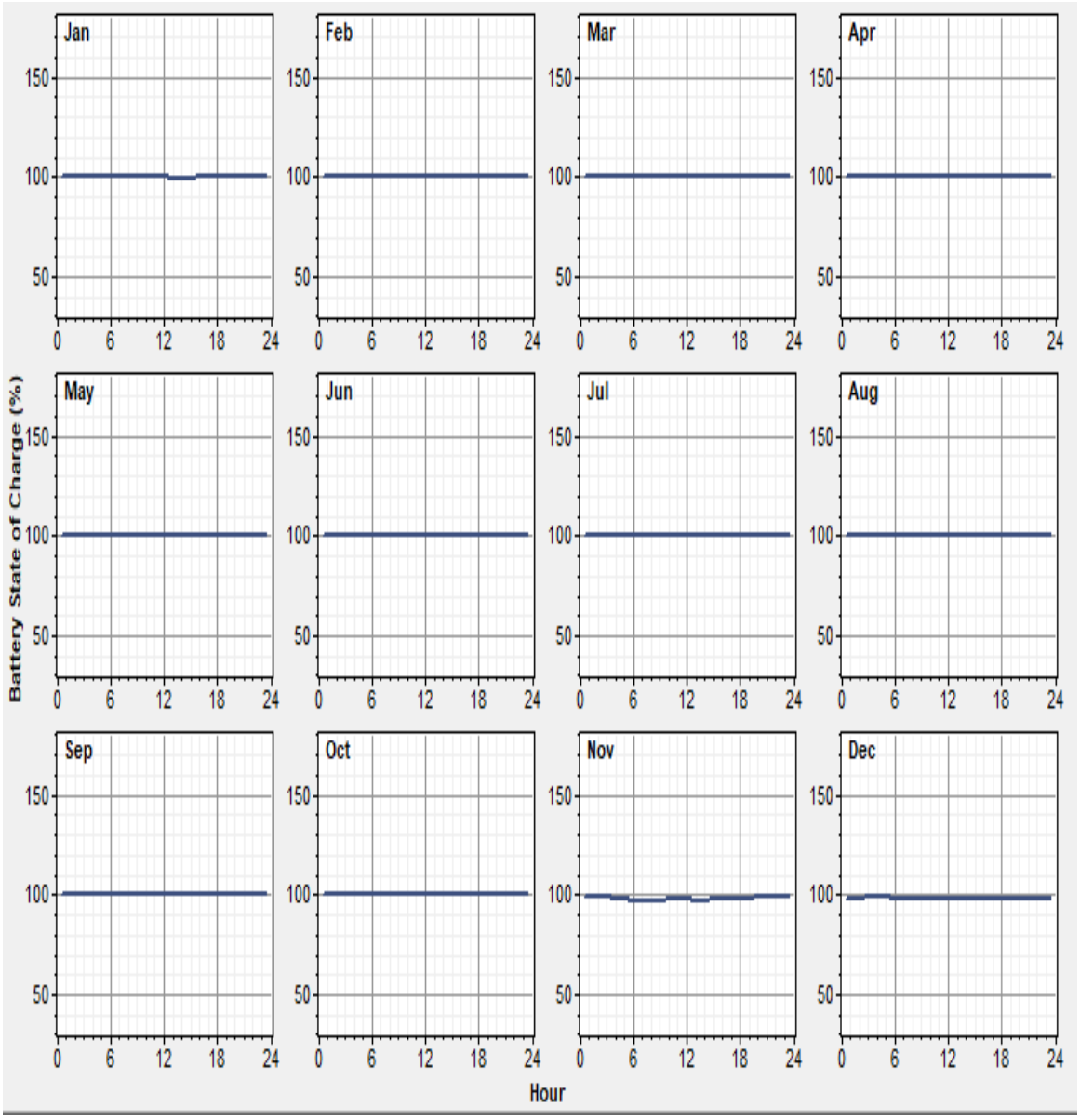

Figure 4. 21: Battery power profile form HOMER

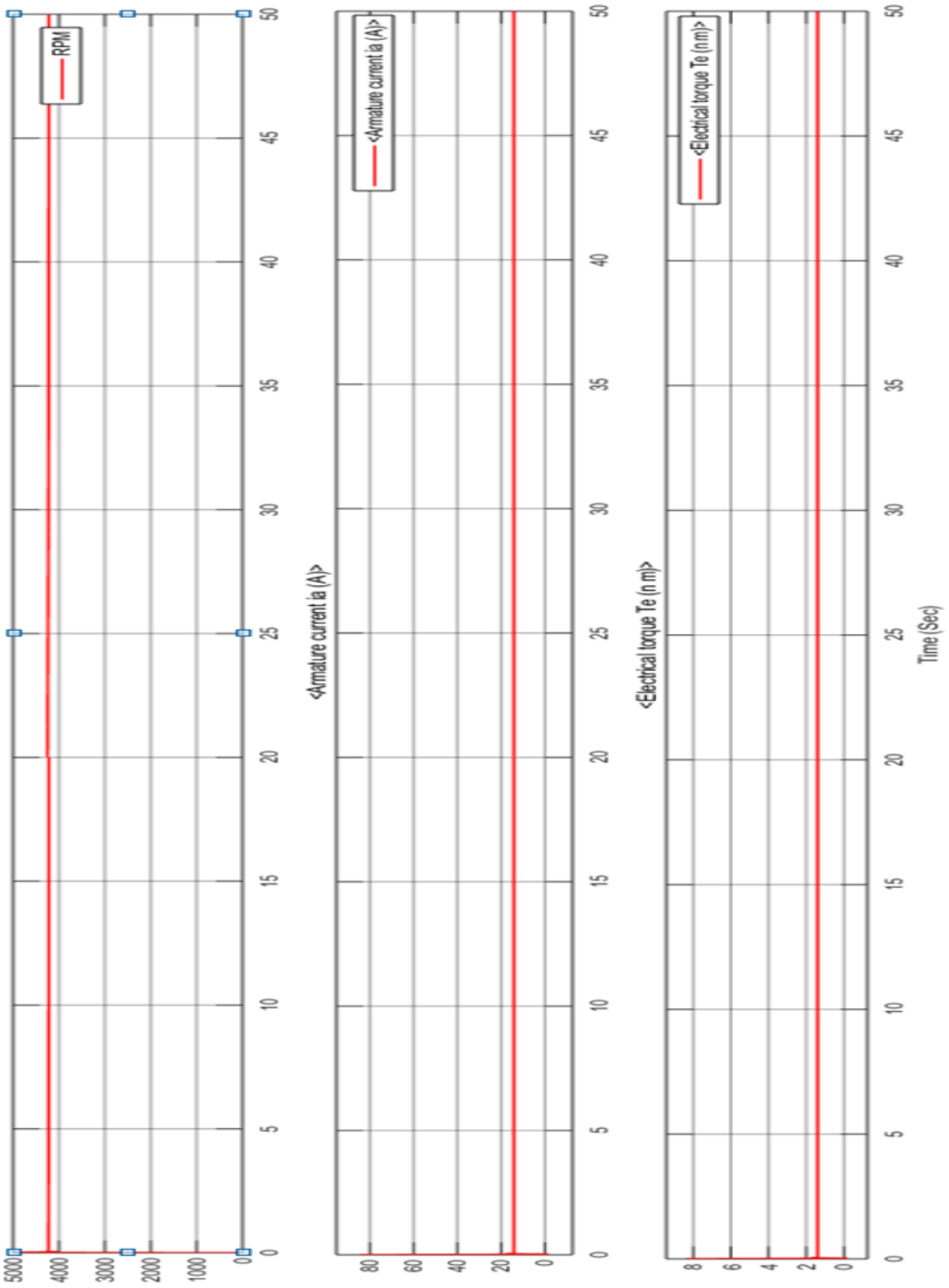

Figure 4. 22: PMDC motor characteristics

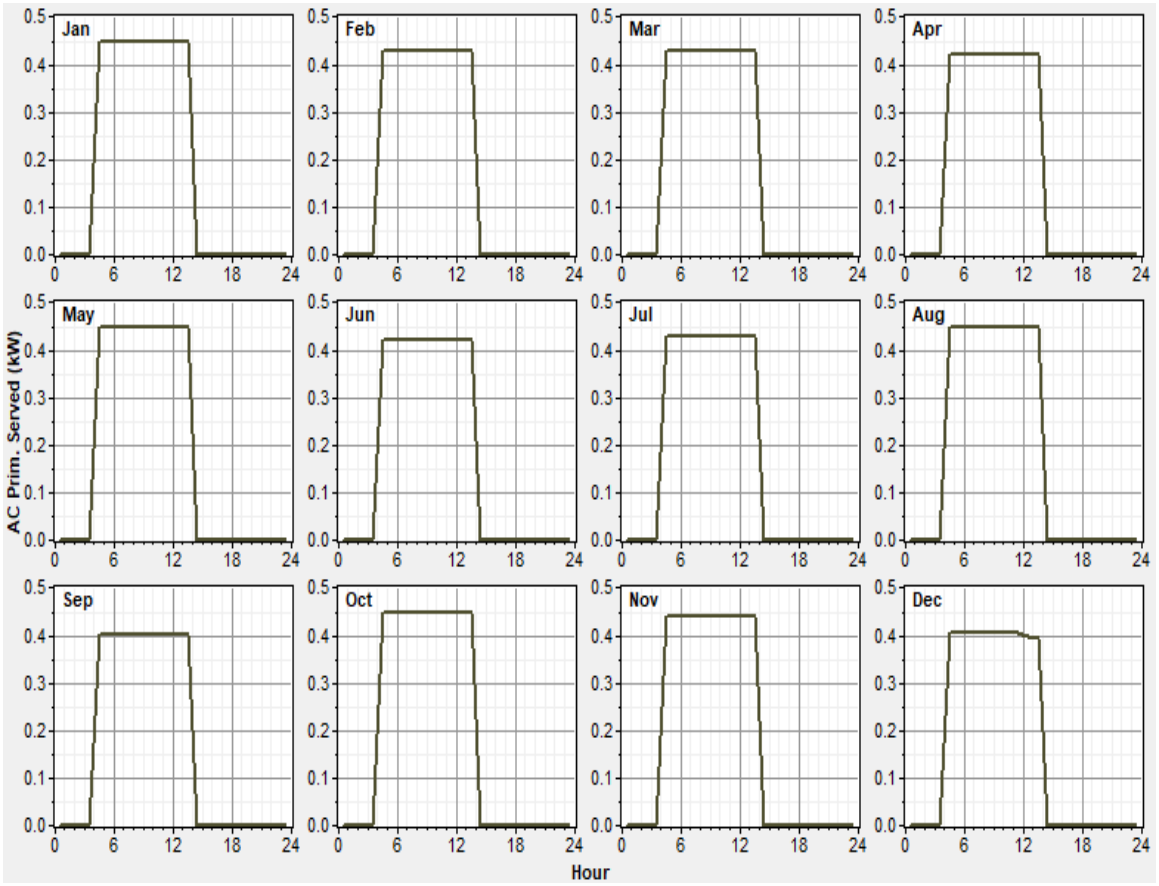

Figure 4. 23: DC motor power profile

The monthly average electric power production from the system (i.e. PV, wind and fuel cell) is shown in Figure 4.24. The solar and wind energy are used to produce oxygen and hydrogen gas by powering an electrolyzer as well as recharging the batteries. The fuel cell power production is low compared to the PV and wind power, due to the integration of the fuel cell into the battery system, which has a large amount of energy to power the DC motor. Table 4.8 shows the results for energy density and specific energy for the storage and total system with the fuel cell. The calculations are based on the total system's mass and weight, which can be illustrated as summations of the storage and fuel cell systems. The estimated results are shown due to the main balance of plant components that were integrated into commercial fuel cells.

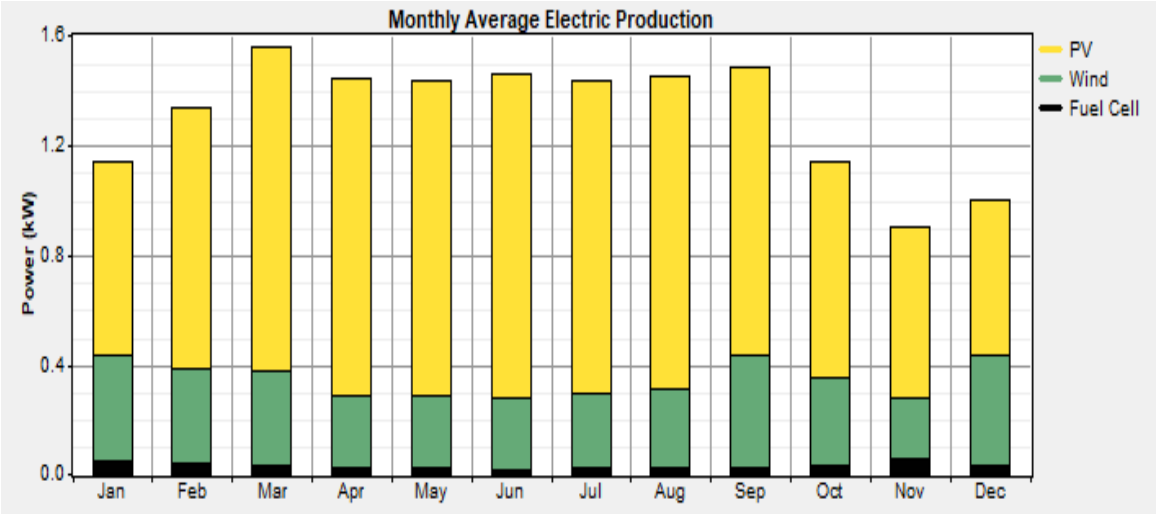

Figure 4. 24: Monthly average electric production

Table 4. 8: SE and ED for storage and total fuel cell

	Storage System		**Total system**	
	SE (kWh/kg)	ED (kWh/L)	SE (kWh/kg)	ED (kWh/L)
L_{O2}/L_{H2}	1.233	1.130	1.024	0.846
C_{O2}/C_{H2}	0.792	0.379	0.701	0.339
Lithium-Ion batteries	0.18	0.36	--	--

Table 4.8 shows a significant improvement in terms of specific energy and energy density, especially for liquid oxygen and hydrogen storage options. In [12], Li-ion batteries have specific energies ranging from 0.165 kWh/kg to 0.207 kWh/kg and energy densities from 0.329 kWh/L to 0.490 kWh/L [12]. The largest improvements are in the specific energy of the fuel cell total systems, compared with the lithium-ion batteries. To show the buoyancy effect on the system, the density can be defined as energy density divided by specific energy, as represented by 4.19 equation [14]:

$$D = \frac{m}{V} = \frac{ED}{SE} \tag{4.19}$$

Figure 4.25 shows the relationship between ED and SE, and the plotting of ED as functions of SE on the X and Y axes is the slope (i.e. X and Y intercept at any point) which is equivalent density at any point. The seawater density (1.03 kg/L) is shown by the dotted line. However, if there is any point above the line, it indicates negative buoyancy or a

density more than seawater. Any point below the line indicates positive buoyancy or less density than seawater. For any given fuel cell power system design that does not require buoyancy, as shown in Figure 4.25, some ballast or float material must be added to meet the buoyancy requirement [14].

The power system's capacity is increased by integrating the fuel cell power system into the MUN Explorer according to the following calculations, 4.20 and 4.21. From figure 1.1 parameters, the assumption made based on these parameters and considered to our system, hydrogen stored at 300 bar equals to 100 litres and oxygen stored at 250 bar equals to 50 litres. The energy capacity of the new system can be calculated to be 36.8 kwh. The tanks to store hydrogen have different sizes, for example 30–40 liters storing 1.3 to 1.5 kg of hydrogen at 350 bars. Two pressure standards have been considered for automotive applications, which are 350 and 700 bars (5,000 and 10,000 psi) [25]. For more details and liquid hydrogen storge options more information can be found in the appendix number 4.

$$\text{Available Energy} = \text{Power} * \text{time} \tag{4.20}$$

$$\text{Watt-hour} = \text{Battery Volt} * \text{Ah} \tag{4.21}$$

The energy capacity is increased by integrating the fuel cell into the system and the number of batteries is reduced by applying equations 4.20 and 4.21. Figures 4.26 and 4.27 illustrate proposed drawing system of the fuel cell and hydrogen / oxygen tanks along with the 8 batteries.

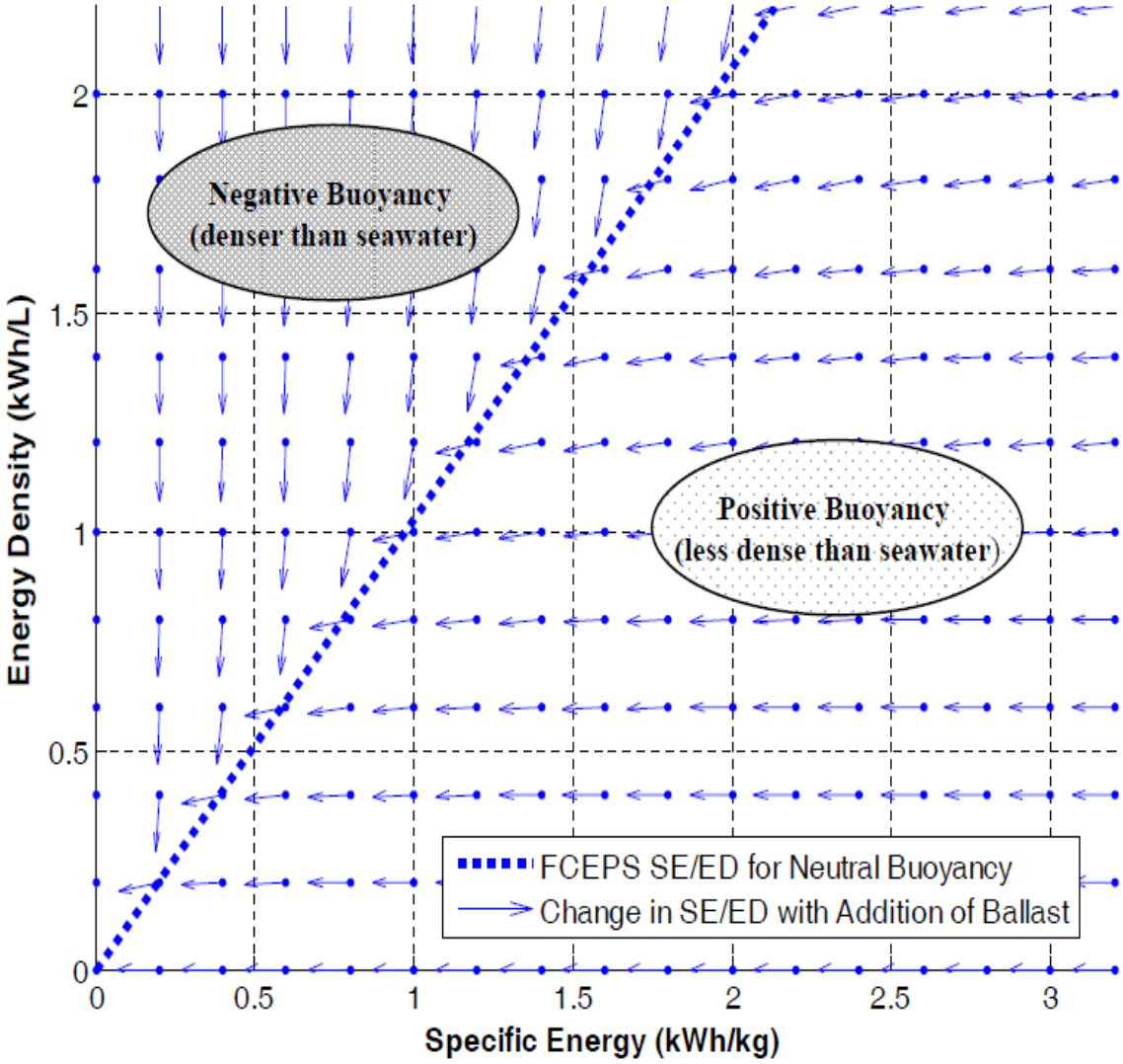

Figure 4. 25: Buoyancy in terms of SE and ED[14]

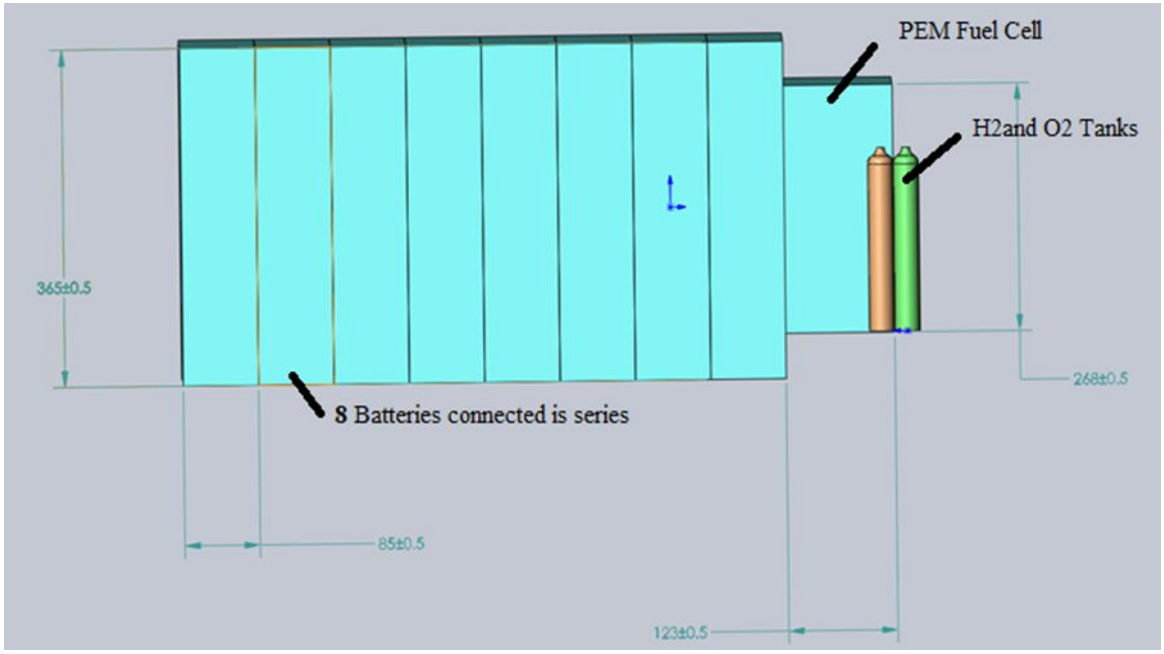

Figure 4. 26: side view of batteries, fuel cell and tanks inside the dry section (dimensions in mm)

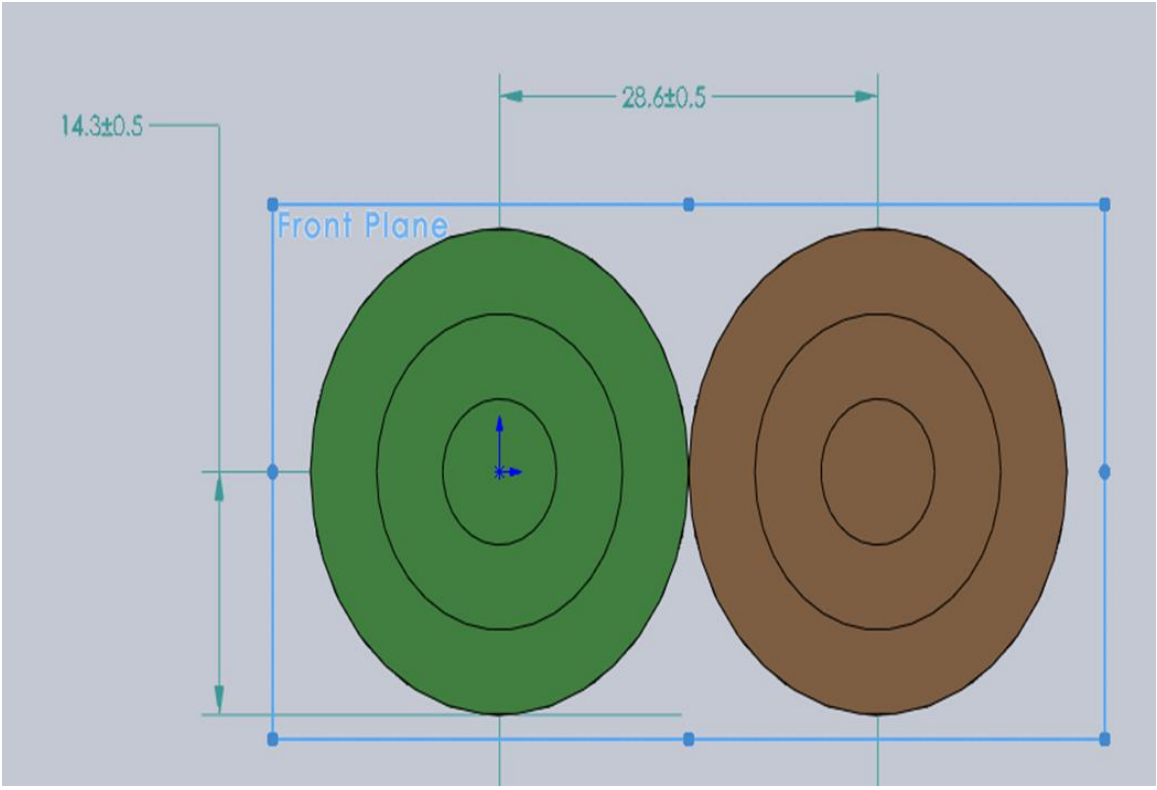

Figure 4. 27: front view of hydrogen and oxygen tanks inside the dry section (dimensions in mm)

4.6. Conclusions

The sizing and modeling of the MUN Explorer's power system were studied and simulated in this chapter. The oxygen and hydrogen tanks were successfully studied in terms of specific energy and energy density. They were also implemented in MATLAB / Simulink as compressed gas storage. The results showed that a fuel cell with hydrogen and oxygen storage options has a higher energy density than batteries alone. The system sizing by HOMER was studied and implemented. The power profiles from HOMER software were illustrated for the fuel cell and DC motor. A 1-kW fuel cell and 8 Li-ion batteries can increase the power system capacity to 36.8 kWh. Installing these options will greatly increase the hours of operation and will help the buoyancy force. The system components are simulated in MATLAB / Simulink.

Future work that builds on this chapter should improve the dynamic model in MATLAB / Simulink by including some controllers in the system. The existing power system for the MUN Explorer should be built and compared with this system (i.e. fuel cell with batteries).

References - Chapter 4

[1] N. P. B. Cai, Q., D. J. Browning, D. J. Brett, “Hybrid Fuel Cell / Battery Power Systems for Underwater Vehicles,” no. June. 2014.

[2] B. Lee, K. Park, and H. M. Kim, “Dynamic simulation of PEM water electrolysis and comparison with experiments,” Int. J. Electrochem. Sci., vol. 8, no. 1, pp. 235–248, 2013.

[3] G. C. Conference, B. J. Speranza, and P. Onsite, “The Effects of Hydrogen Purity on GC Analysis and Column Life,” 2015.

[4] A. Uluoğlu, “Solar-Hydrogen Stand-Alone Power System Design and Simulations,” no. May, 2010.

[5] K. Sopian, M. Z. Ibrahim, W. R. Wan Daud, M. Y. Othman, B. Yatim, and N. Amin, “Performance of a PV-wind hybrid system for hydrogen production,” Renew. Energy, vol. 34, no. 8, pp. 1973–1978, 2009.

[6] S. N. Motapon, A. Lupien-Bedard, L. A. Dessaint, H. Fortin-Blanchette, and K. Al-Haddad, “A Generic Electrothermal Li-ion Battery Model for Rapid Evaluation of Cell Temperature Temporal Evolution,” IEEE Trans. Ind. Electron., vol. 64, no. 2, pp. 998–1008, 2017.

[7] V. K. Kumaraswamy and J. E. Quaicoe, “Tracking techniques for the PEMFC in portable applications,” 2016 IEEE Electr. Power Energy Conf. EPEC 2016, 2016.

[8] J. Gangi and S. Curtin, “Fuel Cell Technologies Market Report 2014,” U.S. Dep.

Energy, p. 66, 2015.

[9] A. T-Raissi, A. Banerjee, and K. G. Sheinkopf, “Current technology of fuel cell systems,” Proc. Intersoc. Energy Convers. Eng. Conf., vol. 3–4, pp. 1953–1957, 1997.

[10] Ø. Hasvold, N. J. Størkersen, S. Forseth, and T. Lian, “Power sources for autonomous underwater vehicles,” J. Power Sources, vol. 162, no. 2 SPEC. ISS., pp. 935–942, 2006.

[11] E. Raugel, V. Rigaud, and C. Lakeman, “Sea experiment of a survey AUV powered by a fuel cell system,” 2010 IEEE/OES Auton. Underw. Veh. AUV 2010, pp. 1–3, 2010.

[12] A. Mendez Guevara, M. A. Herreros, and T. J. Leo, “Fuel Cell Power Systems for Autonomous Underwater Vehicles: State of the Art,” p. d001, 2014.

[13] A. Chakravarty, T. K. Nizami, and C. Mahanta, “Real time implementation of an adaptive backstepping control of buck converter PMDC-motor combinations,” 2017 Indian Control Conf. ICC 2017 - Proc., no. Icc, pp. 277–282, 2017.

[14] K. L. Davies and R. M. Moore, “‘ UUV FCEPS Technology Assessment and Design Process ,’” System, vol. 34, 2006.

[15] K. E. Swider-Lyons, R. T. Carlin, R. L. Rosenfeld, and R. J. Nowak, “Technical issues and opportunities for fuel cell development for autonomous underwater vehicles,” Proc. IEEE Symp. Auton. Underw. Veh. Technol., pp. 61–64, 2002.

[16] G. Griffiths, D. Reece, P. Blackmore, M. Lain, S. Mitchell, and J. Jamieson, “Modeling hybrid energy systems for use in AUVs,” 2005.

[17] M. Uzunoglu, O. C. Onar, and M. S. Alam, “Modeling, control and simulation of a

PV/FC/UC based hybrid power generation system for stand-alone applications," Renew. Energy, vol. 34, no. 3, pp. 509–520, 2009.

[18] H. Görgün, "Dynamic modelling of a proton exchange membrane (PEM) electrolyzer," Int. J. Hydrogen Energy, vol. 31, no. 1, pp. 29–38, 2006.

[19] G. Rigatos and P. Siano, "A PEM fuel cells control approach based on differential flatness theory," 2016 Int. Symp. Power Electron. Electr. Drives, Autom. Motion, SPEEDAM 2016, vol. 2, no. 2, pp. 1004–1009, 2016.

[20] N. M. Souleman, O. Tremblay, and L. A. Dessaint, "A generic fuel cell model for the simulation of fuel cell vehicles," 5th IEEE Veh. Power Propuls. Conf. VPPC '09, pp. 1722–1729, 2009.

[21] S. Njoya Motapon, L. A. Dessaint, and K. Al-Haddad, "A comparative study of energy management schemes for a fuel-cell hybrid emergency power system of more-electric aircraft," IEEE Trans. Ind. Electron., vol. 61, no. 3, pp. 1320–1334, 2014.

[22] Hebertt Sira-Ramirez and Ramón Silva-Ortigoza, Control Design Techniques in Power Electronics Devices. 2006.

[23] R. W. Erickson, "DC/DC power converters," Green Energy Technol., vol. 53, pp. 203–251, 2013.

[24] M. M. Shebani and T. Iqbal, "Dynamic Modeling, Control, and Analysis of a Solar Water Pumping System for Libya," J. Renew. Energy, vol. 2017, pp. 1–13, 2017.

[25] Barbir, Frano. PEM Fuel Cells Theory and Practice, Second Edition /. 2nd ed. Waltham, Mass.: Academic, 2013. Web.

Chapter 5

Dynamic Modeling and Simulation of the MUN Explorer Autonomous Underwater Vehicle with a Fuel Cell System

5.1. Chapter Overview

The actual power system of the MUN Explorer Autonomous Underwater Vehicle (*AUV*) uses 11 Lithium-ion (*Li-ion*) batteries as a main energy source. The batteries are directly connected into the BLDC motor to run the MUN Explorer for the desired operating sequence. This chapter presents a dynamic model of the MUN Explorer AUV, including a fuel cell system, to run under the same operating conditions as suggested by its manual. A PI controller was applied in the dynamic model to maintain the operating conditions such as motor speed, DC bus voltage and the load torque, due to its advantages and simple tuning technique. The MUN Explorer AUV dynamic model with a fuel cell is a proposed system to increase the power capacity. It is advantageous to use a simple controller to observe the system's behaviours. The simulation of the entire system dynamics model along with the proportional-integral (*PI*) controller is done in MATLAB / Simulink. The simulation results are included in the chapter. The DC bus voltage is measured at 48 V, and the motor speed is 20 (rad/s), which is equivalent to 190 (rpm). The power profile of the fuel cell and battery

are presented and plotted against time. The PI controller gives satisfactory results in terms of maintaining the same operating conditions of the MUN Explorer AUV with a fuel cell.

5.2. Introduction

5.2.1. Background

For the design and operations of AUVs, the control system is classified as one of the most important systems, especially when renewable energy systems are implemented on submarines, which include batteries, fuel cells, charging stations, and electrical loads. Management control schemes are used to deal with many issues, such as nonlinearities and the continuation of certain operating conditions, the number of production energy sources and load requirements[1].

Renewable energy sources, storage systems (fuel cells and batteries) as well as the energy demand of many applications such as submarines and AUV applications are essential for sustainability and the reduction of CO2 emissions. To maximize the amount of energy generated by the fuel cell and batteries, a system controller plays a significant role in generating and consuming power precisely and effectively. The energy generation should be maximised, and it should be used directly by the motors and sensors as much as possible. The goal is to reduce losses during energy transfer and conversions in the batteries and fuel cell. Moreover, the energy consumption must be as low as possible to overcome the challenges of limited energy availability in submarines working underwater[2].

A classical Proportional Integral (*PI*) controller is used in the dynamic model systems to control the main performance parameters such as the fuel cell power, battery state of charge (*SOC*), motor speed and *DC* bus voltages. Using a PI feedback controller does not require advanced knowledge to implement, and the tuning can be done online for better tracking. A PI controller is linked to a PWM, especially for fuel cell current control [3], [4].

The MUN Explorer AUV was constructed to do mapping missions of underwater depths as well as survey missions. These missions require a large amount of power in order to reach seabeds (i.e. 3000 meters). 11 rechargeable lithium-ion (*Li-ion*) batteries are carried by the MUN Explorer as the main power source, with a total capacity of 14.6 kWh to 17.952 kWh, and the Explorer can run for 10 hours [5].

Lithium-ion (*Li-ion*) batteries have been enhanced in the last ten years, and they now have higher efficiency, higher energy and power density, and lower self-discharge compared to other batteries such as NiCd, NiMH, and lead acid batteries. To ensure that the Li-ion battery is running at a suitable temperature and state of charge (*SOC*), a battery control system (*BMS*) must be implemented in the system [6].

In this specific case, the Brushless DC motor includes a rotor position sensor as well as a commutation device that has a power inverter bridge and a control circuit. These features are used to accomplish the effective control performance of the motor speed as well as the motor rotations' directions [7].

5.2.2. Literature review

Wang et al. declared that there have been only a small amount of publications dealing with the power's capability and the remaining capacity, concerning the power allocation strategy. They have developed a novel distributed energy management system based on the controller area network. They have also proposed a rule-based control strategy for the distributed energy management system to remain the capacity and the power capability of the energy storage devices. Furthermore, the Bayes Monte Carlo method is used to overcome the initial bias and noises and implemented for co-estimation of the remaining capacity and power capability of the batteries and supercapacitors [8].

Wang et al. built an energy management system for an automobile system for fuel cell, battery, and supercapacitor hybrid source, to be more efficient and manage the energy storage devices. They established an adaptive *PID* controller to regulate the oxygen excess ratio for it to reach its ideal space. This controller, with a fast response speed, smaller steady-state error, and smaller overshoot, showed better traditional feedforward control in terms of transient behaviour. Moreover, the battery and fuel cell as well as battery, supercapacitor and fuel cell hybrid source for portable systems applied an energy management strategy using a new finite state machine [9].

Wang et al. did a comparison between fuel cell, vehicle dynamics and ultracapacitor hybrid power system, along with suboptimal on-line power distribution strategies based on classical robotics and rules. They also used a dynamic programming algorithm as a benchmark to validate the effectiveness of the suggested strategies. Furthermore, the comparison was done by simulations and experiments under different working conditions,

using a semi-physical experimental platform to check the performance of the suggested power distribution approaches[10].

Wang et al. studied three different hybrid propulsion systems, which are:

1. Fuel cell and lithium-ion battery structure
2. Fuel cell and supercapacitor structure, and
3. Fuel cell, lithium-ion battery, and supercapacitor structure.

Each structure has advantages as well as disadvantages; however, the Fuel cell, lithium-ion battery, and supercapacitor structure overcome the problems in systems 1 and 2. This work improved the power dividing strategy for hybrid propulsion systems by using multiple-grained velocity prediction. In order to reach the optimal power divisions for different power sources, the dynamic programming strategy was introduced [11].

5.2.3. Chapter outline and Contributions

This chapter extends the work of the previous chapter [5] to study the dynamic model of the MUN Explorer AUV in more detail by applying a PI controller to the dynamic model with the fuel cell. This controller is implemented to achieve the operating conditions, including motor speed, DC bus voltage and the load torque, during the MUN Explorer's missions. Since the MUN Explorer has challenges related to space in the dry section, this dynamic model with a fuel cell is used to eliminate the number of batteries inside the MUN Explorer body and help the buoyancy force. However, the implementation of a PI controller is a simple approach, to observe the behaviour of the new dynamic model with a fuel cell to verified the values of the actual system of the MUN Explorer(lithium -ion batteries

only). More advanced controllers are proposed for future work. This chapter consists of four sections: The first section is the introduction. Then the second section describes the MUN Explorer power system construction and components, and the third section shows the system control with a PI controller. The fourth section is the results and discussion. The conclusion follows.

5.3. MUN Explorer Power System Construction and Components

The power system of the MUN Explorer Autonomous Underwater Vehicle is designed based on the energy and power necessities for mapping underwater depths. Figure 5.1 illustrates the main components and the most advantages location of the fuel cell. Table 5.1 shows the parameters to be implemented and achieved by using a PI controller.

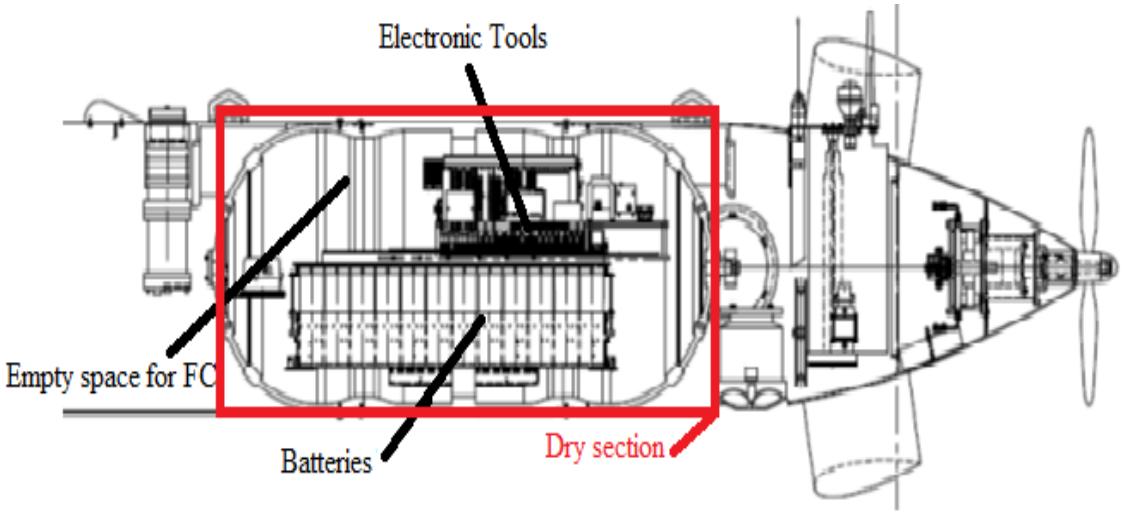

Figure 5. 1: Side view of the MUN Explorer AUV with its components

Table 5. 1: System designing parameters

Design Parameters	Value
Fuel cell power (Min. – Max.)	(600-1200) W
Battery power ((Min. – Max.)	(350- 850) W
Battery state of charge (SOC) (Min. – Max.)	(50-90) %
DC bus voltage (Min. – Max)	(47.5–50) VDC
Fuel cell current maximum	(53)A
Rotor speed	(20) rad/s

5.3.1 Hydrogen / Oxygen Tanks

The oxygen and hydrogen tanks are connected to the fuel cell to feed the required amount of oxygen and hydrogen gases. Both dynamic models of oxygen and hydrogen tanks are built based on equations 5.1 and 5.2.

$$P_b - P_{bi} = CF * \frac{N_{H_2} R T_b}{M_{H_2} V_b} \tag{5.1}$$

$$CF = \frac{P V_m}{RT} \tag{5.2}$$

All the variables in these equations are explained in the Nomenclature. The compressibility factor (*CF*) is equal to one when the pressure is less than 1.37e^7 Pa (2000 *psi*). The *CF* is more than 1 when the pressure is higher than 1.37e^7 Pa (2000 *psi*) at room temperature, which is well known as a function of temperature and pressure[12]. Equations 5.1 and 5.2 are implemented in MATLAB / Simulink and then the pressure of each tank is measured, as presented in previous work [5].

5.3.2 PEM Fuel Cell

A polymer electrolyte membrane (*PEM*) is an important feature of the selected fuel cell that is connected between the electrodes: the anode and cathode. The oxygen gas is injected in the cathode, and the hydrogen gas is injected to the anode side of the fuel cell. The overall electrochemical dynamic can be characterized by equations 5.3, 5.4 and 5.5 [13]:

Cathode: $O_2 + 4H^+ + 4e^- \leftrightarrow 2H_2O$ (5.3)

Anode: $2H_2 \leftrightarrow 4H^+ + 4e^-$ (5.4)

Overall: $2H_2 + O_2 \leftrightarrow 2H_2O + electricity + heat$ (5.5)

The mole conservation equations can be applied for the anode and cathode in any fuel cell, as shown in equations 5.6 and 5.7 [13]:

$$\frac{dP_{H2}}{dt} = \frac{RT}{V_a}[H_{2in} - H_{2used} - H_{2out}] \quad (5.6)$$

$$\frac{dP_{O2}}{dt} = \frac{RT}{V_c}[O_{2in} - O_{2used} - O_{2out}] \quad (5.7)$$

In MATLAB/ Simulink, the dynamic model of the fuel cell stack was built using a controlled voltage source in series with a constant resistance, as shown in Figure 5.4, and it has 42 cells [14].

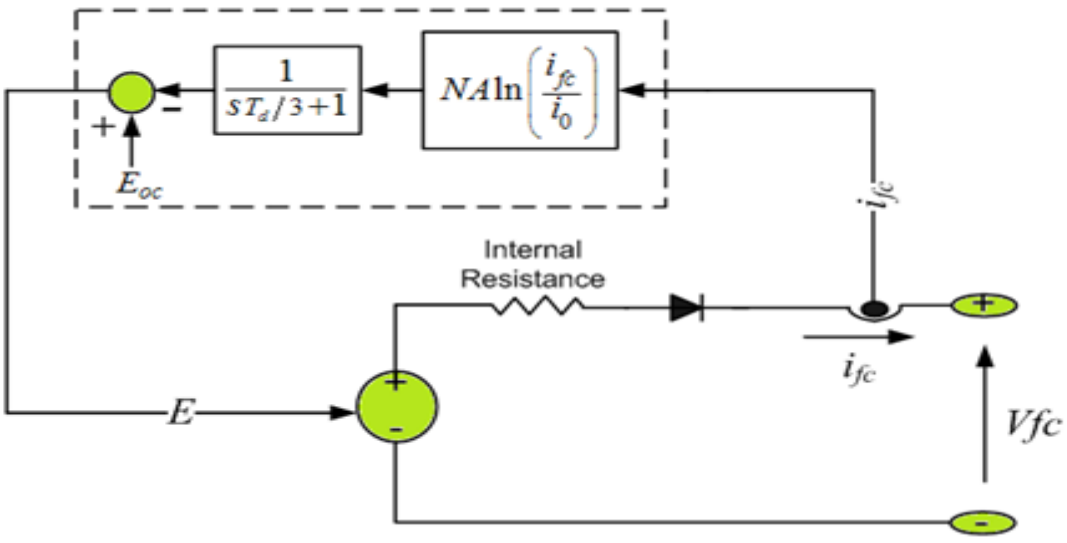

Figure 5. 2: Fuel cell stack model [14]

The controlled voltage source (*E*) can be shown by equation 5.8, so that

$$E = E_{oc} - NAln\left(\frac{i_{fc}}{i_0}\right) * \frac{1}{sT_d/3+1} \tag{5.8}$$

$$V_{fc} = E - R_{ohm} * i_{fc} \tag{5.9}$$

Equations 5.8 and 5.9 show the fuel cell voltage as a function of activation losses because of the slowness of chemical reactions at the electrode surfaces and the total fuel cell voltage, by taking into account the losses due to electrodes and electrolyte resistances (ohmic losses), respectively. To simulate the fuel cell at nominal conditions (pressure and temperature), a simplified model is used to represent a specific fuel cell stack and its parameters can be collected based on the polarization curve, which can be found in the manufacturer's datasheet. Similarly, to prevent the negative current flow into the fuel cell, a diode must be applied to the circuit [14]. Figure 5.5 shows the polarization curves (*V-I and P-I*) from the simulation results, and Figure 5.6 illustrates the polarization curves (*V-I and P-I*) from the data sheet behaviour. Both curves, the simulations, and the

manufacturer's data sheet results, are almost identical. The fuel cell polarization curves' characteristics are defined at sea level and ambient room temperature as the baseline of operating conditions.

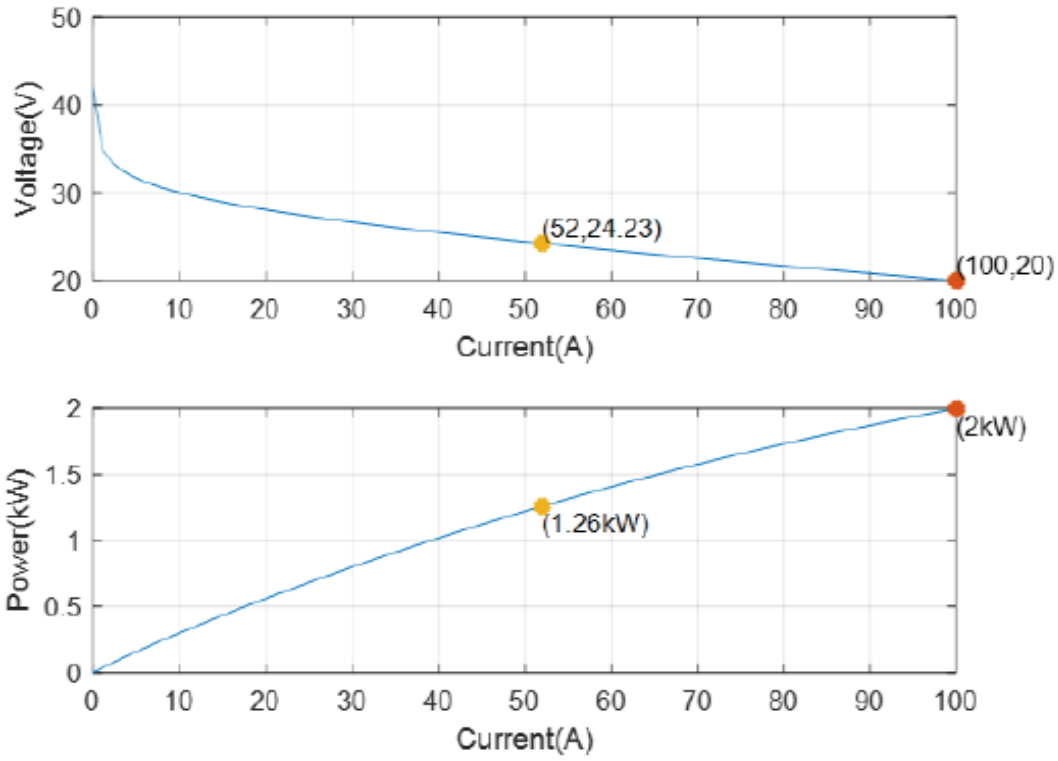

Figure 5. 3: Polarization curves, voltage vs current and power vs current from simulation results [5]

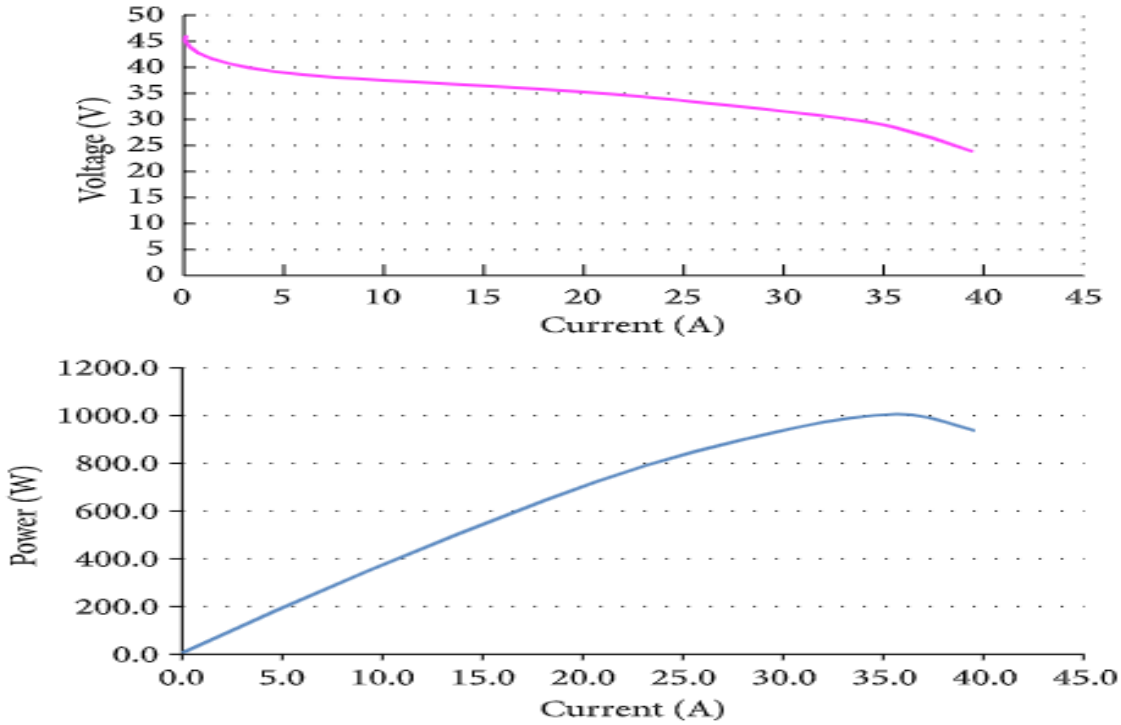

Figure 5. 4: Polarization curves, voltage vs. current and power vs. current from data sheet results[5]

5.3.3 Lithium-Ion Battery

The dynamic model of a Li-ion battery is programmed in MATLAB / Simulink, based on a modified Shepherd curve-fitting model [4]. To ensure the better representation of the battery's SOC effect on the battery performance, the voltage polarization term was added to the battery discharge voltage expression. The filtered battery current is applied as a replacement of the actual battery current for the polarization resistance, solely to improve the simulation stability. The model has two Equations for discharging and charging, as follows [4]:

Discharge Model when i^* is greater than Zero

$$V_{batt} = E_0 - K\frac{Q}{Q-it}\cdot i^* - K\cdot\frac{Q}{Q-it}\cdot it + A\cdot exp(-B\cdot it) - R_b.I \quad (5.10)$$

Charge Model when i^* is less than Zero

$$V_{batt} = E_0 - K.\frac{Q}{it+0.1Q} \cdot i^* - K \cdot \frac{Q}{Q-it} \cdot i + A \cdot \exp(-B \cdot it) \quad (5.11)$$

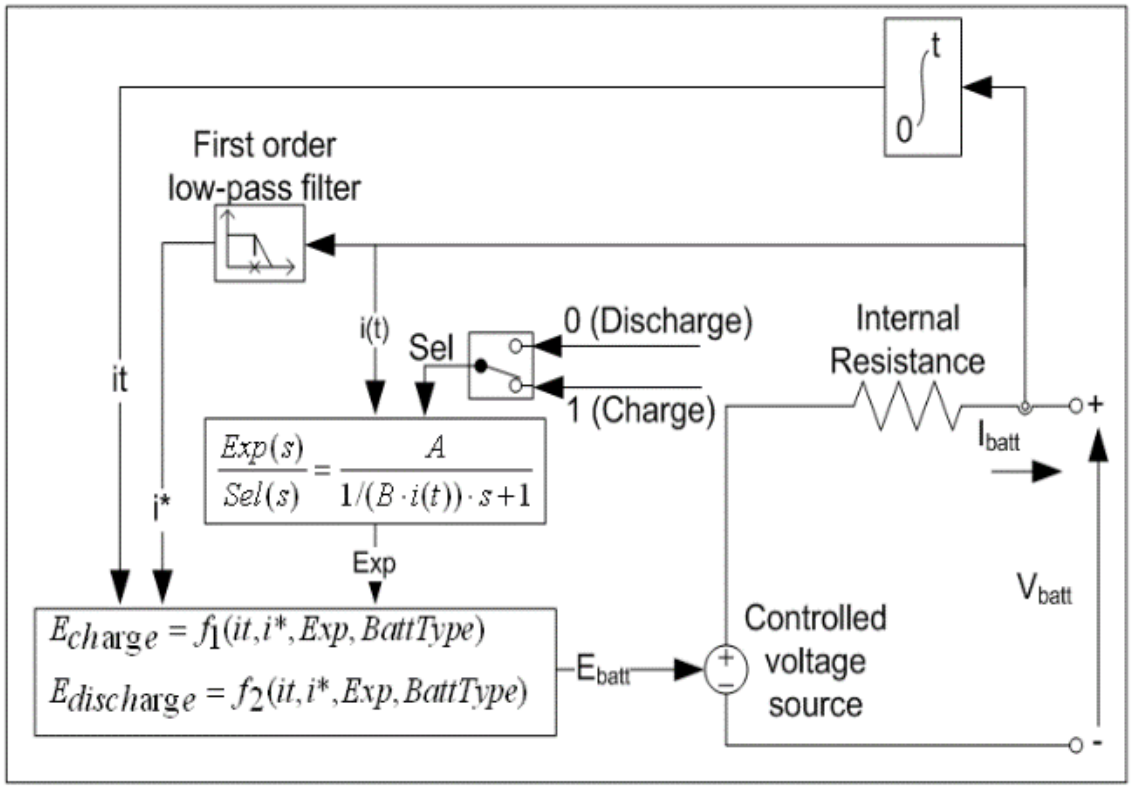

Figure 5. 5: Dynamic model for Li- ion battery [5]

Figure 5.7 demonstrates the dynamic model for a Li-ion battery in MATLAB / Simulink. From the dynamic model, the discharge and charge mode has been calculated to obtain the output voltage from the battery. The variables in equations 5.10 and 5.11 are explained in the Nomenclature section. The simulation discharge curves for the Li-ion battery system (i.e. 48 *V* and 34 *Ah*) are shown in Figure 5.8. Some coefficients are calculated and known by the voltage and ampere-hour curve. This curve also represents the

discharge behaviour and the nominal area with exponential, to better understand the harmless operating strategy to increase the lifetime of the battery.

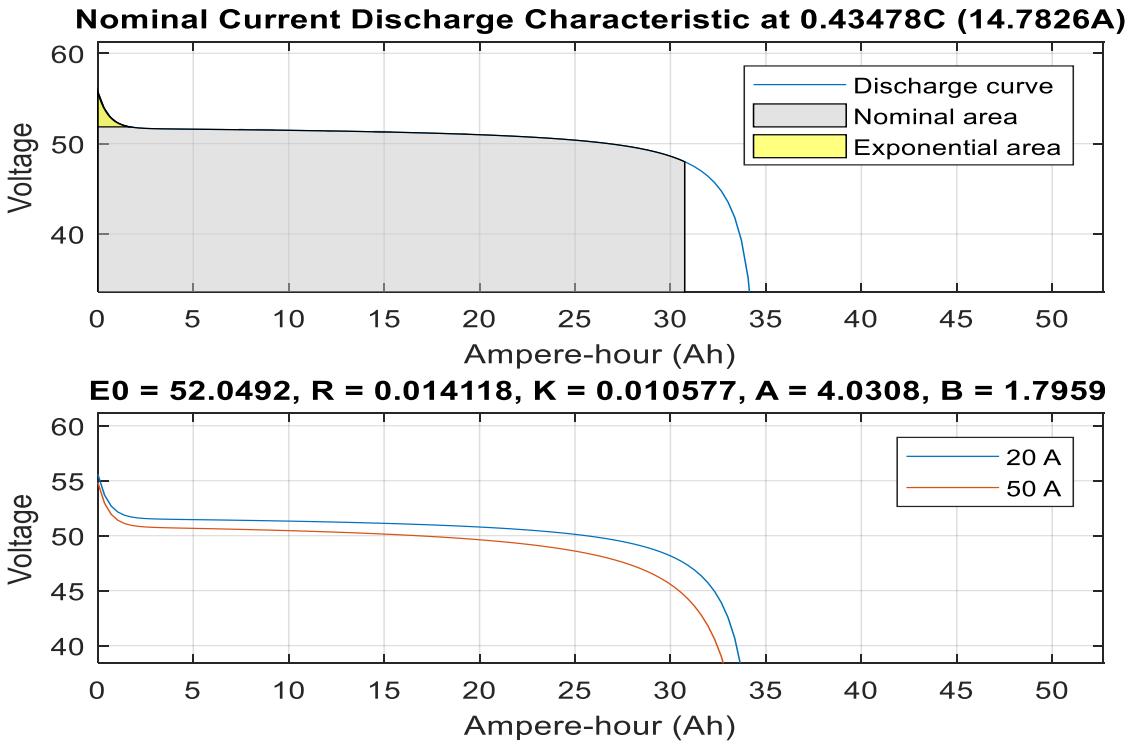

Figure 5. 6: Simulation discharge curves for the Li-ion battery[5]

5.3.4 Brushless DC Motor

A brushless DC motor can be defined as a self-synchronous rotating motor; it has a rotor with a permanent magnet [7]. To control the electronic commutation and rotor position signal, the commutation circuit on the ontology of the motor can be installed independently or integrated into it. The main components of the BLDC motor are the stator with its armature winding and the rotor with a permanent magnet pole, which are very similar to the permanent magnet synchronous motor[7]. The electromagnetic torque model

for the BLDC motor can be represented by equation 5.12, and the dynamic motion can be obtained by equation 5.13 [15].

$$T_e = \frac{1}{\omega_r}(e_a i_a + e_b i_b + e_c i_c) \tag{5.12}$$

$$\frac{d}{dt}\omega_r = \frac{1}{J} * (T_e + T_L + B\omega_r) \tag{5.13}$$

The MUN Explorer uses a propulsion system that has two standard blades (Wageningen B-series propeller type that is 0.65 m in diameter). A BLDC motor is used to drive the propulsion system. Figure 5.9 shows the schematic of the BLDC motor for the MUN Explorer. Table 5.2 shows the parameters of the BLDC motor, which are entered into the brushless DC motor in a MATLAB /Simulink block. These parameters are collected and verified using the MUN Explorer AUV data sheet.

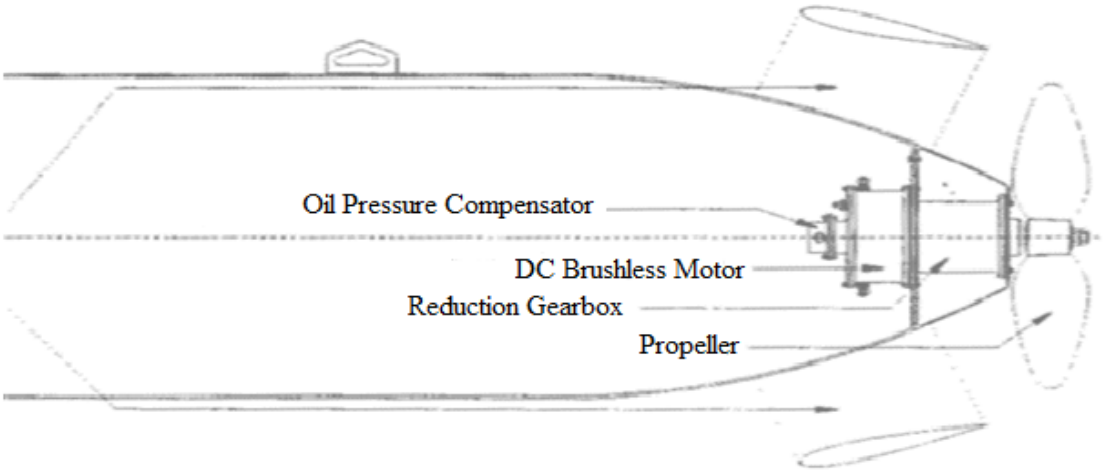

Figure 5. 7: Schematic of the BLDC motor for the MUN Explorer

Table 5. 2 : BLDC motor parameters

Parameters	Value	Unit
Voltage	48	V
Resistance	0.2	Ohms
Inductance	8.5e-3	H
Friction Factor	0.005	N.m/A
Inertia J	0.089	Kg.m^2
Back EMF	120	Degrees

5.4. System Control with a PI Controller

The control system is important to maintain certain operating conditions, such as control of the motor speed, reduction of hydrogen gas consumption and improvement of overall system efficiency. These conditions can be maintained by controlling the power outcome of the *PEM* fuel cell and the battery to the BLDC motor through the convertors, using a PI controller.

In [4], the *PI* controller is implemented based on the battery's SOC behaviour, so the PI regulator output is defined (in this case) as the battery power by removing it from the load power to get the fuel cell reference power. When the power of the fuel cell is reduced, the battery's state of charge is above the reference value, which means the battery reaches its full power. When the battery *SOC* is less than the reference value, the fuel cell delivers almost the entire load power. This controller can be tuned easily to get an acceptable response, compared to the other controller. The main function of this controller is to meet the parameters shown in Table 5.1. The dynamic model system using the PI controller is implemented and illustrated in MATLAB/Simulink, as shown in Figure 5.10. The output from the PI controller is the maximum current of the fuel cell that is fed into the

convertor to maintain 48 *VDC*. The two blue boxes are the minimum voltage (47.5 *V*) and the maximum voltage (52 *V*) to give the controller more flexibility for maintaining the desired value (48 *VDC*).

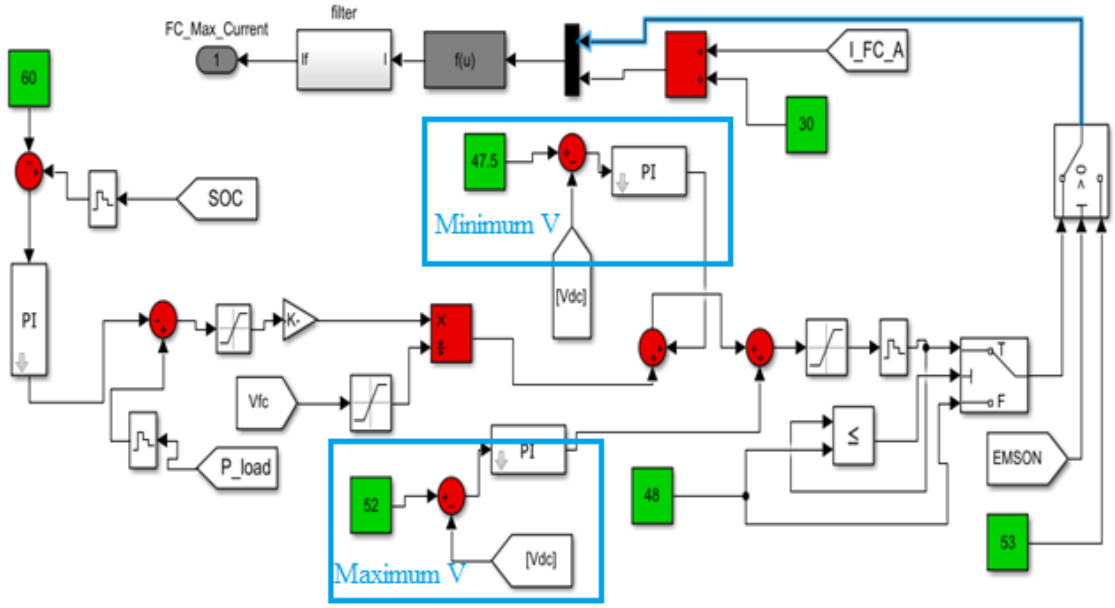

Figure 5. 8: The PI controller for the maximum fuel cell current[4]

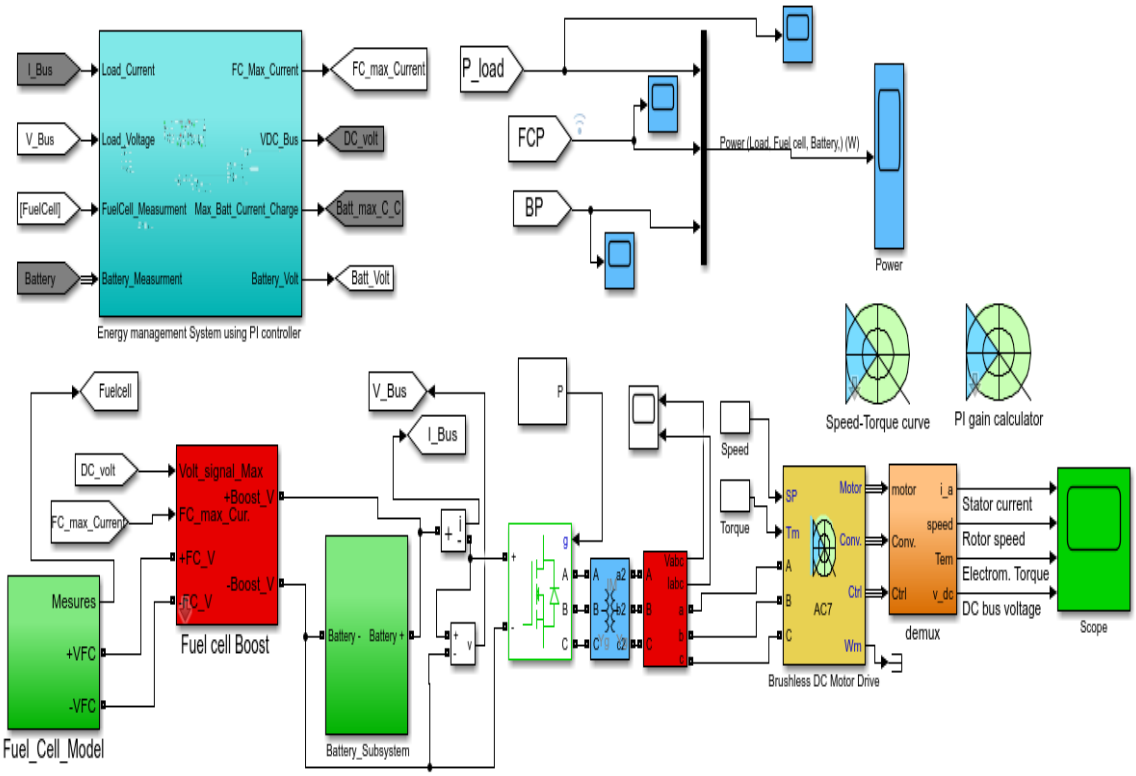

Figure 5. 9: Complete system in MATLAB/ Simulink

The minimum and maximum voltage value represent the allowable voltage range to charge the battery with less harmful effects. If the battery exceeds these values, an explosion and damage can occur. Finally, in MATLAB / Simulink, the complete system was created and modified to show the dynamic model system using the *PI* controller, as shown in Figure 5.11. The main components of the system are the fuel cell system with oxygen and hydrogen tanks, a Li-ion battery, the *BLDC* motor and the energy management block, which controls the output parameters of each block and maintains the parameters shown in Table 5.1. The auxiliary components are boost converters, buck converters, the universal bridge, the speed-torque curve, and the PI gain calculator.

5.5. Results and Discussion

The integration of the fuel cell into the existing battery power system plays a significant role in running the MUN Explorer *AUV* under the desired and proper operating conditions. To maintain these conditions, an energy management system using a PI controller has been implemented into the dynamic model of the MUN Explorer. Figure 5.11 explains the block connections of the complete model with the PI controller energy management system in MATLAB/Simulink. Figure 5. 12 shows the relationship between the load torque and motor speed. This curve can be generated from the Speed-Torque block in Figure 5.11. The Y-axis shows the load torque applied to the motor, and the X-axis represents the speed of the motor. The limits of the operating region illustrate the maximum load torque by which the motor can maintain the desired speed at 20 (rad/s). The yellow region shows the load torque in acceleration, and the gray region illustrates the speed in steady-state operation.

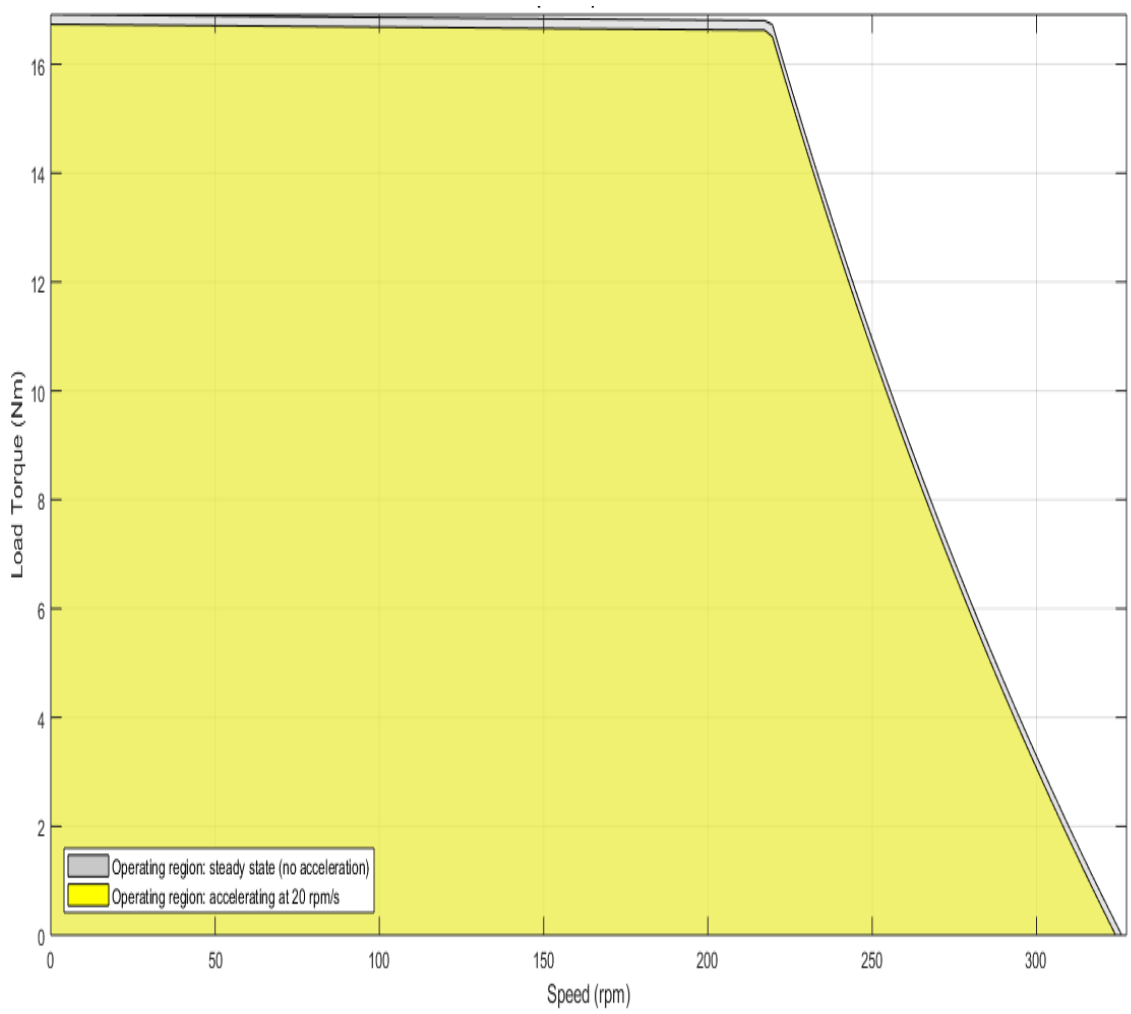

Figure 5. 10: Load torque versus speed motor

The BLDC motor was able to achieve the operating conditions by controlling the torque and speed and maintaining them at the desired points. The curve between the load torque and speed is plotted to illustrate the operating point in the region. The input power of the BLDC motor is decreased when the power of the battery and fuel cell also decrease. Since the fuel cell and battery are directly connected to the BLDC motor, the dropping power causes the mechanical output torque to decrease too. Since the stator current is

proportional to the torque, the stator current is also decreased. The rotor speed is decreased when the input power decreases.

Figure 5.13 shows the simulation results for the stator current, rotor speed, electromagnetic torque and DC bus voltage. From the results, the stator current value is varying between 10 and –10 A, and the rotor speed (*wm*) is 20 rad/s, which is equivalent to 190 (*rpm)*. These values are verified and confirmed by the MUN Explorer manufacturer's data sheet. The electromagnetic torque (*Tem*) is also changing from (10 to -10) N-m. The DC bus voltage has 48 V, which verifies the motor drive voltage. Moreover, there is also a jump of the four physical quantities (stator current, rotor speed, electromagnetic torque and DC bus voltage) due to the fuel cell dynamics and starting points. As noted by the manufacturer of the fuel cell, it takes the cell up to 20 seconds to be turned on and generate the voltage.

The power profile for the load, fuel cell and the battery are illustrated in Figure 5.14. The blue result shows the load power (*W*), which represents the BLDC motor load. Similarly, the red and yellow results show the power profile (*W*) for the fuel cell and battery, respectively. The results illustrate that the fuel cell and battery power follow the load demand, and then the battery power decreases to let the fuel cell generate the maximum power.

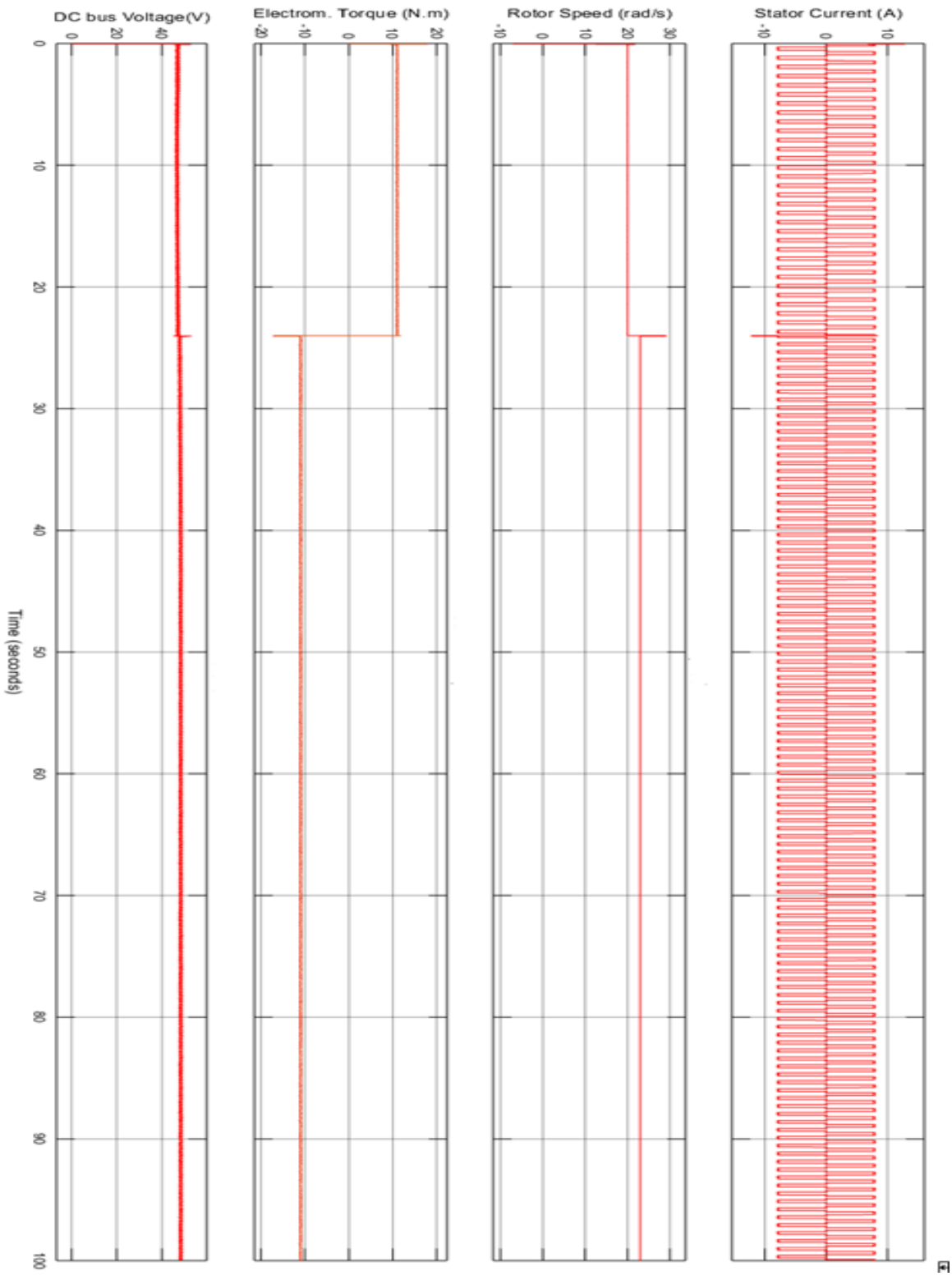

Figure 5. 11: Simulation results for stator current, rotor speed, electromagnetic torque, and DC bus voltage

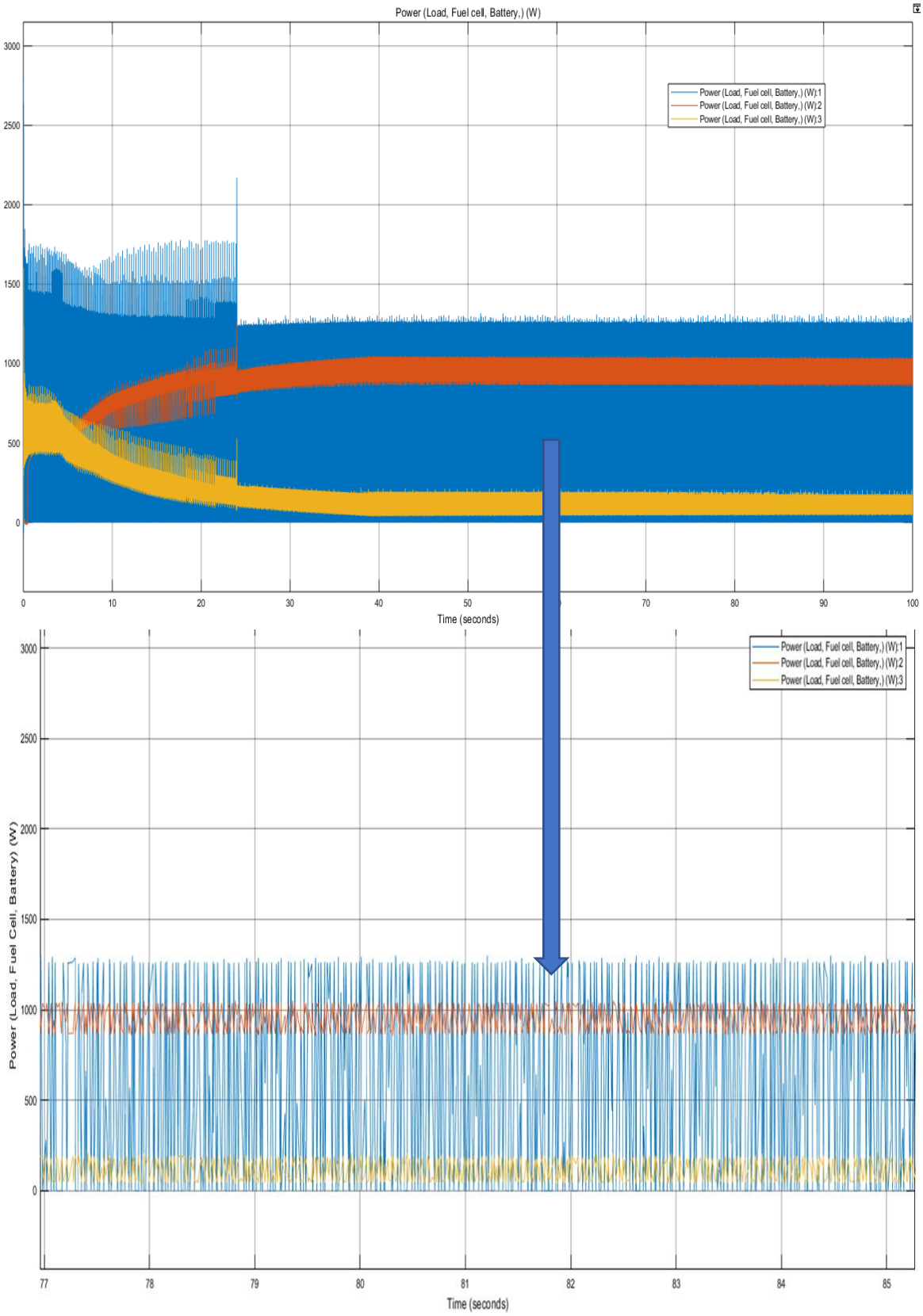

Figure 5. 12: Power profile for the load, fuel cell and the battery in (W)

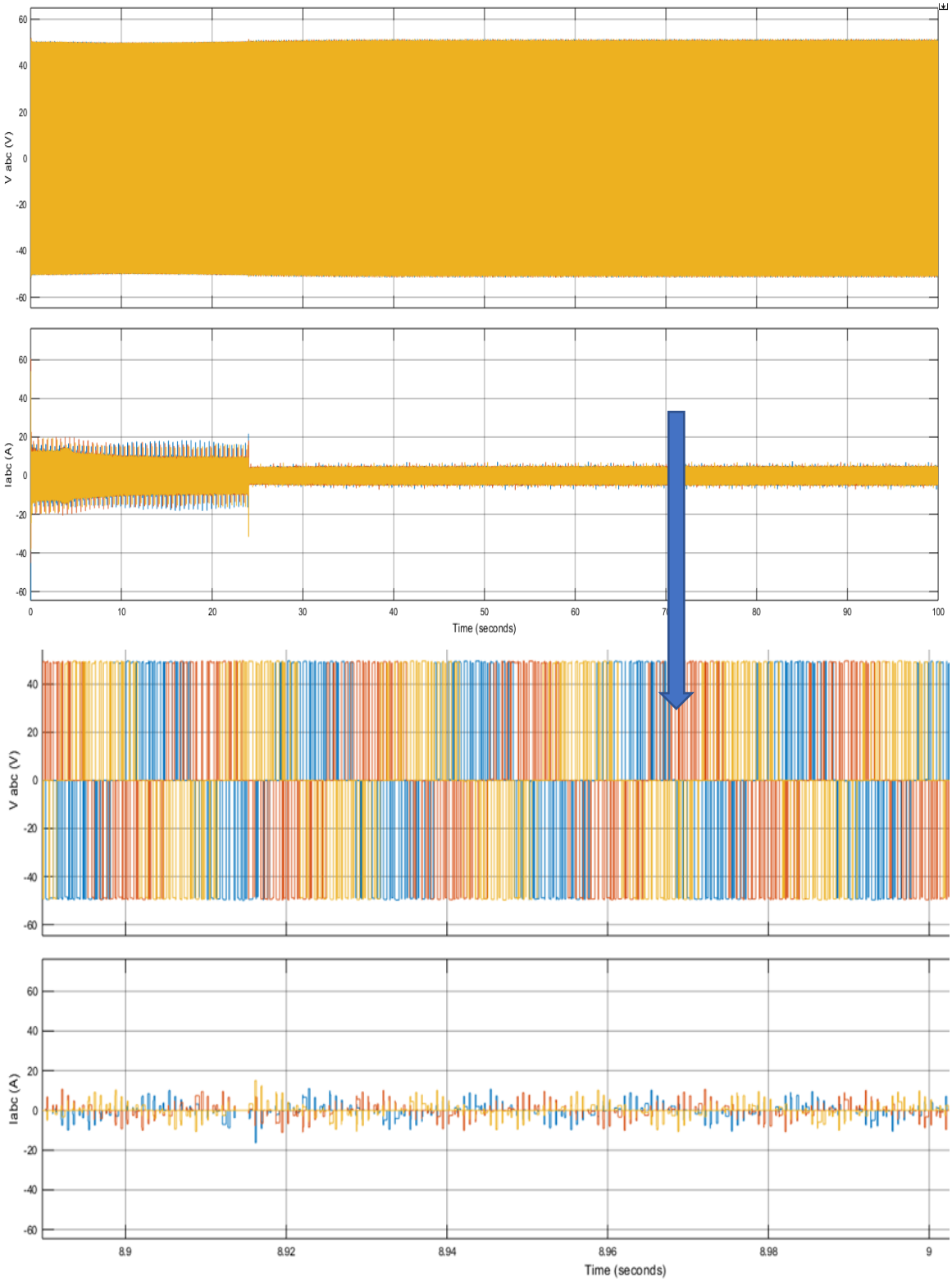

Figure 5. 13: Three-phase voltage and current measurements

Each power profile is plotted in a separate figure that can be seen in the appendix number five (Page number 153-154). From the figures, the changing in the power profile from 20 sec to 30 sec is caused by the fuel cell's starting operating points, due to the dynamic characteristic behaviour.

The simulation runs for 100 (seconds) to ensure the values of Table 5.1 are met and verified. It should have been run for 3600 seconds (1 hr) or at least 1800 seconds (30 min), but the lack of memory prevents it from achieving these times. Figure 5.15 shows the three-phase voltage and current measurements of the model. As seen in Figure 5.15, the results show good agreement in terms of voltage and current measurements.

The hydrogen fuel consumption is illustrated in Figure 5.16. It shows the fuel consumption increase over time. To meet the proposed values in Table 1, the control system using the PI controller is implemented and studied. The classical PI control results show that the battery discharges faster in order to reach the SOC reference point, whereas the fuel cell provides almost all the load power and recharges the battery. The PI controller provides a good result to meet the power requirements, but these results can be improved by implementing a different controller such as a Fuzzy-Logic Controller (*FLC*). An *FLC* will give better results, as documented in the literature.

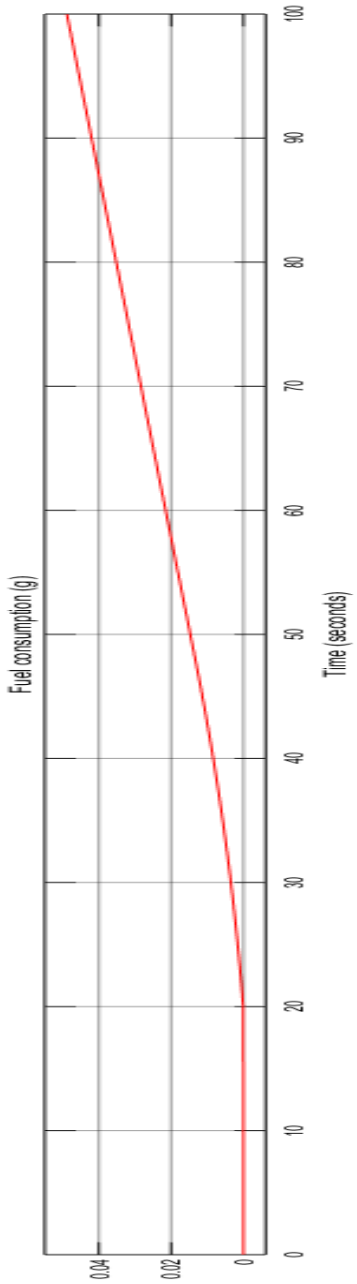

Figure 5. 14: Hydrogen fuel consumption (g)

5.6. Conclusion

The control system using a *PI* controller for the MUN Explorer Autonomous Underwater Vehicle's power system was studied and implemented in this chapter. To ensure that the MUN Explorer ran efficiently and smoothly, some power requirements were imposed and studied, as shown in Table 1. The power profiles for the fuel cell and battery were presented and discussed, as well as the power load profile. All the data for the *BLDC* motor and battery were collected and applied from the manufacturer's data sheet to meet the exact same operating conditions. The *PI* controller showed good results in terms of the response. The *DC* bus voltage was measured at 48 *V*, and the motor speed was 20 (*rad/s*), which is equivalent to 190 (*rpm*). The system components were simulated in MATLAB / Simulink. The *PI* controller is simple to be implemented into the proposed system and easily tuned.

Future work that builds on this research should implement other types of controllers, such as Fuzzy logic controllers or state machine controllers. A Fuzzy controller would be the best choice for such a system. Other future work could experiment with this model to verify the simulation results.

References - Chapter 5

[1] M. Cirrincione *et al.*, "Intelligent energy management system," *IEEE Int. Conf. Ind. Informatics*, no. May 2014, pp. 232–237, 2009.

[2] G. Barchi, G. Miori, D. Moser, and S. Papantoniou, "A Small-Scale Prototype for the Optimization of PV Generation and Battery Storage through the Use of a Building Energy Management System," *Proc. - 2018 IEEE Int. Conf. Environ. Electr. Eng. 2018 IEEE Ind. Commer. Power Syst. Eur. EEEIC/I CPS Eur. 2018*, pp. 1–5, 2018.

[3] V. K. Kumaraswamy and J. E. Quaicoe, "Tracking techniques for the PEMFC in portable applications," *2016 IEEE Electr. Power Energy Conf. EPEC 2016*, pp. 1–6, 2016.

[4] S. Njoya Motapon, L. A. Dessaint, and K. Al-Haddad, "A comparative study of energy management schemes for a fuel-cell hybrid emergency power system of more-electric aircraft," *IEEE Trans. Ind. Electron.*, vol. 61, no. 3, pp. 1320–1334, 2014.

[5] M. M. Albarghot, M. T. Iqbal, K. Pope, and L. Rolland, "Sizing and Dynamic Modeling of a Power System for the MUN Explorer Autonomous Underwater Vehicle Using a Fuel Cell and Batteries," *J. Energy*, vol. 2019, pp. 1–17, 2019.

[6] S. N. Motapon, A. Lupien-Bedard, L. A. Dessaint, H. Fortin-Blanchette, and K. Al-Haddad, "A Generic Electrothermal Li-ion Battery Model for Rapid Evaluation of Cell Temperature Temporal Evolution," *IEEE Trans. Ind. Electron.*, vol. 64, no. 2, pp. 998–1008, 2017.

[7] W. Xie, J. S. Wang, and H. B. Wang, "PI Controller of Speed Regulation of Brushless DC Motor Based on Particle Swarm Optimization Algorithm with Improved Inertia Weights," *Math. Probl. Eng.*, vol. 2019, 2019.

[8] Y. Wang, Z. Sun, and Z. Chen, “Development of energy management system based on a rule-based power distribution strategy for hybrid power sources,” *Energy*, vol. 175, pp. 1055–1066, 2019.

[9] Y. Wang, Z. Sun, and Z. Chen, “Energy management strategy for battery/supercapacitor/fuel cell hybrid source vehicles based on finite state machine,” *Appl. Energy*, vol. 254, no. August, p. 113707, 2019.

[10] Y. Wang, Z. Sun, X. Li, X. Yang, and Z. Chen, “A comparative study of power allocation strategies used in fuel cell and ultracapacitor hybrid systems,” *Energy*, vol. 189, p. 116142, 2019.

[11] Y. Wang, X. Li, L. Wang, and Z. Sun, “Multiple-grained velocity prediction and energy management strategy for hybrid propulsion systems,” *J. Energy Storage*, vol. 26, no. August, 2019.

[12] H. Görgün, “Dynamic modelling of a proton exchange membrane (PEM) electrolyzer,” *Int. J. Hydrogen Energy*, vol. 31, no. 1, pp. 29–38, 2006.

[13] G. Rigatos and P. Siano, “A PEM fuel cells control approach based on differential flatness theory,” *2016 Int. Symp. Power Electron. Electr. Drives, Autom. Motion, SPEEDAM 2016*, vol. 2, no. 2, pp. 1004–1009, 2016.

[14] N. M. Souleman, O. Tremblay, and L. A. Dessaint, “A generic fuel cell model for the simulation of fuel cell vehicles,” *5th IEEE Veh. Power Propuls. Conf. VPPC ’09*, pp. 1722–1729, 2009.

[15] S. Geraee, M. Shafiei, A. R. Sahami, and S. Alavi, “Position sensorless and adaptive speed design for controlling brushless DC motor drives,” *2017 North Am. Power Symp. NAPS 2017*, 2017.

Chapter 6

Conclusion, Contributions and Future Work

6.1. Introduction

Integration of the fuel cell with batteries is an important factor in portable power systems and applicable for many applications, such as electric cars and autonomous underwater vehicles. Two major challenges facing these applications are the limited spaces and heavy weights.

The significance of deploying the MUN Explorer AUV in many different locations to do surveying missions makes it an important topic for research. The need for integration to improve its power system and to overcome some of the limitations of the MUN Explorer AUV has motivated me to contribute to this application by developing a new sizing and dynamic model of the fuel cell with batteries.

In this research, the integration of the PEM fuel cell into existing lithium- ion batteries and hydrogen / oxygen production are addressed by focusing on different areas such as solar energy hydrogen generation; wind energy hydrogen production; sizing the new power system for the Explorer; building the dynamic model for the new power system in MATLAB /Simulink; and maintaining the operating conditions for the MUN Explorer, including motor speed, DC bus voltage and the load torque.

6.2. Conclusion

In this thesis, an investigation of a new dynamic model, approaches and integration have been studied to estimate and manage the MUN Explorer AUV power system. Some of the challenges of the existing MUN Explorer power system have been explored and mitigated. A Fuel Cell Energy / Power System (FCEPS) is used to power the propulsion system of an Unmanned Underwater Vehicle (UUV) application, which has the potential to significantly increase the energy storage in a UUV, compared to the use of rechargeable batteries [1].

The significance of the data collection from the seabed motivates the Responsive AUV Localization and Mapping (REALM) project, which is supported by Memorial University and others, to invest in and improve advanced AUV navigation and performance by developing solutions and enhancements. This thesis is focused on the same direction, to improve the power system of the MUN Explorer by enhancing and increasing the power system capacity. The proposed power system is sized by HOMER software and the dynamic model is built in MATLAB / Simulink to observe the systems behaviour and shows close results between the old and the proposed system. This thesis is also focused on hydrogen / oxygen gas production from renewable energy sources, as well as battery recharge to complete a certain mission. The proposed system of the MUN Explorer has increased the power capacity from 17.952 kWh to 36.8 kWh. The results from hydrogen production systems (solar and wind) is measured to be 7.0 ml/min.

Finally, this thesis provides and contributes to the MUN Explorer AUV application by enhancing a variety of solutions in terms of power capacity and reducing some components as well as augmenting the industry applications. Yet, some of the challenges cannot be resolved, due to the lack of equipment and financial support, such as of implementation the proposed dynamic model system into the actual the MUN Explorer AUV. The information and data presented in this thesis are beneficial and can be used for similar applications.

6.3. Contributions

This research contributions are achieved and listed as following,

1. Solar energy hydrogen production is investigated experimentally and from simulation.
2. Wind energy hydrogen production is investigated experimentally and from simulation.
3. A PEM Fuel Cell is integrated into an AUV existing power system.
4. A new AUV power system is sized and created using HOMER and MTLAB / Simulink.
5. A PI controller is applied to maintain the MUN Explorer operating conditions for the MUN Explorer.

6.4. Recommendations for Future Research Work

In this dissertation, the developments of new approaches and findings have been investigated and have enhanced / extended the MUN Explorer's power and energy system capacity. Some of the recommendations and potential future work are discussed below:

1. Hydrogen production was generated from small renewable energy sources' equipment and the hydrogen and oxygen stored in small tanks. The model can be improved and extended by having a larger scale in order to obtain more results and run for a longer time.
2. In this thesis, the proposed power system of the MUN Explorer AUV is sized and the dynamic model is built in MATLAB/ Simulink. However, the experimental set-up is highly recommended to give more validated results.
3. The MUN Explorer AUV is owned by the Responsive AUV Localization and Mapping (REALM) project, supported by the Atlantic Canada Opportunities Agency Atlantic Innovation Fund, Research & Development Corporation Newfoundland and Labrador, Fugro GeoSurvey's Inc. and Memorial University of Newfoundland. It would be helpful to expand its availability, in order to apply this research to the actual MUN Explorer AUV.
4. The AUV is working under specified operating conditions to complete its mission. In this thesis, the PI controller is implemented in the proposed dynamic model in order to maintain these conditions. However, it is highly recommended to implement other controllers such as Fuzzy logic.

6.5. A List of Publications and Co-Authorship Statement

I, Mohamed Albarghot, take a primary author status for all the chapters in this thesis. Yet, each manuscript is co-authored by my supervisors and colleagues, whose contributions have assisted the development of this thesis as illustrated below.

- **Albarghot, M. and Rolland, L., 2016, October. MATLAB/Simulink modelling and experimental results of a PEM Electrolyzer powered by a solar panel. In 2016 IEEE Electrical Power and Energy Conference (EPEC) (pp. 1-6). IEEE.**

Statement: I am the primary author and have done most of the simulation and experimental analysis. I have drafted the manuscript and included all the comments after review from the co-author in the final manuscript. As co-author, Luc Rolland helped in providing the experimental equipment, reviewed the model and results. He also contributed in reviewing and revising the manuscript.

- **Albarghot, M., Sasi, M. and Rolland, L., 2016. MATLAB/Simulink Modeling and Experimental Results of a PEM Electrolyzer Powered by a Solar Panel. Journal of Energy and Power Engineering, 10, pp.779-785.**

Statement: I am the primary author and I did the simulation and experimental work. I prepared the manuscript and included all the comments after review from the co-author in the final manuscript. As co-author, Mahmud Sasi helped with the registration fees. As co-author, Luc Rolland supplied the experimental equipment evaluated the model and results. He also contributed in reviewing and modifying the manuscript.

- **Albarghot, M. and Rolland, L., 2017, June. Comparison of experimental results with simulation of a PEM Electrolyzer powered by a horizontal wind turbine. In 2017 International Conference of Electrical and Electronic Technologies for Automotive (pp. 1-6). IEEE.**

Statement: I am the primary author and have done the simulation and experimental setup. I have outlined the manuscript and included all the comments after review from the co-author in the final manuscript. As co-author, Luc Rolland helped in providing the experimental equipment reviewed the model and results. He also contributed to the review and revision of the manuscript.

- **Albarghot, M.M., Iqbal, M.T., Pope, K. and Rolland, L., 2019. Sizing and Dynamic Modeling of a Power System for the MUN Explorer Autonomous Underwater Vehicle Using a Fuel Cell and Batteries. Journal of Energy, 2019.**

Statement: I am the primary author and have done the sizing of the system in HOMER software and the dynamic modeling simulation in MATLAB / Simulink. I have written the manuscript and included all the comments after review from co-authors in the final manuscript. As co-author, Tariq Iqbal helped in sizing techniques, reviewed the model and results, and co- authors Kevin Pope and Luc Rolland also contributed to the review and revision of the manuscript.

- **Albarghot, M.M., Iqbal, M.T., Pope, K. and Rolland, L., 2020. Dynamic modeling and simulation of the MUN Explorer autonomous underwater vehicle with a fuel cell system. AIMS Electronics and Electrical Engineering, 4(1), p.114.**

Statement: I am the primary author and created the dynamic modeling for the simulation in MATLAB/ Simulink. I have written the manuscript and included all the comments after review from co-authors in the final manuscript. As co-author, Tariq Iqbal helped in managing ideas, reviewed the model and results. He also contributed in reviewing and revising the manuscript. As co-author, Kevin Pope helped in revising and reviewing the manuscript. As co-author, Luc Rolland assisted in modifying and evaluating the manuscript.

Mohamed Musbah Albarghot

References – Chapter 6

[1] K. L. Davies and R. M. Moore, "‘ UUV FCEPS Technology Assessment and Design Process ,’" *System*, vol. 34, 2006.

Appendixes

Appendix -Chapter 1

Figure number 1 references:

1) https://www.google.com/search?q=wind+turbine+symbol&source=lnms&tbm=isch&sa=X&ved=2ahUKEwjigpfDupfnAhVRCM0KHX8ZBNwQ_AUoAXoECA0QAw&biw=1366&bih=608#imgrc=jq3_Fk7JCq403M:
2) https://www.google.com/search?biw=1366&bih=608&tbm=isch&sa=1&ei=02IoXq2yIou1tAa9z7TgDg&q=isolated+dc+dc+converter+symbol&oq=dc+dc+converter+symbol+&gs_l=img.1.1.0i30j0i5i30j0i8i30.11660.11660..21136...0.0..0.126.475.0j4.....0....1..gws-wiz-img.....0j0i7i30.nV6cVc9nN3U#imgrc=aAosyB_M9LuutM:
3) https://www.google.com/search?biw=1366&bih=657&tbm=isch&sa=1&ei=c7UUXteWLIa5tQb54Jow&q=electrolyzer+symbol&oq=electrolyzer+symbol&gs_l=img.12..0.30635081.30643085..31424068...0.0..0.142.1610.0j13.....0....1..gws-wiz-img.....0i67j0i7i30j0i7i10i30j0i10.Url130a-ykQ&ved=0ahUKEwiXnPTt9_HmAhWGXM0KHXmwBgYQ4dUDCAc#imgrc=0dfE9-lgmz5mfM:
4) https://www.powerelectronicsnews.com/wp-content/uploads/2016/06/Technique-improves-efficacy-of-fuel-cells.gif?fit=657%2C456
5) https://ca.images.search.yahoo.com/search/images?p=lituim+ion+battery+symble&fr=mcafee&imgurl=https%3A%2F%2Fmedia.istockphoto.com%2Fvectors%2Fliion-car-battery-icon-lithiumion-symbol-vector-vector-id995535630%3Fk%3D6%26m%3D995535630%26s%3D612x612%26w%3D0%26h%3D7k14r38ZUQ10Ru6orBCEDEg5WKi6vStrMcfftpt2PRQ%3D#id=4&iurl=https%3A%2F%2Fmedia.istockphoto.com%2Fvectors%2Fliion-car-battery-icon-lithiumion-symbol-vector-vector-id995535630%3Fk%3D6%26m%3D995535630%26s%3D612x612%26w%3D0%26h%3D7k14r38ZUQ10Ru6orBCEDEg5WKi6vStrMcfftpt2PRQ%3D&action=click
6) https://www.google.com/search?biw=1366&bih=657&tbm=isch&sa=1&ei=OxQWXtqCO6GvggfrgbeQDg&q=brushless+DC+motors+symbel+&oq=brushless+DC+motors+symbel+&gs_l=img.3...9594.22419..23220...4.0..0.151.1438.9j5.....0....1..gws-wiz img.....0i67j0i7i30j0i8i30j0i24j0i10i24j0i5i30j0i30.yVtvVbTPyPM&ved=0ahUKEwiajICyxvTmAhWhl-AKHevADeIQ4dUDCAc&uact=5#imgrc=7jPyYxcZYixoZM:

Appendix -Chapter 2

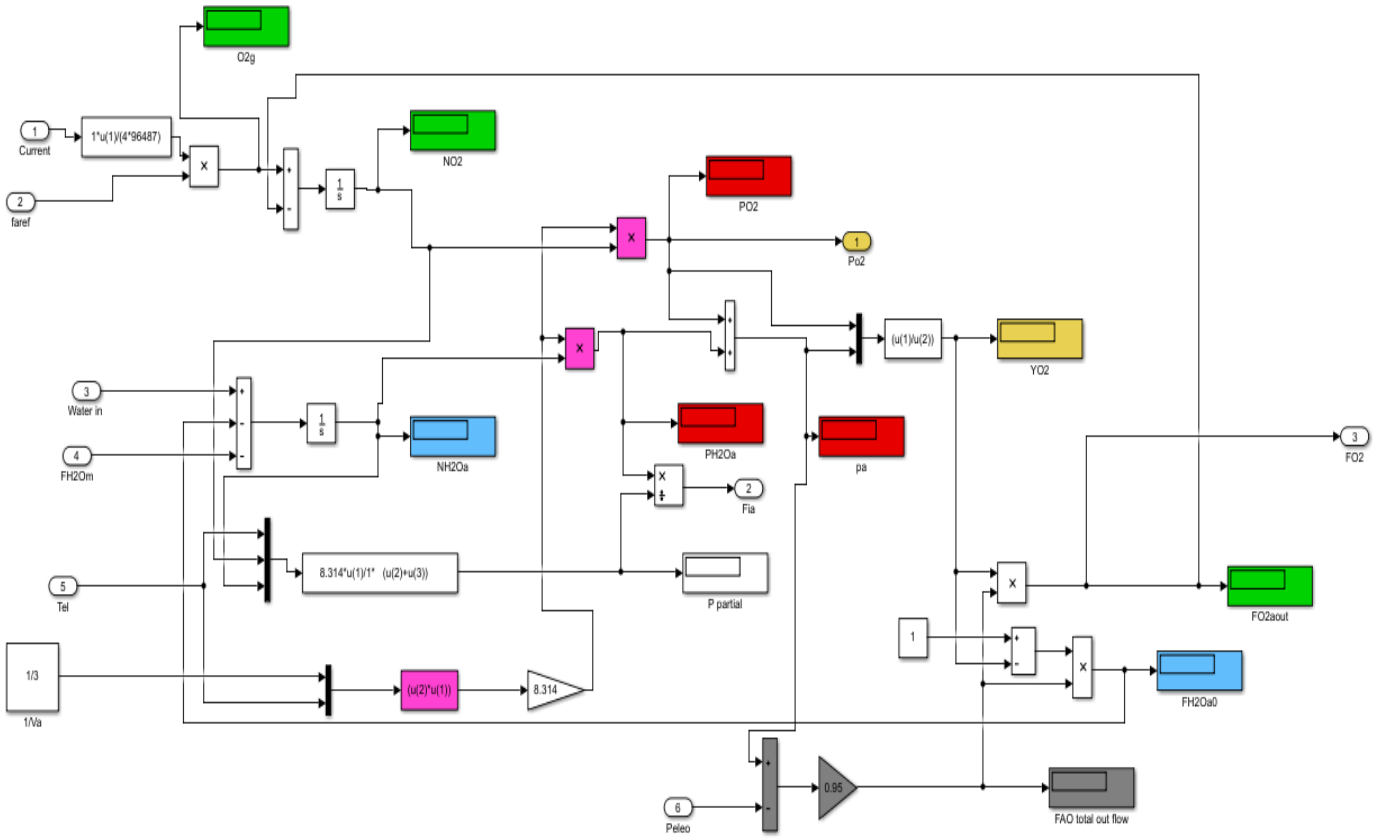

Anode mathematical details in Electrolyzer

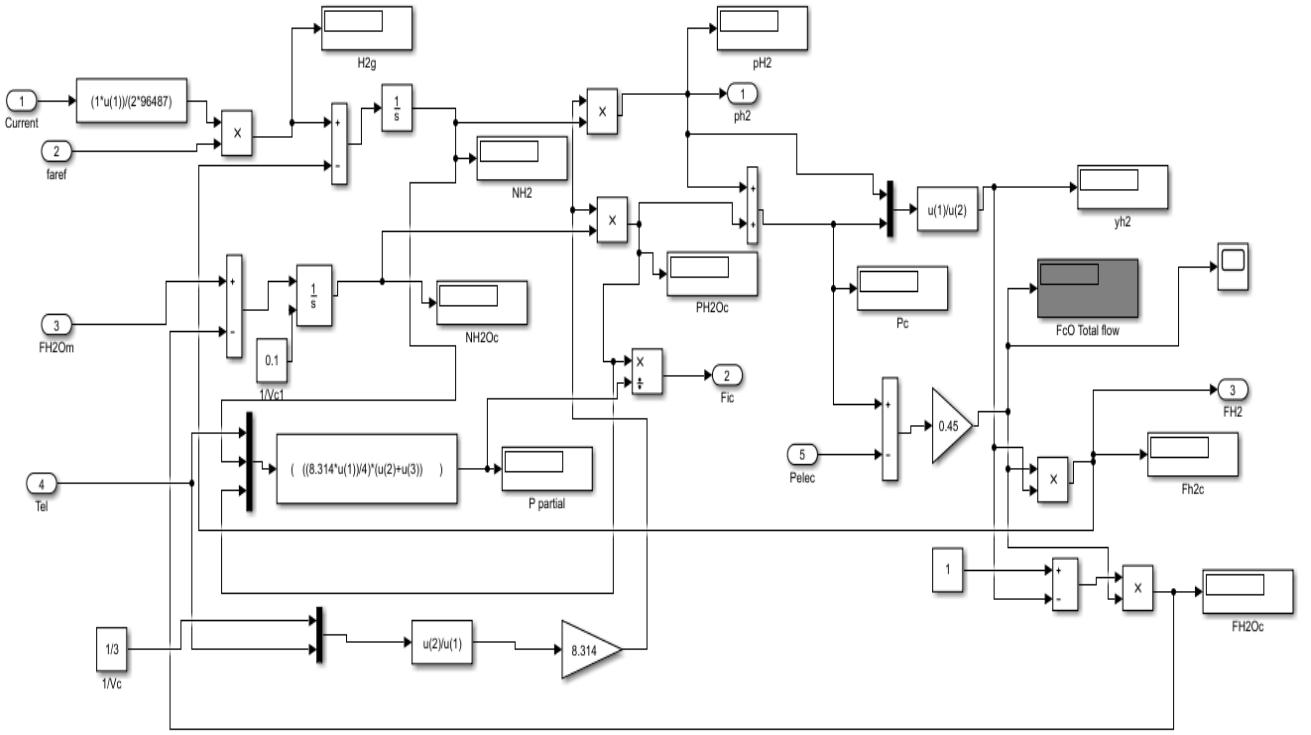

Cathode mathematical details in Electrolyzer

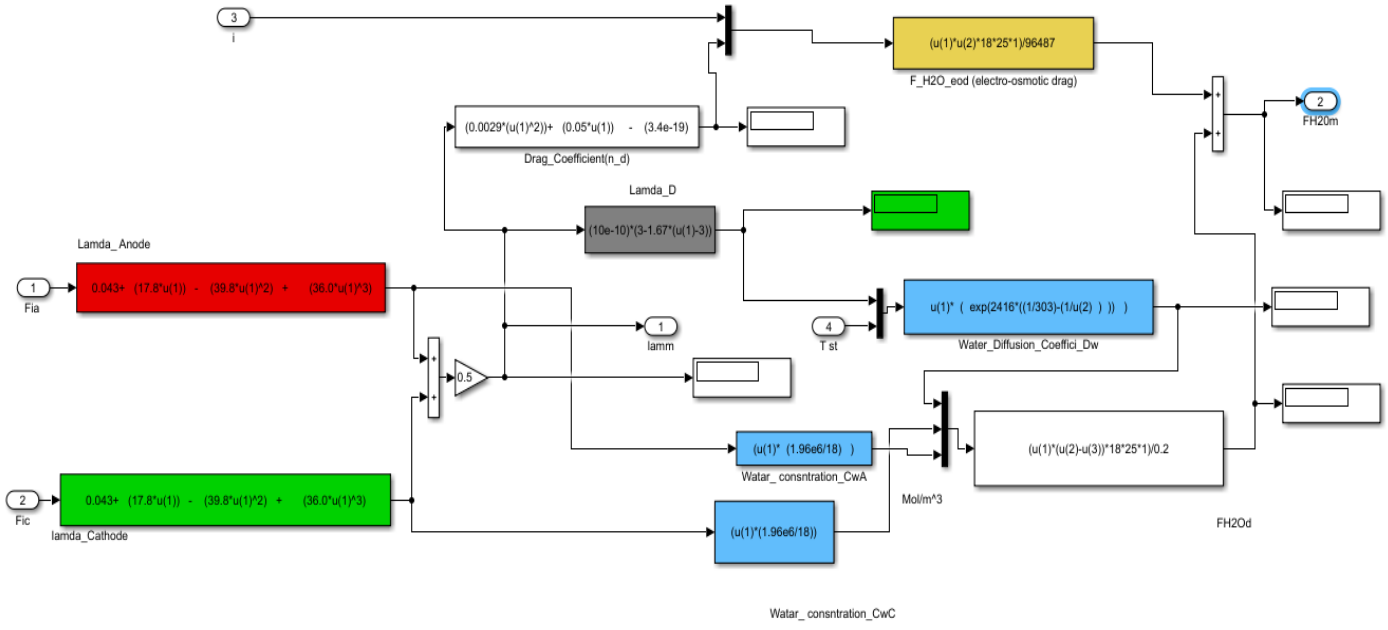

Membrane mathematical details in Electrolyzer

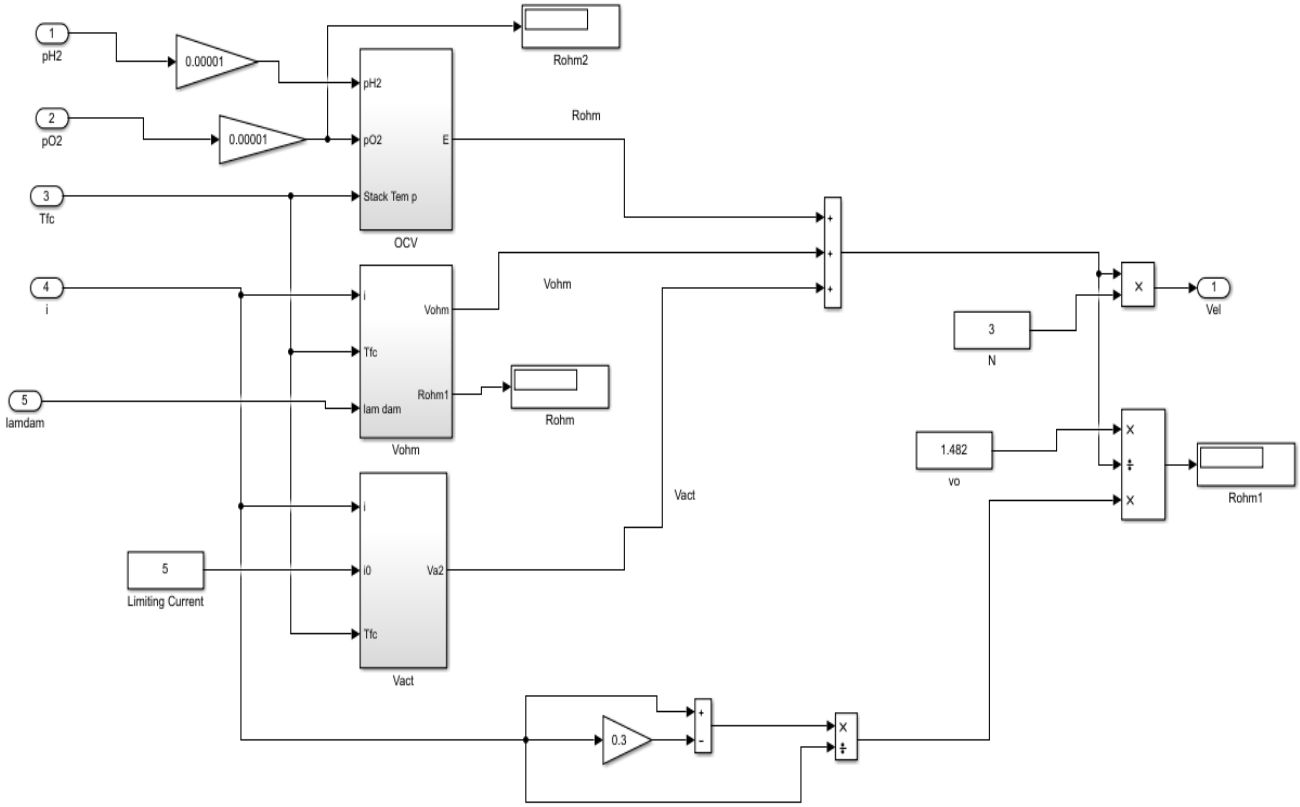

Voltage ancillary mathematical details in Electrolyzer

Appendix -Chapter 4

Sensitivity analysis

“For example, image that a modeler doing a preliminary analysis of a wind-diesel system was uncertain about three variables: the annual average wind speed, the average fuel price over the life of the project, and the interest rate. To determine the sensitivity of the system's cost of energy to those three variables, she did a sensitivity analysis using HOMER. Her best estimate for the wind speed was 6 m/s, for the fuel price was $0.50/L, and for the interest rate was 8%. But she entered multiple values for each variable, covering the range of uncertainty of each. HOMER produced the spider graph shown below, showing that the cost of energy is most sensitive to the wind speed (the wind speed line is the steepest). As a result, the modeler chose to invest more time and money to obtain a more accurate estimate of the wind speed” [Homer Help Sources].

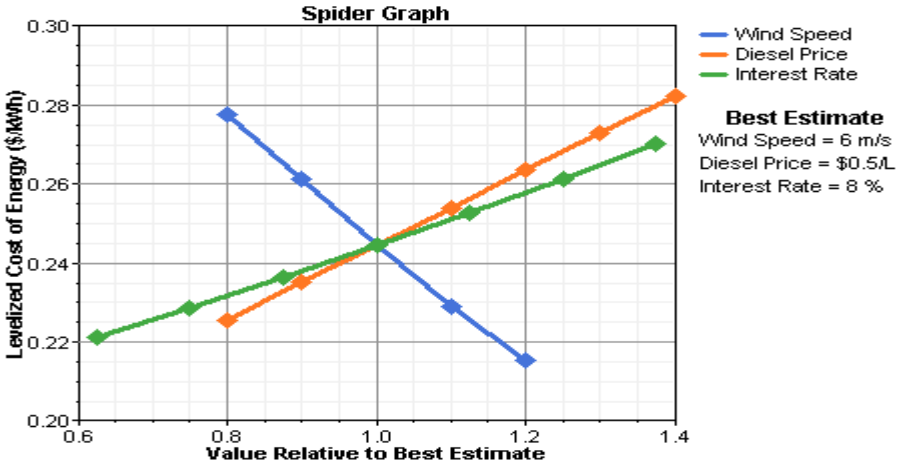

Components	Cost
Fuel cell (500/1k) W	$3084/ $4284
Electrolyzer	$1509
Hydrogen Tank	$915
Battery	$840
Wind turbine	$800
PV panel	$3600
DC Motor	$60

Specifications

Characteristics	Specifications
Length	5.3 m
Diameter	0.69 m
Dry Weight	830 kg
Energy	17.6 kWh
Maximum Depth	3000 m with 10% safety factor
Typical Crusing Speed	1.5 m/s
Speed Range	0.5 m/s to 2.5 m/s
Power Source and Capacity	11 x 1.6 kWh E-One Moli Energy Li-Ion Cobalt rechargeable battery modules
Computer	Rack mount cPCI system for vehicle control and payload control computer
Hydroplanes	4 NACA 0026 stern planes 2 NACA 0026 fore planes
Navigation INU Type	iXsea PHINS III

https://www.mun.ca/engineering/research/facilities/centres/oerc/facilities/merlin/explorerauv.php

Fuel Cell Properties	
Number of Cells	48
Rated Power	1000W (1kW)
Rated Performance	28.8V @ 35A
Hydrogen Supply Valve Voltage	12V
Purging Valve Voltage	12V
Blower Voltage	12V
Reactants	Hydrogen and Air
Ambient Temperature	5 - 30C (41 - 86F)
Max Stack Temperature	65 C (149 F)
Hydrogen Pressure	0.45 - 0.55 Bar
Humidification	Self-humidified
Cooling	Air (integrated cooling fan)
Controller Weight	400g (± 30g)
Stack Weight (with Fan & Casing)	4kg ± 100g
Hydrogen Flow Rate at Max Output	13 L/min
Stack Size	268 x 219 x 122.5mm (10.5" x 8.6" x 4.8")
Hydrogen Purity Requirement	≥ 99.995% (dry H2)

https://www.fuelcellstore.com/fuel-cell-stacks/high-power-fuel-cell-stacks/horizon-1000watt-fuel-cell-h-1000

2.3 Module Electrical Specification

Capacity	
ONYX +48V (per module nominal)	
M70X48V034P	34Ah
Module Charge	
V_{min}	+42VDC
V_{max} = Charge Voltage	+54.0VDC
Current	
$I_{discharge(peak: less\ than\ 30\ seconds)}$	-20A
$I_{discharge(continuous)}$	-15A
$I_{charge(peak: less\ than\ 30\ seconds)}$	+20A
$I_{charge(continuous)}$	+15A
Discharge Temperature Range	
$T_{min(Discharge)}$	-20℃ (-4℉)
$T_{max(Discharge)}$	60℃ (140℉)
Charge Temperature Range	
$T_{min(Charge)}$	0℃ (32℉)

Technical data

E206:

Item name: ..... Electrolyser H2/02 65
Item no: E206
H x W x D: ..... 250 x 250 x 120 mm
Weight: ..... 950 g
Number of cells: 2
Electrode dimensions: ..... 40 x 40 mm
Operating medium: .... distilled water, $\sigma < 2$ µS/cm
Fill volume H2O, H2-side: ..... approx. 90 ml
Fill volume H2O, O2-side: ..... approx. 130 ml
Permissible operating voltage: ..... 0 - 4.0 VDC
Permissible operating current: ..... 0 - 4.4 A
Rated power consumption: ..... approx. 16 W
Gas production H2 at rated power output: ... approx. 65 cm^3/min
Gas production O2 at rated power output: ... approx. 32.5 cm^3/min

E207:

Item name: ..... Electrolyser H2/02 230
Item no: E207
H x W x D: ..... 250 x 330 x 200 mm
Weight: ..... 1850 g
Number of cells: 7
Electrode dimensions: ..... 40 x 40 mm
Operating medium: .... distilled water, $\sigma < 2$ µS/cm
Fill volume H2O, H2-side: ..... approx. 90 ml
Fill volume H2O, O2-side: ..... approx. 130 ml
Permissible operating voltage: ..... 0 - 14.0 VDC
Permissible operating current: ..... 0 - 4.4 A
Rated power consumption: ..... approx. 56 W
Gas production H2 at rated power output: ... approx. 230 cm^3/min
Gas production O2 at rated power output: ... approx. 115 cm^3/min

https://www.fuelcellstore.com/hydrogen-equipment/electrolyzer-230-e107

https://www.alibaba.com/product-detail/cheapest-1000W-wind-alternator-48v-for_60158460072.html

https://www.alibaba.com/product-detail/48v-brushless-dc-motor-nema34220w_60500232517.html?spm=a2700.7724838.2017115.96.57493907yRTCES

-

Metal Hydride Properties	
Hydrogen Capacity - Alloy A	34 standard liters (1.3 scf)*
Hydrogen Capacity - Alloys L, M, or H	30 standard liters (1.14 scf)*
Hydrogen Pressure when Charging or Discharging	The hydrogen pressure when charging or discharging a SOLID-H™ container is something you select when you order. Four standard pressure ranges are offered; Alloy A (1-10 bar at room temperature), Alloy L (2-3 bar at room temperature), Alloy M (4-5 bar at room temperature) and Alloy H (8-12 bar at room temperature).
Discharge Rate	The discharge rate depends on many variables. We can help you select a SOLID-H™ metal hydride alloy and hydrogen container(s) that will meet your hydrogen flow requirements. In general, you should not expect to empty the entire hydrogen capacity in a matter of minutes. Hours are required to withdraw 90% or more of the hydrogen capacity from a standard** metal hydride container. The largest SOLID-H™ containers require days to discharge completely. **It is possible to discharge a metal hydride in a matter of seconds. This requires extraordinary heat transfer enhancement inside and outside of the container. We can provide heat transfer enhancement to improve the charging and discharging rates of our SOLID-H™ containers.
Recharge Time	About 4 hours - The specified recharge time is for cooling by still air at 20°C and the charging pressure specified in the SOLID-H™ manual for Alloys A, L, M or H. A fan will shorten charging time.
Cylinder Diameter	1.125 inch (28.6 mm)
Overall Length	7.8 inch (198 mm)
Mass	0.96 lb (438 grams)
Destructive Proof Test	>5000 psig (350 bar)
Pressure Relief Valve Set	<550 psig (37 bar)
Materials Included	Stainless Steel Cylinder with Brass Fittings

https://www.fuelcellstore.com/bl-30-metal-hydride

Fuel cell nominal parameters:
  Stack Power:
    -Nominal = 1259.96 W
    -Maximal = 2000 W
  Fuel Cell Resistance = 0.061871 ohms
  Nerst voltage of one cell [En] = 1.115 V
  Nominal Utilization:
    -Hydrogen (H2)= 99.92 %
    -Oxidant (O2)= 1.813 %
  Nominal Consumption:
    -Fuel = 15.22 slpm
    -Air = 36.22 slpm
  Exchange current [i0] = 0.027318 A
  Exchange coefficient [alpha] = 0.308

Fuel cell signal variation parameters:
  Fuel composition [x_H2] = 99.95 %
  Oxidant composition [y_O2] = 21 %
  Fuel flow rate [FuelFr] at nominal Hydrogen utilization:
    -Nominal = 12.2 lpm
    -Maximum = 23.46 lpm
  Air flow rate [AirFr] at nominal Oxidant utilization:
    -Nominal = 2400 lpm
    -Maximum = 4615 lpm
  System Temperature [T] = 328 Kelvin
  Fuel supply pressure [Pfuel] = 1.5 bar
  Air supply pressure [PAir] = 1 bar

https://www.fuelcellstore.com/hydrogen-equipment/hydrogen-storage/bl-20-metal-hydride

https://www.fuelcellstore.com/bl-60-metal-hydride

For the selection of the three hydrogen tanks, the cost of each one has entered HOMER Software inputs based on their sizes (kg) as listed in the table below.

Costs

Size (kg)	Capital ($)	Replacement ($)	O&M ($/yr)
0.307	2685	895	0
0.400	2745	915	0
0.636	3963	1321	0

And the capacity and pressure are listed below:

For 0.307 Kg

Hydrogen Capacity of 20-21 standard liters (0.76-0.80 scf)

Hydrogen Pressure when Charging or Discharging is 1-12 bar at room temperature

For 0.400 Kg

Hydrogen Capacity of 30-34 standard liters (1.14-1.3 scf)

Hydrogen Pressure when Charging or Discharging is 1-12 bar at room temperature

For 0.636 Kg

Hydrogen Capacity of 60-69 standard liters (2.28-2.64 scf)

Hydrogen Pressure when Charging or Discharging is 1-12 bar at room temperature

Table for compressed hydrogen

Required Volume to Store 1 kg of Hydrogen as Compressed Gas at 20°C

Pressure MPa	Volume Liters
0,1013	11,934.0
100	128.7
200	68.4
300	48.4
350	42.7
450	34.9
700	25.7

Appendix – Chapter 5

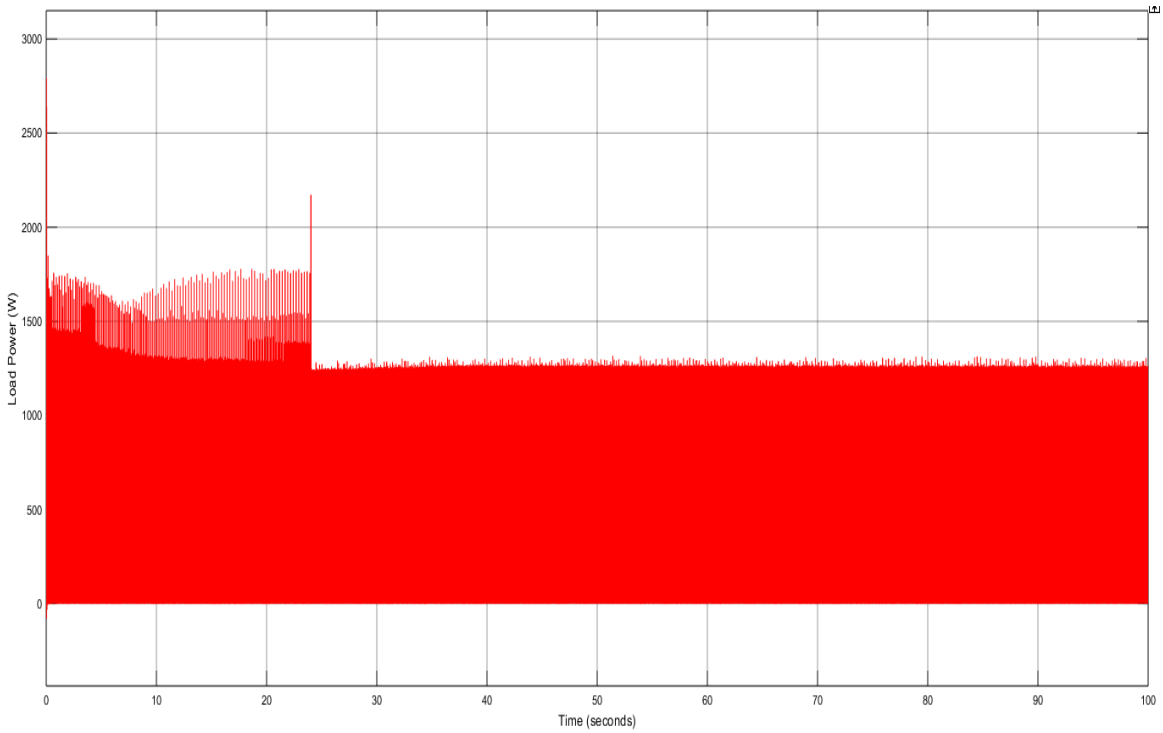

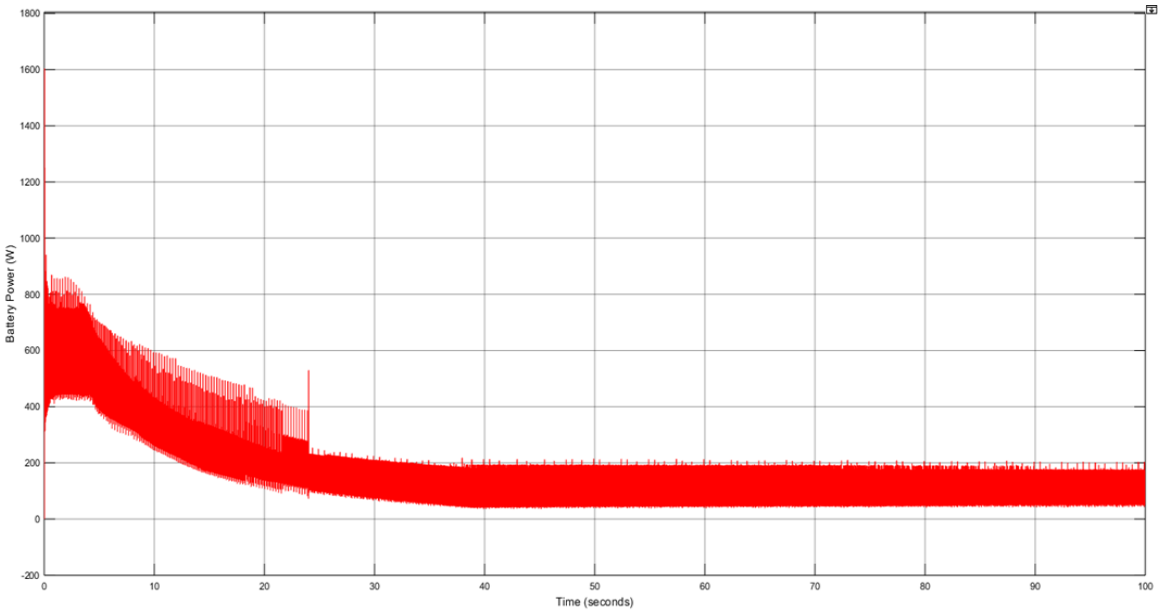
Battery Power (W)
Time (seconds)
1800
1600
1400
1200
1000
800
600
400
200
0
-200
0
10
20
30
40
50
60
70
80
90
100

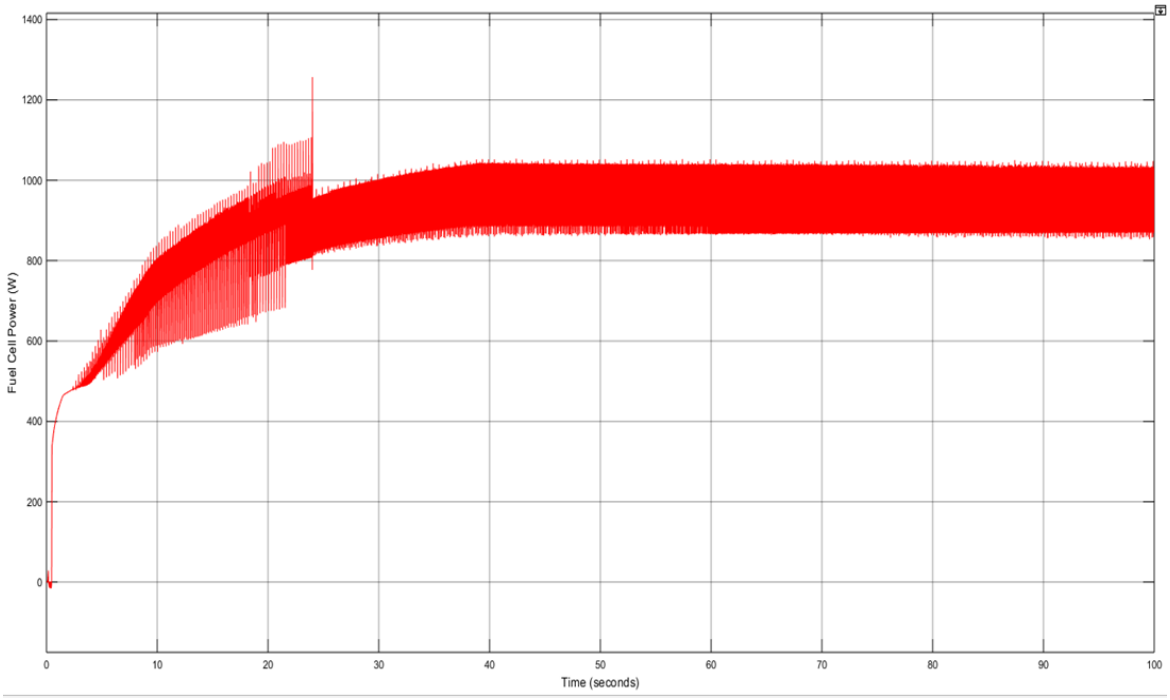

4.3 PROPULSION SYSTEM

4.3.1 Motor

Manufacturer	Hathaway Emoteq, Inc
Model	HT07001-H01
Design voltage (V) DC	48
Maximum current (Amp) (input to motor controller)	32
Maximum RPM in water – @ 2.5 m/s	300
Max continuous power (W) (input to motor controller	1630 @ 51 VDC

4.3.2 Motor controller

Manufacturer	Hathaway Emoteq, Inc
Model	B2Q04840
Peak current (Amp) (Output of motor controller)	40
Minimum D.C. supply (V)	40
Maximum D.C. supply (V)	60